UNIVERSITY OF CALIFORNIA

Santa Barbara

Pluripotent Stem Cell-Derived Retinal Pigmented Epithelium: Methods, Lines, and Behaviors

A dissertation submitted in partial satisfaction of the
requirements for the degree Doctor of Philosophy
in Molecular, Cellular and Developmental Biology
by

Roxanne Helene Croze

Committee in charge:

Professor Dennis O. Clegg, Chair

Professor Peter J. Coffey, University College London

Professor Stuart Feinstein

Professor Carol Vandenberg

June 2015

The dissertation of Roxanne Helene Croze is approved.

_____

Peter J. Coffey

_____

Stuart Feinstein

_____

Carol Vandenberg

_____

Dennis O. Clegg, Committee Chair

June 2015

Pluripotent Stem Cell Derived Retinal Pigmented Epithelium:
Methods, Lines, and Behaviors

by

Roxanne Helene Croze

ACKNOWLEDGMENTS

I would first like to thank my advisor Professor Dennis O. Clegg for accepting me into his lab and for his mentorship over the past five years. He has provided me with the perfect combination of freedom and structure, allowing me to be experimentally creative and keeping me focused on achieving my goals. His comic relief and personal stories have been indispensable in helping guide me through my own adventures while in graduate school.

I also want to thank the many graduate students, technicians and professors who have lent me reagents and equipment, and more importantly brainstormed ideas and helped me troubleshoot experimental issues. This list includes: the entire Clegg Lab, especially Lyndsay Leach, whom had a major part in the compilation of Chapter 3, David Buchholz, Sarah Benbow, Irene Whitney, Patrick Keeley, Amanda Kautzman, Misty Riddle and the Stem Cell Lab especially, Sherry Hikita, Michelle Maloney and Cassidy Hinman. I have also had the assistance of three amazing undergraduates, Josh Dorst, William Thi and Gabi Reeder whom I hope have learned as much from me as I have learned from them. I would also like to acknowledge my family and friends outside of graduate school whom I would not have been able to get through these five years without.

In addition, I would like to thank Carolyn and Monte Radeke for technical support while performing the microarray experiments, Mary Raven for microscopy training and assistance, and Lincoln Johnson, Dean Bok, James Thomson and David Gamm for their generous gifts of fetal and iPSC cells.

This work was supported by the Garland Initiative for Vision, grant DR1-0144 from the California Institute for Regenerative Medicine, Fight for Sight, The Foundation Fighting Blindness Wynn-Gund Translational Research Acceleration Program, the UCSB Institute for Collaborative Biotechnologies through grant W911NF-09-0001 from the U.S. Army Research Office, the Bright Focus Foundation (M2011064, MJR) and the California Institute for Regenerative Medicine (LA1-02086 (PJC); DR1-01444, CL1-00521, TG2-01151 (DOC) and Major Facilities grant FA1-00616. RHC is a fellow of the California Institute for Regenerative Medicine. The content of the information does not necessarily reflect the position or the policy of the Government, and no official endorsement should be inferred.

VITA OF ROXANNE HELENE CROZE

June 2015

EDUCATION

University of California, Santa Barbara
PhD Candidate, September 2010 to June 2015
Molecular, Cellular and Developmental Biology

University of California, Santa Barbara
Masters of Arts, June 2012
Molecular, Cellular and Developmental Biology

University of California, Davis
Bachelor of Science, December 2007
Biological Sciences**:** Cell and Molecular Biology, with honors

University of California Center, Siena, Italy
Education Abroad Program, April 2006 - June 2006
International studies in Italian language and culture

RESEARCH EXPERIENCE

PhD Candidate, Dr. Dennis Clegg, University of California, Santa Barbara
Molecular, Cellular and Developmental Biology Department, Research focus: The effects of ROCK Inhibition on hESC-RPE (April 2011-June 2015)
• Examining the effects of Rho kinase inhibitors on hESC-RPE and fRPE differentiation, proliferation, apoptosis and wound healing.
• Creating fluorescent reporters to monitor hESC-RPE cell behavior and function to examine cells after transplantation into a rat model of retinal dysfunction.
• Continuing lab efforts to reprogram keratinocytes directly into RPE.
• Collaborated with Dr. David Buchholz in developing a rapid and efficient protocol for hESC derived RPE.

Research Assistant, Dr. Bruce Levy and Dr. Charles Serhan, Brigham and Women's Hospital, Harvard School of Medicine
Pulmonary Division, Research focus: The role of lipid mediators on the resolution of Aspiration Pneumonia (September 2008- August 2010)
• Created and carried out protocols for both *in vivo* and *in vitro* aspiration pneumonia, acute lung injury, and asthma experiments to study the effects of lipid mediators on the active resolution process in the lung or using epithelial cell lines and primary cultures.
• Worked with Dr. Troy Carlo on creating and maintaining a mouse colony of PDP1 knockout mice, examined the effects of acute lung injury on these knockout mice and created a stable clone *in vitro* of PDP1 protein for laboratory use.

• Studied the differences in metabolic rate between RvD1 and AT-RvD1
• Participated in seminars and journal clubs, presented my data and recent important publications to the division and throughout the research community.
• Maintained a precise lab notebook, and continued my education on laboratory ethics and procedures.

Research Laboratory Intern, Dr. R. Wu, UC Davis School of Medicine
UC Davis Department of Internal Medicine, Research focus: The role of IL-17 on immune regulation in lung epithelial cells (January 2007- December 2007).
• Worked with Dr. Sharlene Velichko to investigate the signaling cascade of the IL-17 receptor on respiratory epithelial cells and cloned an IL-17 receptor-A fusion protein containing the IL-17RA cytoplasmic domain and the CD8+ ectodomain to serve as a shortcut for cell stimulation.
• Worked with Dr. Phillip Thai performing stem cell research to examine differentiation of epithelial airway cells' response to cigarette smoke, and worked on cloning promoters of respiratory epithelial cells into GFP-Topo plasmids for easy recognition of differentiation.
• Learned proper techniques for creating well organized laboratory records.
• Furthered my knowledge of Laboratory Health, Safety and Environment rules and laboratory management protocols.

Research Laboratory Intern, Dr. L. Sparger, UC Davis School of Veterinary Medicine
UC Davis Department of Immunology, Research focus: Improving the Feline Immunodeficiency Virus (FIV) vaccine by using plasmid recombination (Winter 2006).
• Worked with Dr. Robert Dubie, performing basic laboratory techniques including electrophoresis, electroporation, PCR, MiniPreps, MaxiPreps and other introductory procedures to help progress research on the FIV vaccine.
• Gained lab experience and knowledge of Laboratory Health, Safety and Environment rules in addition to laboratory management protocols.

AWARDS

Attendee of the Lindau Nobel Laureate Meeting: Physiology and Medicine (June/July 2014)
Best Poster Award, UCSB MCDB Symposium (2013, 2014)
Doreen J. Putrah Travel Award (2013)
Excellence in Neuroscience Research Junior Award, 19th Annual UCSB Neuroscience Symposium (January 23th, 2013)
CIRM Trainee Grant, University of California, Santa Barbara (2012-2015)
Best Poster Award, Beckman Initiative for Macular Research Annual Meeting (2012)
Clark -Carbon Fellowship, University of California, Santa Barbara (2010-2011)
Full Athletic Soccer Scholarship, University of California, Davis (2003-2007)

Reserve Fund Scholarship, University of California, Davis (2007)
Outstanding Senior Award Recipient, University of California, Davis, Class of 2007
Student-Athlete Honor Roll, University of California, Davis (2003-2007)

LEADERSHIP AND ACTIVITIES

Get WiSE member, Women in Science and Engineering outreach (2014-present)
EMBODI member, Engineering, Medicine, Biology, Discovery, Innovation (2013-present)
Co-reviewer for the Investigative Ophthalmology and Visual Science (May 2015)
Co-reviewer for Stem Cells (April 2015)
Co-reviewer for the Journal of Biomaterials Science: Polymer Edition (October 2013)
Stem Cell Awareness Day Speaker, Santa Barbara High School (October 2013, 2014, 2015)
UCSB Graduate Committee, Graduate Student Representative (2013-2015)
Mentor, CIRM Research Mentorship Program, University of California, Santa Barbara (2015 summer)
Mentor, Summer Applied Biotechnology Research Experience (SABRE), Institute for Collaborative Biotechnologies University of California, Santa Barbara (2012 summer)
Teaching Assistant, Biology 1A Laboratory, University of California, Santa Barbara (fall 2010, fall 2011)
Teaching Assistant, Biology 1B Laboratory Curriculum Development, University of California, Santa Barbara (winter 2011)
Player, Women's UC Davis Intercollegiate Division I Soccer (2003- 2007)
Nominee, NCAA Leadership Conference (April 2005)
Captain, UCD Women's Soccer Team (2006-2007 season)
Captain, UCD Women's Soccer Team (2005 winter/spring season)
Women's Varsity Soccer Assistant Coach, Will C. Wood High School, Vacaville, CA (February-May 2007)
Under 15 Girls Soccer Assistant Coach, Davis Legacy Club, Davis, CA (2007-2008 season)

SKILLS

• Human embryonic stem cell and induced human pluripotent stem cell culture techniques
• Eight years of cell culture work; human embryonic stem cell derived retinal pigmented epithelium, primary keratinocytes, primary bronchial epithelial cells, adipose stem cells, and cell lines: adipose stem cells, HUVEC, MEWO, A549, Calu3, AMJ2C8, HEK293T, CHO, 3T3, ARPE19 and MDCK
• Two years of *in vivo* mouse work using acute lung injury, pneumonia, peritonitis, and asthma models, knowledge of appropriate handling techniques, colony maintenance

and breeding, anesthesia, tail vein injections, bronchial alveolar lavage, lung fixation for histological analysis, organ extraction, cardiac blood extraction, euthanasia
• Gel electrophoresis, immunoprecipitation, coimmunoprecipitation, western blot analysis, *in vitro* cell stimulation, protein purification, immunohistochemistry, immunocytochemistry, flow cytometry, electroporation, transformation, transfection, transduction, molecular cloning, fluorescence and confocal microscopy, lentiviral manipulation, lentivirus production, ELISA, DNA/RNA isolation, primer design, PCR, RT-QPCR (Sybergreen and Taqman), microarray, MTT assay, TUNEL assay, AnnexinV staining, phagocytosis assay, radiolabelled phosphorylation, audioradiography, lipid extractions, bacterial handling and plating, media and buffer preparation
• Experience using Microsoft Word, Excel, PowerPoint, SigmaPlot, Prism, Adobe Illustrator, Image J, Adobe Photoshop, VersaAnalyzer in PC and Mac platforms

PUBLICATIONS

Croze, R.H., Buchholz, D.E., Radeke, M., Thi, W., Hu, Q., Coffey, P.J., and Clegg, D.O. (2014) *ROCK inhibition extends passage of human embryonic stem cell derived retinal pigmented epithelium*. Stem Cells Translational Medicine 3:1066-1078.

Croze R.H. and Clegg D.O. (2014) "Differentiation of pluripotent stem cells into retinal pigmented epithelium". Dev Ophthalmol. 53:81-96.

Buchholz, D.E., Pennington, B.P., **Croze, R.H.,** Hinman, C.R., Coffey, P.J., and Clegg, D.O. (2013) *Rapid and Efficient Directed Differentiation of Human Pluripotent Stem Cells Into Retinal Pigmented Epithelium.* Stem Cells Translational Medicine 2:384-393.

Clegg, D.O., Hikita, S.T., Hu, Q., Buchholz, D.E., Rowland, T.J., Conti, L., Pennington, B., **Croze, R. H.,** Leach, L., Tsie, M., and Johnson, L.V. (2013) "Derivation of retinal pigmented epithelial cells from pluripotent stem cells", in Stem Cells Handbook, Second Edition, S. Sell, Ed., Springer Publishing.

Rogerio A. P., Haworth, O., **Croze, R**., Oh, S.F., Uddin, M., Carlo, T., Pfeffer, M.A., Priluck, R., Serhan, C.N., and Levy, B.D. (2012) *Resolvin D1 and its Aspirin-Triggered Epimer Resolvin D1 Promote the Resolution of Allergic Airways Responses.* Journal of Immunology 189:1983-1991.

Eickmeier, O., Seki, H., Haworth, O., Hilberath, J.N., Gao, F., Uddin, M., **Croze, R.H**., Carlo, T., Pfeffer, M.A., and Levy, B.D. (2012) Aspirin-triggered resolvin D1 reduces mucosal inflammation and promotes resolution in a murine model of acute lung injury. Mucosal Immunology 6:256-266.

Hilberath, J.N., Carlo, T., Pfeffer, M.A., **Croze, R.H.**, Hastrup, F., Levy, B.D. (2011) *Resolution of Toll-like receptor 4-mediated acute lung injury is linked to eicosanoids and suppressor of cytokine signaling 3.* FASEB 25:1827-1835.

Planagumà A, Pfeffer MA, Rubin G, **Croze R**, Uddin M, Serhan CN, Levy BD. (2010) *Lovastatin decreases acute mucosal inflammation via 15-epi-lipoxin A4.* Mucosal Immunology 3:270-279.

Meeting Presentations

Croze, R.H., Leach, L., Sandra Nakasone, Radeke, M., and Clegg, D.O., "Monitoring stem cell transplants in ocular disease." Regenerative Medicine: From the Bench to the Bedside, Cambridge, UK (2014).

Croze, R.H., Leach, L., Sandra Nakasone, Radeke, M., and Clegg, D.O., "Monitoring stem cell transplants in ocular disease." International Society for Stem Cell Research, Boston, MA (2013).

Croze, R.H., Leach, L., Sandra Nakasone, Radeke, M., and Clegg, D.O., "Monitoring stem cell transplants in ocular disease." CIRM Trainee Grant Meeting, San Francisco, CA (2013).

Croze, R.H., Leach, L., Radeke, M., and Clegg, D.O., "Monitoring stem cell transplants in ocular disease." Beckman Conference, Irvine, CA (2012). *Best poster winner

Buchholz, D.E., **Croze, R.H.**, Hinman, C.R., Leach, L.L., Pennington, B.O., and Clegg, D.O. "Rapid and Efficient Directed Differentiation of Human Embryonic Stem Cells into Retinal Pigmented Epithelium." 6th Annual Translational Stem Cell Research Conference of the New York Stem Cell Foundation, New York, NY (2011).

Buchholz, D. E., **Croze, R. H.**, Leach, L. L. Clegg, D. O. "Specification of the Early Eye Field from Human Embryonic Stem Cells." 9th Annual Meeting of the International Society for Stem Cell Research, Toronto, Canada (2011).

Eickmeier, O., Seki, H., Haworth, O., Hilberath, J.N., Gao, F., Uddin, M., **Croze, R.H.,** Carlo, T., Pfeffer, M.A., and Levy, B.D. "Aspirin-triggered resolvin D1 reduces mucosal inflammation and promotes resolution in a murine model of acute lung injury." American Thoracic Society Conference, New Orleans, LA (2010).

ABSTRACT

Pluripotent Stem Cell Derived Retinal Pigmented Epithelium:
Methods, Lines, and Behaviors

by

Roxanne Helene Croze

Ocular diseases affect millions world-wide and dramatically influence the quality of life. Although much is known about ocular biology and disease pathologies, effective treatments are still lacking. The eye is well suited for application of emerging cell-based therapies. This dissertation will explore the development of stem cell-based treatments for age-related macular degeneration (AMD), a prevalent ocular disease in the elderly. Retinal pigmented epithelium (RPE), a cell type implicated in AMD, has been derived from both human induced pluripotent stem cells (iPSC) and human embryonic stem cells (hESC). Rapidly advancing research has generated various methods of RPE differentiation and several transplantation strategies. The following chapters will provide an in-depth overview and characterization of hESC-RPE and iPSC-RPE across two methods of derivation.

Pluripotent stem cell derived RPE have unique cellular characteristics. This dissertation will also examine various RPE behaviors upon manipulation with a synthetic kinase inhibitor and describe the creation and production of exogenous reporters that can be used for real-time monitoring of cellular transplantations.

Human embryonic stem cell derived retinal pigmented epithelium (hESC-RPE) is in clinical trials for the treatment of macular diseases. Currently, these cells take over three months to derive and subsequent months to mature and characterize. After only four to five passages the cells begin to undergo an epithelial-to-mesenchymal transition and are unsuitable for cellular therapies. We show in this dissertation that inhibition of Rho-associated coiled-coil kinase (ROCK) using specific inhibitor, Y-27632, can increase the lifespan and proliferation rate of hESC-RPE in culture. hESC-RPE maintain typical cuboidal morphology, gene expression, protein localization, factor secretion, and phagocytic abilities up to passage 13 following ROCK inhibition.

In addition, this dissertation will elucidate other effects of ROCK inhibition on hESC-RPE. ROCK inhibition is known to affect cytoskeletal rearrangements and we will show that ROCK inhibition can promote wound closure and attachment through increased cell cycle activation and cell spreading respectively. Elucidating these effects and beginning to understand the mechanisms of wound healing and attachment is critical when considering ROCK inhibition as a novel treatment for geographic atrophy, a late stage phenotype of AMD, and as a potential combinational therapy with cellular replacement to enhance engraftment.

In the final chapter, the creation of a molecular tool basket will be described. As hESC-RPE progress through the phases of clinical trials, it will be important to gain a better understanding of how the cells behave in vivo to address any potential caveats within the clinical trials. Fluorescent reporters that monitor transplanted cell migration,

function and mitotic stage have been created to examine, in real time, how the stem cell derived transplant is affected by the endogenous retinal milieu.

The findings within this dissertation have tremendous implications in understanding the variability between hESC-RPE and iPSC-RPE and the various methods of derivation as these cellular therapies move into the clinics. In addition, the benefits of ROCK inhibition on hESC-RPE and iPSC-RPE could lead to combinational therapies and help produce large intermediate cell banks if clinical trials prove efficient and a large scale cell production is required.

TABLE OF CONTENTS

LIST OF FIGURES

LIST OF TABLES

Chapter I

Differentiation of Pluripotent Stem Cells into Retinal Pigmented Epithelium

Introduction

Age-related macular degeneration (AMD) is a progressive disease leading to the loss of high-acuity vision. More than 200,000 people are diagnosed per year, making AMD the leading cause of blindness in the elderly in the developing world [1]. Around 7.2 million people in the US alone suffer from this devastating disease with annual medical costs exceeding US$250B [2]. The disease primarily affects a small region in the back of the eye responsible for central vision called the macula. Loss or dysfunction of macular RPE, which provides crucial supportive functions for the photoreceptors, is thought to play a crucial role in disease progression. There are two general forms of the disease, wet (exudative) AMD and dry (non-exudative) AMD, with over 90% of patients suffering from the more slowly progressing dry form [3, 4]. Wet AMD is characterized by a quick progression of choroidal neovascularization (CNV), leading to rapid degradation of RPE and photoreceptors and impaired vision. However, this form of the disease is successfully treated in most patients using inhibitors of the vascular endothelial growth factor (VEGF), such as ranibizumab, bevacizumab, and aflibercept [1, 5-7]. The advanced form of AMD not involving CNV growth, termed geographic atrophy, results in extensive RPE and photoreceptor death, which causes substantial vision loss as the fovea becomes threatened or involved directly [8, 9]. This extensive loss of vision impairs daily activities including reading, driving, face recognition, and mobility. Currently, there are no reliable, effective treatments for dry AMD [10, 11]. Although some experimental autologous transplants and retinal translocation surgeries have been performed, they are fraught with obstacles and complications that have yet to be overcome [12].

AMD is a multifactorial disease with numerous genetic and environmental risk factors [13, 14]. Polymorphisms within multiple complement system genes, including alternate complement factors H, B, and I, in addition to components 2 and 3, lead to substantial genetic predisposition to AMD [15-21]. These findings suggest a chronic inflammatory state in the disease and potentially a progressive immune attack on RPE. Mutations in non-inflammatory related genes, Apolipoprotein E *(APOE)* [22], hepatic triglyceride lipase *(HL)* [23], cholesteryl ester transfer protein *(CETP)* [23], vascular endothelial growth factor *(VEGF)* [24], and regions surrounding the tissue inhibitor metalloproteinase 3 *(TIMP3) [23],* also correlate with AMD onset. Genes associated with AMD also include Age-related Maculopathy Susceptibility 2 *(ARMS2)* [21] and HTR1A serine peptidase 1 *(HTRA1)* [25], although little is known about their mechanisms of action. A mutation in the ATP-binding cassette transporter gene sub-family A (ABCA4) leads to Stargardt disease, causing early onset macular degeneration, often rendering patients blind before the age of 20 [26]. ABCA4 mutations may also be associated with some cases of AMD [27]. Environmental factors that influence AMD development and progression include, age, smoking, non-African decent, poor eating habits, and low physical activity [14]. The precise mechanism of AMD causation is still not completely understood.

The presence of drusen deposits is the hallmark pathology of both forms of AMD. Drusen are composed of lipids, carbohydrates, proteins, and cellular components, including secreted inflammatory proteins [28, 29]. These deposits build up in between the basal laminar side of the RPE and the surface of the Bruch's membrane, a multilaminar extracellular matrix barrier separating the RPE and choroid. The

monolayer of RPE is disrupted by drusen and may play a role in RPE dysfunction. However, the direct effect of drusen on RPE and in AMD is still unclear [28]. Drusen biogenesis might cause RPE dysfunction, or RPE damage could lead to defective degradation of cellular components and consequent formation of deposits [30]. Regardless, drusen are present in AMD where RPE undergo apoptosis, contributing to photoreceptor death [31, 32].

RPE are critical to photoreceptor viability [33, 34]. The RPE create the blood-retina barrier and have multiple roles in maintaining photoreceptor health and visual function. RPE phagocytose rod outer segments, absorb of stray light, secrete trophic factors, and assist in visual cycle retinol conversion and nutrient diffusion from the choroid. Therefore, dysfunctional RPE leads to the subsequent damage and death of photoreceptors. Photoreceptor loss within the macula causes central vision impairment with disease progression expanding the extent of vision loss.

Retinitis pigmentosa (RP), Leber congenital amaurosis (LCA) and Best disease are also associated with RPE dysfunction and might benefit from novel cell replacement therapies. Current treatments, in various stages of development, involve gene therapy using associated adenoviral injections [35, 36]. Promising research using merTK gene therapy in mouse models of retinal dysfunction could lead to a novel RP treatment; merTK is a receptor located on the apical side of RPE, critical in phagocytosis of photoreceptor outer segments. RPE65 gene therapy is currently in clinical trials for LCA treatment. RPE65 is an RPE specific enzyme involved in the retinoid visual cycle, necessary for continual photoreceptor function [36]. To gain a better mechanistic understanding of these diseases, iPSC lines are being generated from patients. The

Gamm group has created several iPSC-RPE lines from Best disease patients to elucidate the normal and aberrant function and localization of Bestrophin, the protein genetically altered in this disease [37].

The Case for Cellular Therapies

Current available treatment options for dry AMD are limited. Vitamin and mineral therapy can reduce the incidence of CNV but does not seem to affect the development of GA [38]. Although cell based therapies have challenges including, cellular production and characterization, immune rejection, inflammatory response, tumor formation, and integration and survival of the transplant, the eye has many advantages that make this approach feasible. The macula averages 6mm in diameter, requiring approximately 120,000 RPE cells for complete coverage. The sub-retinal space is immune-privileged, lacking significant immune cell infiltration. Lastly, the eye is accessible, and refined surgical techniques and tools are available for efficient subretinal transplantation. In addition, good end point parameters of transplant success can be measured. Visual acuity can be determined using simple tests (EDTRS Eye Charts) as well as more complex microperimetry. Advanced imaging techniques, such as optical coherence tomography (OCT) and fundus autofluorescence (FAF) can be done to assess transplant placement, RPE integrity, photoreceptor integrity, RPE-photoreceptor integration, choroidal thickness, and complications such as retinal edema and CNV. Progress in imaging is continuing at a rapid pace, with the development of novel, non-invasive adaptive optic methods that can resolve single RPE and photoreceptor cells [39].

Proof of concept for RPE transplantation comes from studies in rodents and humans that began 20 years ago. Extensive research has been carried out using a variety of cell types, transplantation methods and tools, and retinal dysfunction models [12]. In rodents, while there is no ideal model for AMD, the Royal College of Surgeons (RCS) rat is used as a model of RPE dysfunction. It is important to note that rats do not have a macula (including a cone-rich fovea), and the RCS rat model does not recapitulate some critical aspects of human AMD (e.g., abnormalities in Bruch's membrane structure and composition). RCS rats harbor mutations in the merTK gene, which encodes a cell surface receptor required for the critical RPE process of photoreceptor outer segment phagocytosis. Without proper phagocytosis, RPE fail to maintain photoreceptor viability, causing substantial vision loss 3 months after birth. A number of cell types will rescue vision in this model. Suspensions of transformed and spontaneously derived RPE cells, h1RPE7 and ARPE19, injected into the subretinal space show improved visual performance and histology compared to sham-treated RCS rats [40-43]. Isolated fetal human neural cortical precursor (hNPCs) cells also rescue visual function after injection. These precursors migrate to the retina and form a multilayer on Bruch's membrane, increasing retinal sensitivity and function [44]. Although fibroblasts will not effectively rescue vision in the RCS rat some salutary effects are observed in animals undergoing subretinal injection without cell delivery [45]. In addition, the photoreceptor rescue effect often extends hundreds of microns beyond the border of the transplanted cells [43]. Therefore, it seems likely that secretion of trophic factors and activation of endogenous macrophages that clean up the debris zone contribute to the rescue and preservation of photoreceptors.

To date, human RPE transplantation has utilized three types of RPE: autologous, allogenic, and stem cell-derived. Autologous RPE transplantation involves excision of a patch of healthy RPE plus choroid from the ocular periphery and placement under the macula. Macular translocation, another form of autologous surgery, originally used to treat exudative AMD patients, involves retinal detachment and rotation, locating healthy RPE and Bruch's membrane under the macula. However, when macular translocation is done to treat GA, GA develops rather rapidly under the new location of the fovea for unknown reasons [46]. Fetal and cadaver RPE have been injected in suspension, small sheets, or gelatin matrices into patients with varying ocular diseases to improve visual performance [12]. There is a suggestion that better results have been obtained with patches or sheets, rather than suspensions of cells [47, 48]. The results of RPE transplantation studies in AMD patients have been variable, however, and time will tell which method proves to be superior [49]. The relatively few documented cases of visual improvement following RPE transplantation demonstrate the cellular therapy is feasible and may be a useful approach for treating selected AMD patients.

A number of important issues must be addressed for cell-based AMD therapy to be optimized, e.g., long-term cell survival (independent of immune rejection), identification of the stage(s) of the disease most appropriate for surgical intervention, and development of a safe, simple surgical technique. A critically important issue also involves identification of sources of cells for transplantation. Apart from ethical concerns, fetal RPE are not available in abundance and cannot be propagated indefinitely (abnormal morphology is evident by the fifth passage in most cases), which limits their commercial utility. The ideal cell source for therapies would have infinite

expansion properties, reproducible and well-defined differentiation capabilities, and stable cryopreservation and shipment abilities. Human pluripotent stem cells meet the starting cell material criteria for the large source of RPE needed for ocular disease cell therapy.

In this chapter, we will discuss the methods of RPE derivation from pluripotent stem cells and the various transplantation methods undergoing development as cell therapies move forward into the clinics. While many excellent reviews have been written on this topic [47, 50-52], the field is developing fast enough to warrant a new discussion.

Derivation of RPE from Pluripotent Stem Cells

There are two main types of human pluripotent stem cells: human embryonic stem cells (hESCs) and induced pluripotent stem cells (iPSCs). hESCs are harvested from the inner cell mass of a 3-5 day old fertilized embryo. hESCs can be cultured indefinitely with maintained stem cell characteristics and the potential to differentiate into all three germ layers [53]. The first five hESC lines generated in 1998 by Prof. Jamie Thomson's laboratory at the University of Wisconsin are still in use today. Theoretically these lines could be used to supply enough cells for research and treatment of all patients of any disease for which cellular therapies are developed, including AMD. iPSCs are derived from differentiated somatic cells that have been reprogrammed to revert back to a pluripotent state. This reprogramming was first accomplished using integrative viral vectors encoding specific embryonic transcription factors associated with pluripotency. The stem cell colonies that formed, like hESCs, could divide infinitely and differentiate into any cell type in the body [54, 55]. The potential advantage of

iPSCs over hESCs is that patient-specific cells could be generated that might avoid immune rejection after autologous transplantation. While initial reports suggested that autologous undifferentiated iPSCs might still be rejected [56], more recent studies have shown that differentiated cells are immune compatible [57, 58]. Improved methods for generation of iPSCs that lack integrating vectors have been discovered that utilize excisable transgenic systems, micro RNAs, modified mRNAs, and small molecules[59-63]. Thus, both iPSCs and hESCs are promising sources for future cellular therapies.

Numerous cell types have been derived from both hESCs and iPSCs including RPE. RPE differentiation from hESCs was first described in 2004 by Klimanskaya et al., and since then multiple groups have optimized the protocol for producing a pure population of hESC- and iPSC-derived RPE (hESC-RPE) (iPSC-RPE) [40, 47, 50, 64-74]. In culture, stem cells and RPE need to be grown on a substrate to support their attachment and growth. hESCs and iPSCs originally were grown on inactivated mouse or human embryonic fibroblasts; however, Matrigel, a composite of extracellular matrix proteins from a mouse sarcoma, and mouse PA6 stromal cells have also been used [53-55, 64, 75]. Endogenous RPE normally reside on an extracellular matrix layer called Bruch's membrane. In culture, a similar substrate is needed to facilitate RPE attachment, differentiation, and survival. Several substrates have been used: human Bruch's membrane explants, gelatin, laminin, vitronectin, bovine corneal endothelial cell extracellular matrix, and Matrigel. Comparisons show that Matrigel, laminin, vitronectin, and bovine corneal endothelial cell extracellular matrix lead to the purest RPE phenotype [76-78]. Ideally a xenofree (non-animal containing) protocol would be used throughout the entire differentiation process.

The Continuous Adherent Culture Method

Derivation of RPE from either pluripotent starting source can be achieved in a continuous adherent culture. Stem cells are allowed to overgrow on a feeder cell layer of mitotically inactivated mouse embryonic fibroblasts (MEF) or Matrigel. Stem cell colonies become confluent and multilayered. They lose their tight borders and begin to differentiate. At this time, the media is changed from a stem cell supporting media, to a differentiating media without basic fibroblast growth factor (bFGF) to further promote differentiation. Cultures maintained in this bFGF-free media will begin to show small spots of pigmentation after 1-8 weeks. These spots are differentiating RPE. Overtime, the pigmented spots multiply and expand within the culture. Although there are other differentiated cell types in the cultures, the spontaneously derived RPE are easy to distinguish because of their pigment granules, a major advantage in hESC/iPSC-RPE differentiation. When the pigmented RPE spots become frequent and large, they can be mechanically dissected and passaged [40, 65-67, 73, 79, 80]. The excised cells are grown to a monolayer and exhibit the RPE-distinctive cobblestone morphology and pigmentation patterns (Figure 1). The downside of this RPE enrichment method is that the manual isolation technique is difficult to fit within the Good Manufacturing Practice (GMP) production guidelines. This limitation could prevent advancing hESC/iPSC-RPE cellular therapies into human clinical trials. Therefore, enzymatic techniques are under investigation to separate RPE from other differentiated cell types [80].

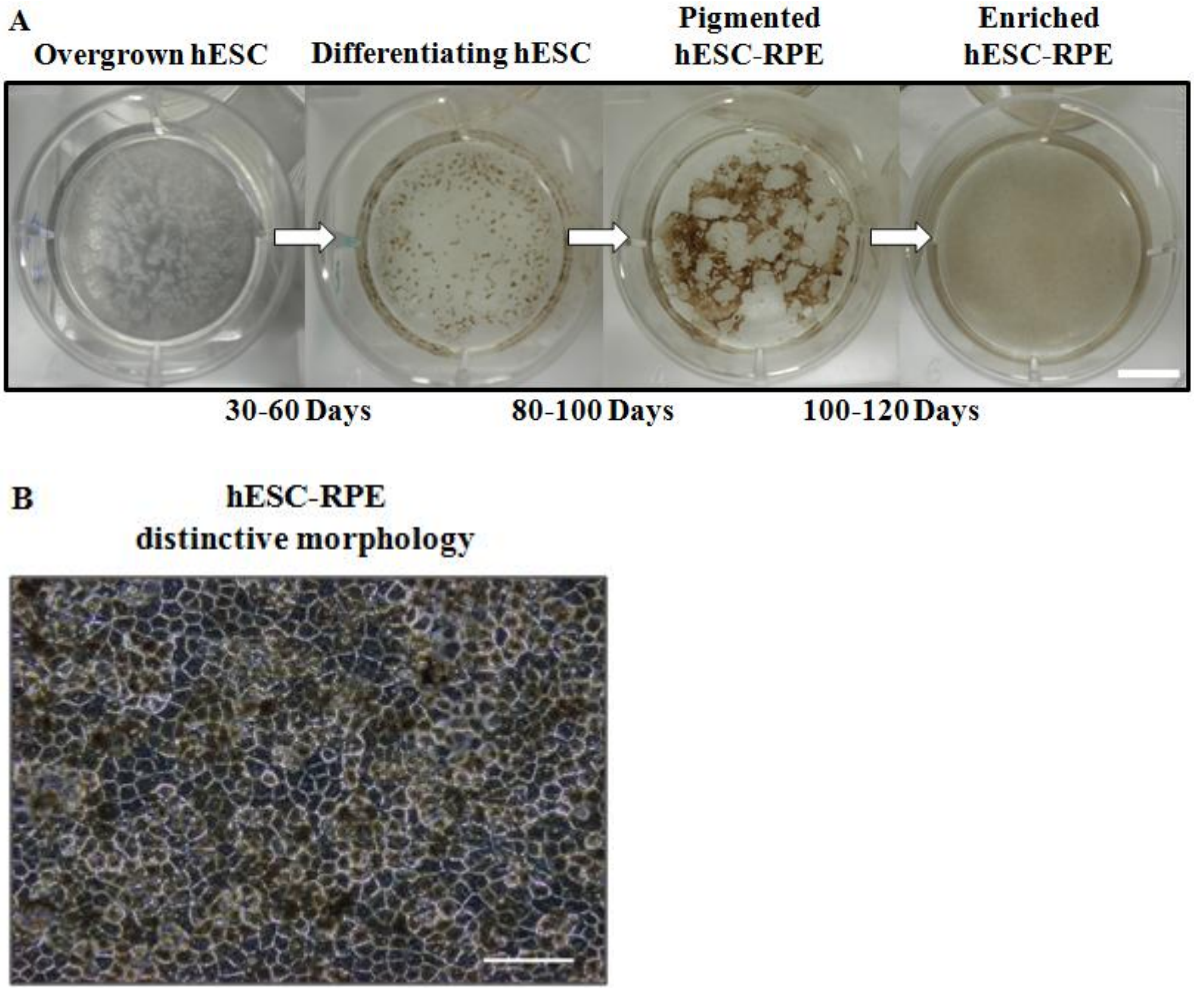

Figure 1. Depiction of spontaneous retinal pigmented epithelium (RPE) differentiation from human embryonic stem cells (hESCs) using a continuous adherent culture method. (A) From left to right, overgrown hESCs through the spontaneous differentiation process. Pigmented colonies are manually excised after 100 days in culture and re-plated to yield a mostly homologous population of RPE cells. (B) Enriched RPE exhibit typical cobblestone cuboidal morphology and pigmentation. Scale bar (A) 10mm. Scale bar (B) 100μm.

After the pigmented RPE are enriched and plated, quality control must be performed to ensure these derived cells express similar gene expression patterns and function as endogenous RPE. Assays to establish RPE identity and potency must be created. Quantitative real-time PCR (QRT-PCR) can be done to compare transcript levels of hESC and iPSC-RPE to human RPE. A number of RPE genes (e.g., RPE specific transcription factors, microphthalmia-associated transcription factor (MITF) and orthodenticle 2 isoform b homeobox protein (OTX2); visual cycle proteins, cellular retinaldehyde-binding protein (CRALBP) and retinal pigmented epithelium protein 65kDa (RPE65); secreted factors, pigment epithelium-derived factor (PEDF); tight junction marker, zona occludens 1 (ZO-1); and phagocytosis component, mer tyrosine kinase (MERTK)) are analyzed by QRT-PCR to ensure mRNA levels coincide with human fetal RPE (fRPE) [40, 65-67, 73, 79]. Current data suggest some differences between fRPE, the benchmark comparison. Overall, bioinformatics analyses show that hESC-RPE are very similar to fRPE but may correspond to a less mature RPE state [73]. RPE65, a mature RPE marker, appears to increase with culture of hESC-RPE, and could also be used as a biomarker to determine RPE identity. It is interesting to note that fRPE share a much more similar gene profile with hESC-RPE than iPSC-RPE [73]. In addition, hESC-RPE and fRPE show equivalent low levels of genes associated with aging, energy metabolism, and the complement system, all factors associated with AMD pathophysiology [73] (Hikita et al. unpublished).

Stem cell-derived RPE must also be tested to ensure these cells carry out critical physiological processes. As described previously, RPE are responsible for phagocytosing photoreceptor outer segments to maintain photoreceptor homeostasis.

Phagocytosis can be tested using an assay in which fluorescently labeled outer segments are incubated with cultured RPE, and the amount of internalized segments is quantified. hESC-RPE and several iPSC-RPE lines have phagocytic abilities comparable to fRPE [66, 67, 73, 76, 79]. Several studies have implanted both types of stem cell-derived RPE into rodent models of retinal dysfunction and shown improved visual performance [40, 65, 68, 81]. In addition, subretinally injected iPSC-RPE enhanced visual acuity in a model of RP with no tumor formation [82]. Currently, all clinical trials involving hESC-RPE require immunosuppression, which could potentially be avoided if a well-defined, rapidly developed iPSC-RPE line could be generated. One example of such an approach, uses only Oct4 to reprogram into iPSCs in combination with small molecules [83]. These lines have been derived into RPE and hold great potential for clinical application of autologous RPE grafts.

The Embryoid Body Approach

hESCs and iPSCs can also be differentiated into RPE using a second strategy called the embryoid body approach. Although this method may not be as efficient as the continuous adherent approach, it still yields viable RPE and is a spontaneous differentiation protocol [65]. To apply this method, stem cells are grown on feeder cells or substrate until 50-75% confluent. Colonies are dissociated using an enzyme, such as collagenase, and sectioned into pieces. The pieces are plated in a serum- and bFGF-free differentiation media on plates coated with a neutrally charged hydrophilic hydrogel to diminish attachment. The cells will form spherical aggregates called embryoid bodies (EBs). These bodies can differentiate into all three germ layers and show pigmentation. Twenty days following EB formation, the aggregates are passed onto a coated plate,

allowing for cell attachment. Within 24 hours cells will attach and begin to spread. Over time, distinct RPE sheets will form. These RPE colonies can be excised manually and passaged onto another coated dish, creating a mostly homogenous RPE cell population [68, 69, 72, 79, 84]. Gene expression profiles of resultant hESC -RPE cells show patterns similar to fRPE, with robust expression of RPE specific genes: MITF, OTX2, CRALBP, RPE65, PEDF, ZO-1, MERTK [68, 69, 72, 74, 84]. In addition, these cells can phagocytose outer segments and rescue visual performance in rodent models of retinal dysfunction [68, 72, 79, 84]. This desired phenotype can also be achieved deriving RPE from iPSCs [69, 71, 85-87].

Directed Differentiation

Spontaneous differentiation of RPE is time consuming and efficiency varies between cell lines. Therefore, a number of groups have focused on improved protocols to speed up this process. The strategy is to mimic normal human RPE development by adding small molecules to initiate signaling cascades at the correct time to promote retinal cell fate in vitro [69-71, 84]. These efforts have not only focused on hESC and iPSC differentiation into RPE, but also on a range of retinal cell types [88]. RPE are ectoderm and originate from the anterior neural plate neuroepithelium during optic cup development. A range of signaling cascades including the transforming growth factor-beta (TGFβ) superfamily, Wingless-related integration site (Wnt), and fibroblast growth factor (FGF) pathways are involved in RPE specification [33, 89]. Stem cells must first be directed towards a retinal progenitor fate before terminal RPE differentiation. Several groups have directed differentiation by using Wnt and NODAL inhibitors, Dkk-1 and Lefty-A, to induce a neural fate [70, 71, 74, 84]. Further neural and

retinal induction has been obtained utilizing supplements, N2 or B27 and heparin. Following differentiation into retinal progenitors, RPE can be specified by epithelial driving factors. Activin A, BMP4, Wnt3A and an FGF inhibitor (SU5402) stimulate RPE derivation from neural retinal progenitors [69]. A class B vitamin, nicotinamide, also promotes RPE differentiation, and this effect is enhanced when added in combination with Activin A [72]. Appropriate timing and duration of each molecule is critical to yield pigmented, functional RPE. In 2012, Zahabi et al. reduced the time from beginning human iPSC differentiation to enrichment to 40 days using basic FGF (bFGF), TGFβ receptor inhibitor (SB431542), noggin, retinoic acid (RA), and sonic hedgehog (shh) throughout their protocol [90]. A new method of deriving RPE from pluripotent stem cells was published by the Tanaka group in January, 2013. They described the formation of epithelial cysts, mimicking neural tube morphology, arising 5 days after pluripotent cells are embedded in Matrigel. The cysts are extracted, re-plated onto Matrigel-coated wells using an RPE supporting media with supplemental factors, and develop into RPE within 30 days. These RPE become pigmented, express RPE65 and BEST1, show appropriate transepithelial resistance levels, and phagocytose rod outer segments. In addition, following transplantation into the RCS rat, they increase the thickness of the outer nuclear layer within the retina [91]. Recently an improved protocol of directed differentiation from hESCs to RPE has been achieved, producing enrichable RPE sheets within only 14 days [75]. This protocol has been refined further through the use of CHIR99021, leading to a further increase in RPE derivation efficiency [92] (See Figure 2 for a comparison of all differentiation methods.)

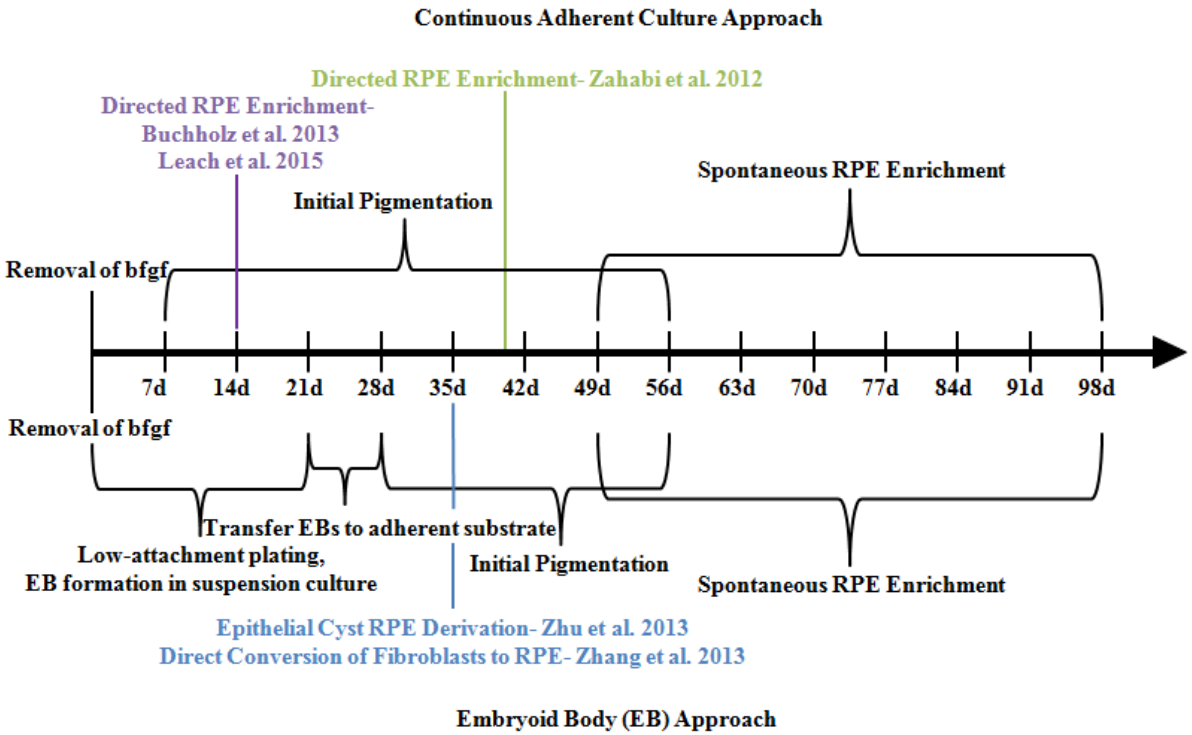

Figure 2. Time course comparison of the continuous adherent culture and embryoid body culture methods of spontaneous derivation of RPE from pluripotent stem cells. Colored lines indicate time to enrichment for other RPE differentiation methods.

Other sources of RPE

While pluripotent stem cells are the best source of RPE, other stem cell types are under investigation. Both rat neural stem cells, harvested from the cerebral cortex, and mesenchymal stromal cells (MSC), isolated from human lipo-aspirate, were reported to yield cells with some RPE characteristics using the same differentiation strategy [93, 94]. Co-cultures with rat RPE, or conditioned media from human RPE, in combination with vaso-intestinal peptide (VIP) produced cells with some morphological features of RPE [93, 94]. The MSC-derived RPE were further characterized and showed some induction of BEST1 and RPE65, mature human RPE markers [94]. However, the levels of expression were not compared to fRPE, so it is difficult to be sure how RPE-like these cells are. Another group used bone marrow-derived mesenchymal stem cells cultured with human RPE-conditioned media and photoreceptor outer segments to generate RPE that express RPE65 and phagocytose porcine rod outer segments [95]. Another potential alternate source of RPE is retinal stem cells (RSCs) from the ciliary margin. Coles et al. reported that there are 10,000 multipotent RSCs in each eye that can yield all retinal cell types, including RPE [96]. After transplantation of RSCs into mice, the cells survived, integrated, and differentiated into the retina. However, a subsequent study questioned whether these were actually RSCs [97]. It is unclear if these cells can be expanded into a pure RPE population, and more characterization is needed. During development, RPE are plastic cells, and some groups have harnessed this potential in mature RPE, claiming RPE can dedifferentiate into a multipotent stem cell which can then take on other cell phenotypes [98].

A direct conversion of human fibroblasts to RPE-like cells has also been achieved through over expression of key RPE transcription factors and additional supplements. This protocol yields cells expressing some mature RPE markers within 35 days. The function of these RPE-like cells, however, has not yet been reported [99].

iPSC or hESC-derived RPE?

An unanswered question remains: which starting source, hESCs or iPSCs is better for clinical use? A potential drawback to the iPSCs having the same genetic makeup and immunocompatibility as the patient is that they carry the same inherited defects predisposing to the disease. Another caveat is that these cells show increased mutations, copy number variations, and abnormal methylation patterns when compared to hESCs, which could hinder their therapeutic value [86, 100-104]. hESC-RPE are a younger cell type and are not manipulated by viruses or small molecules. Although, allogeneic hESC-RPE can be free of disease-associated mutations, they might be rejected by the immune system. The subretinal space is an immune privileged sight, but this privilege is relative and not absolute. Moreover, patients may have a compromised blood-brain barrier, which could allow a larger than normal immune response within the eye. A benefit of hESC-RPE is they can be ready for transplantation immediately following diagnosis in appropriately selected patients. Currently, patient-specific iPSC-RPE would be extremely time consuming to produce and characterize before transplantation. In patients with rapidly progressing disease, this delay in treatment might result in significant loss of vision. Finally, generation of autologous cells would be costly and require a nine month tumorigenicity study under current FDA policies. However banks of HLA-matched iPSCs might overcome this problem.

iPSC-RPE also show memory of their previous terminal fate and show differences in gene profiles from fRPE [105]. These differences, however, vary from cell line to cell line, and with new non-integrative systems, iPSC-RPE appear to be more similar to fRPE [55, 73, 83]. There is great variability between cell lines for both hESC- and iPSC-derived RPE, which has yet to fully be explained and could lead to clinical complications for either source [69, 85, 106, 107]. More hESC-RPE and iPSC-RPE research is needed to elucidate the optimal starting cell material. Therapies moving forward with either cell line must take precautions to ensure reliable and fully characterized cells are manufactured for transplantation.

Transplantation Strategies

In addition to the debate over whether to use hESCs or iPSCs to derive RPE for transplantation, there is also a question about how to deliver the cells. Grafted cells must integrate and function properly with the existing retina to prevent further photoreceptor damage and decrease progression of disease. Two main techniques are being studied currently. The first technique administers a bolus injection of dissociated RPE into the subretinal space. Both hESC-RPE and iPSC-RPE have been delivered with this approach, and both showed photoreceptor rescue and preserved vision in rodent models of retinal dysfunction [40, 65, 72, 81]. An important study in 2009 showed some transplanted cells, in two distinct rat models of ocular disease, survived the duration of the 220 day experiment with no teratoma formation [68]. This study is crucial in proof of principle that cells implanted into the eye can possess the longevity needed to slow disease progression without tumor formation [68]. However, efficiency of cell survival and integration are still in question. Some reports have concluded that the majority of

injected cells form aggregates in the subretinal space, do not integrate into the RPE monolayer, and are unaccounted for after a period of time. Importantly, only a subset of injected dissociated cells possesses the ability to phagocytose rod outer segments [81]. These results are not surprising. It is known that epithelial cells, like RPE, need to maintain contact with a basement membrane to function properly and remain viable [12]. Cells in suspension undergo 'anoikis,' a term coined by Ruoslahti to describe cells that undergo apoptosis after being displaced from their anchor of extracellular matrix proteins [108]. Bruch's membrane has specific extracellular matrix proteins that are required for RPE adhesion, survival and function [34]. It is also crucial that RPE cells form tight junctions to fulfill their necessary barrier functions.

The above considerations suggest a second strategy for RPE transplantation: grow RPE on a scaffold substrate that mimics the support of the Bruch's membrane and allows the RPE to be transplanted as a fully differentiated, polarized monolayer. The idea behind the scaffold technique is that RPE cells will survive longer and remain located over the diseased retinal area, leading to greater functionality and improved visual performance. In addition, RPE grown on substrates can polarize and be implanted in the correct orientation with their apical microvilli facing the photoreceptor outer segments [109]. In AMD, Bruch's membrane deteriorates along with the RPE, therefore transplanting healthy RPE on a biomimetic scaffold could improve the functionality and long-term survival of the RPE transplant [110].

A variety of scaffolds have been investigated. Natural biomaterial scaffolds include: human amniotic membranes (hAM) [111-115], human lens capsule [116, 117], and explants of Bruch's membrane [118, 119]. Using these unaltered natural tissue

supports could lead to issues with disease transmission from host and would be difficult to conform to FDA guidelines for transplantation production [120]. Natural polymers could be more advantageous and are currently being purified and used to grow hESC-RPE and iPSC-RPE. Extracellular matrix (ECM) proteins secreted from RPE [121] and corneal endothelial cells [121, 122], isolated gelatins and collagens [118, 121, 123-126], alginates [109], hyaluronic acid [109], fibrinogens [127], vitronectin [118, 119], laminins [118, 119, 122], and fibronectins [119, 122] all can support RPE growth. In addition to human purified proteins, a combination of ECM proteins derived from the mouse Englebreth-Holm-Swarm tumor called Matrigel is also efficient for culturing RPE [125]. The caveats to using ECM proteins are the lot-to-lot variation in composition and the difficulties to regulate production using GMP due to the animal source of the substrate.

Search for a synthetic polymer to support RPE growth and maturation has yielded several promising candidates. These compounds can be manufactured with knowledge of specific composition, are tailored to optimize RPE growth, and can be mass produced. In addition, adhesive peptides and growth factors can be embedded within the polymers to promote attachment and survival. Materials are non-immunogenic and can be biodegradable or biostable supports. Parylene, poly (lactic-co-glycolic acid) (PGLA), poly (L-lactic acid) (PLLA), polycaprolactone (PCL), poly (glycerol sebacate) (PGS), and polyhydroxyalkanoates (PHAs) are among those that have been investigated [109]. The polymers that successfully allowed culturing of RPE include: PLGA [128-132], PLLA [128, 132, 133], a polyethylene glycol (PEG)-PLLA [130], polydimenthylsiloxane (PDMS) [134], poly (hydroxybutyrate-cohydroxyvalerate) (PHB-

co-PHV) [135], polyether urethanes [136, 137], and parylene [138]. Parylene is already approved for use in the eye, and it can be micromachined to include ultrathin areas that mimic the permeability of Bruch's membrane. Hydrogels composed of methacrylate and (meth) acrylamide also promote RPE growth [115]. Current research is making progress toward completely xeno-free derivation of RPE from hESC and iPSC, and discovering the optimal synthetic scaffold would allow the entire process from differentiation to transplantation to be xeno-free. This approach provides benefits when creating GMP protocols and potentially eliminates complications from using animal products within the transplant [85, 139].

Clinical Trial Progression

Many groups are well on their way to bringing pluripotent stem cell-derived RPE cells to the clinic for treating ocular diseases like AMD. The first clinical trial was granted approval after long-term safety experiments and proof of concept were documented in rodents. Clinical trials began with two patients, one with Stargardt macular dystrophy and one with AMD. A bolus injection of dissociated hESC-RPE cells was administered into one eye of human patients. A preliminary report was published four months post transplantation [140]. Improved visual performance in the Stargardt disease patient was documented in the surgical eye only, but there is some controversy regarding this result [141]. The AMD patient showed improvement in the uninjected eye as well as in the injected eye, even though the immunosuppressive regimen was not followed. Perhaps the most important result from this preliminary study is that patients presented no loss of vision or formation of ocular tumors. The next round of patients enrolled in the study will receive a greater number of hESC-RPE cells with the intent of

increasing integration and efficiency [140]. Trials for wet and dry AMD using monolayers of hESC-RPE on scaffolds are soon to begin in London and California, and a trial using autologous iPSC-RPE has been approved in Japan. Other trials for AMD using non-RPE cells (neural stem cells and cord blood) have also been initiated. Because the eye has many advantages for developing cellular therapies, a number of groups have seized upon the opportunity. It seems likely, based on proof of concept studies in both rodent and human, that these trials have tremendous potential for the treatment of AMD as well as other ocular diseases.

This chapter published as Croze et. al (2014) in *Developmental Ophthalmology*, has outlined the ocular diseases and cell type of interest in the Clegg lab and the work being performed throughout the research community to create effective novel therapeutics to treat those affected by vision loss. The second chapter will compare several iPSC-RPE lines and two different methods of RPE differentiation to show the variability and caution that must be taken when choosing iPSC-RPE lines to use in the clinic. The third chapter, published as Croze et. al 2014 in *Stem Cells Translational Medicine*, and fourth chapter will examine the effects of Rho-associated coiled-coil kinase (ROCK) inhibition on various behaviors of hESC-RPE and iPSC-RPE including: passage length, proliferation, EMT, wound healing and attachment. Lastly, Chapter 5 will describe molecular tools that have been created in order to gain valuable insight into how RPE behave after transplantation in a rat model of retinal dysfunction, in real time.

References

1. Gehrs, K.M., et al., *Age-related macular degeneration--emerging pathogenetic and therapeutic concepts.* Ann Med, 2006. **38**(7): p. 450-71.
2. Klein, R., et al., *Prevalence of age-related macular degeneration in the US population.* Arch Ophthalmol, 2011. **129**(1): p. 75-80.
3. Ferris, F.L., 3rd, et al., *Clinical classification of age-related macular degeneration.* Ophthalmology, 2013. **120**(4): p. 844-51.
4. Klein, R., et al., *Fifteen-year cumulative incidence of age-related macular degeneration: the Beaver Dam Eye Study.* Ophthalmology, 2007. **114**(2): p. 253-62.
5. Cho, H., et al., *Aflibercept for exudative AMD with persistent fluid on ranibizumab and/or bevacizumab.* Br J Ophthalmol, 2013. **97**(8): p. 1032-1035.
6. Bakall, B., et al., *Aflibercept Therapy for Exudative Age-related Macular Degeneration Resistant to Bevacizumab and Ranibizumab.* Am J Ophthalmol, 2013. **156**(1): p. 15-22 e1.
7. Kaiser, P.K., *Emerging therapies for neovascular age-related macular degeneration: drugs in the pipeline.* Ophthalmology, 2013. **120**(5 Suppl): p. S11-5.
8. Curcio, C.A., N.E. Medeiros, and C.L. Millican, *Photoreceptor loss in age-related macular degeneration.* Invest Ophthalmol Vis Sci, 1996. **37**(7): p. 1236-49.
9. Young, R.W., *Pathophysiology of age-related macular degeneration.* Surv Ophthalmol, 1987. **31**(5): p. 291-306.
10. Buschini, E., et al., *Age related macular degeneration and drusen: neuroinflammation in the retina.* Prog Neurobiol, 2011. **95**(1): p. 14-25.
11. Damico, F.M., et al., *New approaches and potential treatments for dry age-related macular degeneration.* Arq Bras Oftalmol, 2012. **75**(1): p. 71-6.
12. da Cruz, L., et al., *RPE transplantation and its role in retinal disease.* Prog Retin Eye Res, 2007. **26**(6): p. 598-635.
13. Leveziel, N., et al., *Genetic factors associated with age-related macular degeneration.* Ophthalmologica, 2011. **226**(3): p. 87-102.
14. Melville, H., et al., *Stem cells: a new paradigm for disease modeling and developing therapies for age-related macular degeneration.* J Transl Med, 2013. **11**(1): p. 53.
15. Haines, J.L., et al., *Complement factor H variant increases the risk of age-related macular degeneration.* Science, 2005. **308**(5720): p. 419-21.
16. Gold, B., et al., *Variation in factor B (BF) and complement component 2 (C2) genes is associated with age-related macular degeneration.* Nat Genet, 2006. **38**(4): p. 458-62.
17. Spencer, K.L., et al., *Protective effect of complement factor B and complement component 2 variants in age-related macular degeneration.* Hum Mol Genet, 2007. **16**(16): p. 1986-92.
18. Jakobsdottir, J., et al., *C2 and CFB genes in age-related maculopathy and joint action with CFH and LOC387715 genes.* PLoS One, 2008. **3**(5): p. e2199.
19. Maller, J.B., et al., *Variation in complement factor 3 is associated with risk of age-related macular degeneration.* Nat Genet, 2007. **39**(10): p. 1200-1.
20. Yates, J.R., et al., *Complement C3 variant and the risk of age-related macular degeneration.* N Engl J Med, 2007. **357**(6): p. 553-61.

21. Edwards, A.O., et al., *Complement factor H polymorphism and age-related macular degeneration.* Science, 2005. **308**(5720): p. 421-4.
22. Baird, P.N., et al., *The epsilon2 and epsilon4 alleles of the apolipoprotein gene are associated with age-related macular degeneration.* Invest Ophthalmol Vis Sci, 2004. **45**(5): p. 1311-5.
23. Chen, W., et al., *Genetic variants near TIMP3 and high-density lipoprotein-associated loci influence susceptibility to age-related macular degeneration.* Proc Natl Acad Sci U S A, 2010. **107**(16): p. 7401-6.
24. Haines, J.L., et al., *Functional candidate genes in age-related macular degeneration: significant association with VEGF, VLDLR, and LRP6.* Invest Ophthalmol Vis Sci, 2006. **47**(1): p. 329-35.
25. Dewan, A., et al., *HTRA1 promoter polymorphism in wet age-related macular degeneration.* Science, 2006. **314**(5801): p. 989-92.
26. Cideciyan, A.V., et al., *Mutations in ABCA4 result in accumulation of lipofuscin before slowing of the retinoid cycle: a reappraisal of the human disease sequence.* Hum Mol Genet, 2004. **13**(5): p. 525-34.
27. Allikmets, R., et al., *Mutation of the Stargardt disease gene (ABCR) in age-related macular degeneration.* Science, 1997. **277**(5333): p. 1805-7.
28. Hageman, G.S., et al., *An integrated hypothesis that considers drusen as biomarkers of immune-mediated processes at the RPE-Bruch's membrane interface in aging and age-related macular degeneration.* Prog Retin Eye Res, 2001. **20**(6): p. 705-32.
29. Curcio, C.A., et al., *Subretinal drusenoid deposits in non-neovascular age-related macular degeneration: morphology, prevalence, topography, and biogenesis model.* Retina, 2013. **33**(2): p. 265-76.
30. Leu, S.T., et al., *Drusen are Cold Spots for Proteolysis: Expression of Matrix Metalloproteinases and Their Tissue Inhibitor Proteins in Age-related Macular Degeneration.* Exp Eye Res, 2002. **74**(1): p. 141-54.
31. Del Priore, L.V., Y.H. Kuo, and T.H. Tezel, *Age-related changes in human RPE cell density and apoptosis proportion in situ.* Invest Ophthalmol Vis Sci, 2002. **43**(10): p. 3312-8.
32. Dunaief, J.L., et al., *The role of apoptosis in age-related macular degeneration.* Arch Ophthalmol, 2002. **120**(11): p. 1435-42.
33. Bharti, K., et al., *The other pigment cell: specification and development of the pigmented epithelium of the vertebrate eye.* Pigment Cell Res, 2006. **19**(5): p. 380-94.
34. Strauss, O., *The retinal pigment epithelium in visual function.* Physiol Rev, 2005. **85**(3): p. 845-81.
35. Deng, W.T., et al., *Tyrosine-mutant AAV8 delivery of human MERTK provides long-term retinal preservation in RCS rats.* Invest Ophthalmol Vis Sci, 2012. **53**(4): p. 1895-904.
36. Hufnagel, R.B., et al., *Gene therapy for Leber congenital amaurosis: advances and future directions.* Graefes Arch Clin Exp Ophthalmol, 2012. **250**(8): p. 1117-28.
37. Singh, R., et al., *iPS cell modeling of Best disease: insights into the pathophysiology of an inherited macular degeneration.* Hum Mol Genet, 2013. **22**(3): p. 593-607.

38. Group, A.R., *Lutein/Zeaxanthin and Omega-3 Fatty Acids for Age-Related Macular Degeneration. The Age-Related Eye Disease Study 2 (AREDS2) Controlled Randomized Clinical Trial*, 2013, JAMA: National Institute of Health.
39. Morgan, J.I., et al., *Light-induced retinal changes observed with high-resolution autofluorescence imaging of the retinal pigment epithelium.* Invest Ophthalmol Vis Sci, 2008. **49**(8): p. 3715-29.
40. Lund, R.D., et al., *Human embryonic stem cell-derived cells rescue visual function in dystrophic RCS rats.* Cloning Stem Cells, 2006. **8**(3): p. 189-99.
41. Coffey, P.J., et al., *Long-term preservation of cortically dependent visual function in RCS rats by transplantation.* Nat Neurosci, 2002. **5**(1): p. 53-6.
42. Wang, S., et al., *Morphological and functional rescue in RCS rats after RPE cell line transplantation at a later stage of degeneration.* Invest Ophthalmol Vis Sci, 2008. **49**(1): p. 416-21.
43. Lund, R.D., et al., *Subretinal transplantation of genetically modified human cell lines attenuates loss of visual function in dystrophic rats.* Proc Natl Acad Sci U S A, 2001. **98**(17): p. 9942-7.
44. Wang, S., et al., *Long-term vision rescue by human neural progenitors in a rat model of photoreceptor degeneration.* Invest Ophthalmol Vis Sci, 2008. **49**(7): p. 3201-6.
45. Sauve, Y., et al., *Preservation of visual responsiveness in the superior colliculus of RCS rats after retinal pigment epithelium cell transplantation.* Neuroscience, 2002. **114**(2): p. 389-401.
46. Cahill, M.T., et al., *Recurrence of retinal pigment epithelial changes after macular translocation with 360 degrees peripheral retinectomy for geographic atrophy.* Arch Ophthalmol, 2005. **123**(7): p. 935-8.
47. Rowland, T.J., D.E. Buchholz, and D.O. Clegg, *Pluripotent human stem cells for the treatment of retinal disease.* J Cell Physiol, 2012. **227**(2): p. 457-66.
48. Binder, S., et al., *Transplantation of the RPE in AMD.* Prog Retin Eye Res, 2007. **26**(5): p. 516-54.
49. Gullapalli VK KM, W.H., Sugino IK, Madreperla S, Zarbin MA, *Transplantation Frontiers*. 2013, Retina: Elsevier. 2058-2077.
50. Bharti, K., S.S. Miller, and H. Arnheiter, *The new paradigm: retinal pigment epithelium cells generated from embryonic or induced pluripotent stem cells.* Pigment Cell Melanoma Res, 2011. **24**(1): p. 21-34.
51. Stern, J.H. and S. Temple, *Stem cells for retinal replacement therapy.* Neurotherapeutics, 2011. **8**(4): p. 736-43.
52. John Sudhakar, S.N., Periyasamy Parikumar, Mahesh Shanmugam, Rajappa Senthikumar, David William Green, Samuel J.K. Abraham *Choice of Cell Source in Cell-Based Therapies for Retinal Damage due to Age-Related Macular Degeneration: A Review.* Journal of Ophthalmology, 2013. **2013**: p. 1-9.
53. Thomson, J.A., et al., *Embryonic stem cell lines derived from human blastocysts.* Science, 1998. **282**(5391): p. 1145-7.
54. Takahashi, K., et al., *Induction of pluripotent stem cells from adult human fibroblasts by defined factors.* Cell, 2007. **131**(5): p. 861-72.
55. Yu, J., et al., *Induced pluripotent stem cell lines derived from human somatic cells.* Science, 2007. **318**(5858): p. 1917-20.

56. Zhao, T., et al., *Immunogenicity of induced pluripotent stem cells.* Nature, 2011. **474**(7350): p. 212-5.
57. Guha, P., et al., *Lack of immune response to differentiated cells derived from syngeneic induced pluripotent stem cells.* Cell Stem Cell, 2013. **12**(4): p. 407-12.
58. Boyd, A.S., et al., *Concise review: Immune recognition of induced pluripotent stem cells.* Stem Cells, 2012. **30**(5): p. 797-803.
59. Stadtfeld, M., et al., *Induced pluripotent stem cells generated without viral integration.* Science, 2008. **322**(5903): p. 945-9.
60. Yu, J., et al., *Human induced pluripotent stem cells free of vector and transgene sequences.* Science, 2009. **324**(5928): p. 797-801.
61. Narsinh, K.H., et al., *Generation of adult human induced pluripotent stem cells using nonviral minicircle DNA vectors.* Nat Protoc, 2011. **6**(1): p. 78-88.
62. Solanki, A. and K.B. Lee, *A step closer to complete chemical reprogramming for generating iPS cells.* Chembiochem, 2010. **11**(6): p. 755-7.
63. Yu, J., et al., *Efficient feeder-free episomal reprogramming with small molecules.* PLoS One, 2011. **6**(3): p. e17557.
64. Gong, J., et al., *Effects of extracellular matrix and neighboring cells on induction of human embryonic stem cells into retinal or retinal pigment epithelial progenitors.* Exp Eye Res, 2008. **86**(6): p. 957-65.
65. Vugler, A., et al., *Elucidating the phenomenon of HESC-derived RPE: anatomy of cell genesis, expansion and retinal transplantation.* Exp Neurol, 2008. **214**(2): p. 347-61.
66. Buchholz, D.E., et al., *Derivation of functional retinal pigmented epithelium from induced pluripotent stem cells.* Stem Cells, 2009. **27**(10): p. 2427-34.
67. Carr, A.J., et al., *Molecular characterization and functional analysis of phagocytosis by human embryonic stem cell-derived RPE cells using a novel human retinal assay.* Mol Vis, 2009. **15**: p. 283-95.
68. Lu, B., et al., *Long-term safety and function of RPE from human embryonic stem cells in preclinical models of macular degeneration.* Stem Cells, 2009. **27**(9): p. 2126-35.
69. Meyer, J.S., et al., *Modeling early retinal development with human embryonic and induced pluripotent stem cells.* Proc Natl Acad Sci U S A, 2009. **106**(39): p. 16698-703.
70. Osakada, F., et al., *Stepwise differentiation of pluripotent stem cells into retinal cells.* Nat Protoc, 2009. **4**(6): p. 811-24.
71. Osakada, F., et al., *In vitro differentiation of retinal cells from human pluripotent stem cells by small-molecule induction.* J Cell Sci, 2009. **122**(Pt 17): p. 3169-79.
72. Idelson, M., et al., *Directed differentiation of human embryonic stem cells into functional retinal pigment epithelium cells.* Cell Stem Cell, 2009. **5**(4): p. 396-408.
73. Liao, J.L., et al., *Molecular signature of primary retinal pigment epithelium and stem-cell-derived RPE cells.* Hum Mol Genet, 2010. **19**(21): p. 4229-38.
74. Nistor, G., et al., *Three-dimensional early retinal progenitor 3D tissue constructs derived from human embryonic stem cells.* J Neurosci Methods, 2010. **190**(1): p. 63-70.

75. Buchholz DE, P.B., Croze RH, Himan CR, Coffey PJ, Clegg DO, *Rapid and Efficient Directed Differentiation of Human Pluripotent Stem Cells Into Retinal Pigmented Epithelium.* Stem Cells Transl Med, 2013. **2**: p. Ahead of Print.
76. Rowland, T.J., et al., *Differentiation of human pluripotent stem cells to retinal pigmented epithelium in defined conditions using purified extracellular matrix proteins.* J Tissue Eng Regen Med, 2012.
77. Song, M.K. and G.M. Lui, *Propagation of fetal human RPE cells: preservation of original culture morphology after serial passage.* J Cell Physiol, 1990. **143**(1): p. 196-203.
78. Campochiaro, P.A. and S.F. Hackett, *Corneal endothelial cell matrix promotes expression of differentiated features of retinal pigmented epithelial cells: implication of laminin and basic fibroblast growth factor as active components.* Exp Eye Res, 1993. **57**(5): p. 539-47.
79. Klimanskaya, I., et al., *Derivation and comparative assessment of retinal pigment epithelium from human embryonic stem cells using transcriptomics.* Cloning Stem Cells, 2004. **6**(3): p. 217-45.
80. Maruotti, J., et al., *A simple and scalable process for the differentiation of retinal pigment epithelium from human pluripotent stem cells.* Stem Cells Transl Med, 2013. **2**(5): p. 341-54.
81. Carr, A.J., et al., *Protective effects of human iPS-derived retinal pigment epithelium cell transplantation in the retinal dystrophic rat.* PLoS One, 2009. **4**(12): p. e8152.
82. Li, Y., et al., *Long-term safety and efficacy of human-induced pluripotent stem cell (iPS) grafts in a preclinical model of retinitis pigmentosa.* Mol Med, 2012. **18**: p. 1312-9.
83. Ukrohne, T.U., et al., *Generation of retinal pigment epithelial cells from small molecules and OCT4 reprogrammed human induced pluripotent stem cells.* Stem Cells Transl Med, 2012. **1**(2): p. 96-109.
84. Osakada, F., et al., *Toward the generation of rod and cone photoreceptors from mouse, monkey and human embryonic stem cells.* Nat Biotechnol, 2008. **26**(2): p. 215-24.
85. Hirami, Y., et al., *Generation of retinal cells from mouse and human induced pluripotent stem cells.* Neurosci Lett, 2009. **458**(3): p. 126-31.
86. Feng, Q., et al., *Hemangioblastic derivatives from human induced pluripotent stem cells exhibit limited expansion and early senescence.* Stem Cells, 2010. **28**(4): p. 704-12.
87. Mekala, S.R., et al., *Derivation, characterization and retinal differentiation of induced pluripotent stem cells.* J Biosci, 2013. **38**(1): p. 123-34.
88. Williams, L.A., B.N. Davis-Dusenbery, and K.C. Eggan, *SnapShot: directed differentiation of pluripotent stem cells.* Cell, 2012. **149**(5): p. 1174-1174 e1.
89. Munoz-Sanjuan, I. and A.H. Brivanlou, *Neural induction, the default model and embryonic stem cells.* Nat Rev Neurosci, 2002. **3**(4): p. 271-80.
90. Zahabi, A., et al., *A new efficient protocol for directed differentiation of retinal pigmented epithelial cells from normal and retinal disease induced pluripotent stem cells.* Stem Cells Dev, 2012. **21**(12): p. 2262-72.

91. Zhu, Y., et al., *Three-dimensional neuroepithelial culture from human embryonic stem cells and its use for quantitative conversion to retinal pigment epithelium.* PLoS One, 2013. **8**(1): p. e54552.
92. Leach, L.L., et al., *Canonical/beta-catenin Wnt pathway activation improves retinal pigmented epithelium derivation from human embryonic stem cells.* Invest Ophthalmol Vis Sci, 2015. **56**(2): p. 1002-13.
93. Enzmann, V., et al., *Enhanced induction of RPE lineage markers in pluripotent neural stem cells engrafted into the adult rat subretinal space.* Invest Ophthalmol Vis Sci, 2003. **44**(12): p. 5417-22.
94. Vossmerbaeumer, U., et al., *Retinal pigment epithelial phenotype induced in human adipose tissue-derived mesenchymal stromal cells.* Cytotherapy, 2009. **11**(2): p. 177-88.
95. Huang, C., et al., *Combination of retinal pigment epithelium cell-conditioned medium and photoreceptor outer segments stimulate mesenchymal stem cell differentiation toward a functional retinal pigment epithelium cell phenotype.* J Cell Biochem, 2012. **113**(2): p. 590-8.
96. Coles, B.L., et al., *Facile isolation and the characterization of human retinal stem cells.* Proc Natl Acad Sci U S A, 2004. **101**(44): p. 15772-7.
97. Cicero, S.A., et al., *Cells previously identified as retinal stem cells are pigmented ciliary epithelial cells.* Proc Natl Acad Sci U S A, 2009. **106**(16): p. 6685-90.
98. Salero, E., et al., *Adult human RPE can be activated into a multipotent stem cell that produces mesenchymal derivatives.* Cell Stem Cell, 2012. **10**(1): p. 88-95.
99. Zhang, K., et al., *Direct conversion of human fibroblasts into retinal pigment epithelium-like cells by defined factors.* Protein Cell, 2013.
100. Pera, M.F., *Stem cells: The dark side of induced pluripotency.* Nature, 2011. **471**(7336): p. 46-7.
101. Kim, K., et al., *Epigenetic memory in induced pluripotent stem cells.* Nature, 2010. **467**(7313): p. 285-90.
102. Gore, A., et al., *Somatic coding mutations in human induced pluripotent stem cells.* Nature, 2011. **471**(7336): p. 63-7.
103. Hussein, S.M., et al., *Copy number variation and selection during reprogramming to pluripotency.* Nature, 2011. **471**(7336): p. 58-62.
104. Lister, R., et al., *Hotspots of aberrant epigenomic reprogramming in human induced pluripotent stem cells.* Nature, 2011. **471**(7336): p. 68-73.
105. Hu, Q., et al., *Memory in induced pluripotent stem cells: reprogrammed human retinal-pigmented epithelial cells show tendency for spontaneous redifferentiation.* Stem Cells, 2010. **28**(11): p. 1981-91.
106. Toivonen, S., et al., *Comparative analysis of targeted differentiation of human induced pluripotent stem cells (hiPSCs) and human embryonic stem cells reveals variability associated with incomplete transgene silencing in retrovirally derived hiPSC lines.* Stem Cells Transl Med, 2013. **2**(2): p. 83-93.
107. Lamba, D.A. and T.A. Reh, *Microarray characterization of human embryonic stem cell--derived retinal cultures.* Invest Ophthalmol Vis Sci, 2011. **52**(7): p. 4897-906.
108. Frisch, S.M. and E. Ruoslahti, *Integrins and anoikis.* Curr Opin Cell Biol, 1997. **9**(5): p. 701-6.

109. Hynes, S.R. and E.B. Lavik, *A tissue-engineered approach towards retinal repair: scaffolds for cell transplantation to the subretinal space.* Graefes Arch Clin Exp Ophthalmol, 2010. **248**(6): p. 763-78.
110. Del Priore, L.V., T.H. Tezel, and H.J. Kaplan, *Maculoplasty for age-related macular degeneration: reengineering Bruch's membrane and the human macula.* Prog Retin Eye Res, 2006. **25**(6): p. 539-62.
111. Capeans, C., et al., *Amniotic membrane as support for human retinal pigment epithelium (RPE) cell growth.* Acta Ophthalmol Scand, 2003. **81**(3): p. 271-7.
112. Ohno-Matsui, K., et al., *The effects of amniotic membrane on retinal pigment epithelial cell differentiation.* Mol Vis, 2005. **11**: p. 1-10.
113. Ohno-Matsui, K., et al., *In vitro and in vivo characterization of iris pigment epithelial cells cultured on amniotic membranes.* Mol Vis, 2006. **12**: p. 1022-32.
114. Singhal, S. and G.K. Vemuganti, *Primary adult human retinal pigment epithelial cell cultures on human amniotic membranes.* Indian J Ophthalmol, 2005. **53**(2): p. 109-13.
115. Singh, S., S. Woerly, and B.J. McLaughlin, *Natural and artificial substrates for retinal pigment epithelial monolayer transplantation.* Biomaterials, 2001. **22**(24): p. 3337-43.
116. Lee, C.J., et al., *Microcontact printing on human tissue for retinal cell transplantation.* Arch Ophthalmol, 2002. **120**(12): p. 1714-8.
117. Lee, C.J., H.A. Fishman, and S.F. Bent, *Spatial cues for the enhancement of retinal pigment epithelial cell function in potential transplants.* Biomaterials, 2007. **28**(13): p. 2192-201.
118. Ho, T.C. and L.V. Del Priore, *Reattachment of cultured human retinal pigment epithelium to extracellular matrix and human Bruch's membrane.* Invest Ophthalmol Vis Sci, 1997. **38**(6): p. 1110-8.
119. Tezel, T.H., L.V. Del Priore, and H.J. Kaplan, *Reengineering of aged Bruch's membrane to enhance retinal pigment epithelium repopulation.* Invest Ophthalmol Vis Sci, 2004. **45**(9): p. 3337-48.
120. Niknejad, H., et al., *Properties of the amniotic membrane for potential use in tissue engineering.* Eur Cell Mater, 2008. **15**: p. 88-99.
121. Ho, T.C., L.V. Del Priore, and H.J. Kaplan, *En bloc transfer of extracellular matrix in vitro.* Curr Eye Res, 1996. **15**(9): p. 991-7.
122. Tezel, T.H. and L.V. Del Priore, *Reattachment to a substrate prevents apoptosis of human retinal pigment epithelium.* Graefes Arch Clin Exp Ophthalmol, 1997. **235**(1): p. 41-7.
123. Bhatt, N.S., et al., *Experimental transplantation of human retinal pigment epithelial cells on collagen substrates.* Am J Ophthalmol, 1994. **117**(2): p. 214-21.
124. Huang, J.C., et al., *Preparation and transplantation of photoreceptor sheets.* Curr Eye Res, 1998. **17**(6): p. 573-85.
125. Imai, H., et al., *The upregulation of angiogenic gene expression in cultured retinal pigment epithelial cells grown on type I collagen.* Curr Eye Res, 2007. **32**(10): p. 903-10.
126. Lu, J.T., et al., *Thin collagen film scaffolds for retinal epithelial cell culture.* Biomaterials, 2007. **28**(8): p. 1486-94.

127. Oganesian, A., et al., *A new model of retinal pigment epithelium transplantation with microspheres.* Arch Ophthalmol, 1999. **117**(9): p. 1192-200.
128. Giordano, G.G., et al., *Retinal pigment epithelium cells cultured on synthetic biodegradable polymers.* J Biomed Mater Res, 1997. **34**(1): p. 87-93.
129. Lu, L., C.A. Garcia, and A.G. Mikos, *Retinal pigment epithelium cell culture on thin biodegradable poly(DL-lactic-co-glycolic acid) films.* J Biomater Sci Polym Ed, 1998. **9**(11): p. 1187-205.
130. Lu, L., M.J. Yaszemski, and A.G. Mikos, *Retinal pigment epithelium engineering using synthetic biodegradable polymers.* Biomaterials, 2001. **22**(24): p. 3345-55.
131. Thomson, R.C., et al., *Manufacture and characterization of poly(alpha-hydroxy ester) thin films as temporary substrates for retinal pigment epithelium cells.* Biomaterials, 1996. **17**(3): p. 321-7.
132. Thomson, H.A., et al., *Biodegradable poly(alpha-hydroxy ester) blended microspheres as suitable carriers for retinal pigment epithelium cell transplantation.* J Biomed Mater Res A, 2010. **95**(4): p. 1233-43.
133. Hadlock, T., et al., *Ocular cell monolayers cultured on biodegradable substrates.* Tissue Eng, 1999. **5**(3): p. 187-96.
134. Lim, J.M., et al., *Retinal pigment epithelial cell behavior is modulated by alterations in focal cell-substrate contacts.* Invest Ophthalmol Vis Sci, 2004. **45**(11): p. 4210-6.
135. Tezcaner, A., K. Bugra, and V. Hasirci, *Retinal pigment epithelium cell culture on surface modified poly(hydroxybutyrate-co-hydroxyvalerate) thin films.* Biomaterials, 2003. **24**(25): p. 4573-83.
136. Williams, R.L., et al., *Polyurethanes as potential substrates for sub-retinal retinal pigment epithelial cell transplantation.* J Mater Sci Mater Med, 2005. **16**(12): p. 1087-92.
137. Da Silva, G.R., et al., *Montmorillonite clay based polyurethane nanocomposite as substrate for retinal pigment epithelial cell growth.* J Mater Sci Mater Med, 2013.
138. Hu, Y., et al., *A novel approach for subretinal implantation of ultrathin substrates containing stem cell-derived retinal pigment epithelium monolayer.* Ophthalmic Res, 2012. **48**(4): p. 186-91.
139. Vaajasaari, H., et al., *Toward the defined and xeno-free differentiation of functional human pluripotent stem cell-derived retinal pigment epithelial cells.* Mol Vis, 2011. **17**: p. 558-75.
140. Schwartz, S.D., et al., *Embryonic stem cell trials for macular degeneration: a preliminary report.* Lancet, 2012. **379**(9817): p. 713-20.
141. Huang, J., et al., *Embryonic stem-cell-derived retinal pigment epithelial cells for macular degeneration.* Lancet, 2012. **379**(9831): p. 2050; author reply 2050-1.

Chapter II

Induced pluripotent stem cell-derived retinal pigmented epithelium: A comparative study between cell lines and differentiation methods

Introduction

Induced pluripotent stem cells (iPSCs) were first described in landmark papers by the Yamanka and Thomson laboratories in 2006 and 2007, respectively [1, 2]. They described the reversion of differentiated cells back into a stem cell like state through the forced expression of key pluripotent genes. IPSCs have the potential to differentiate into any cell type in body, allowing for patient-specific cells to be created for possible treatment options [1, 2]. IPSCs hold great potential for novel autologous cellular therapies, disease modeling and research without many of the ethical concerns of using human embryonic stem cells (hESCs) [3]. First reports of iPSC lines were created using integrating vectors; however this could cause unwanted residual effects post differentiation [4]. Therefore, researchers have discovered ways to use non-integrating episomal vectors to derive iPSCs. Using non-integrating iPSC lines is extremely attractive when progressing these novel therapies towards clinical trials [5].

The first iPSC clinical trial is underway in Japan to treat wet age-related macular degeneration (AMD) after several groups showed an improvement in vision following cellular injection in rat models [6-8]. AMD affects 7.2 million people in the United States and is the leading cause of blindness in the elderly population [9, 10]. There are two forms of the disease, wet, or exudative, and dry, or atrophic, AMD. Wet AMD is characterized by neovascularization within the retina while dry AMD presents with drusen, which are lipid deposits of unknown origin [11]. Both forms result in disruption of the retinal pigmented epithelium (RPE), a monolayer of cells situated between the choroid and the neural retina. The RPE are responsible for maintaining the

health of the photoreceptors; therefore when the RPE become compromised, the photoreceptors begin to die resulting in a loss of vision [12].

As iPSC-RPE begin to be used in clinical trials it is imperative that a more complete understanding of these cells is achieved to understand the variability that is known to exist between lines [13]. In addition, there are currently several methods for deriving RPE from hESCs and iPSCs; however, there has not been in-depth analysis of derivation methods for different lines of iPSCs [14, 15]. This article will provide a comparative study of three iPSC-RPE lines and two differentiation protocols: the spontaneous continuously adherent culture (SCAC) differentiation method [8, 15-19] and the 14-day directed differentiation protocol [20, 21].

In addition to an in-depth comparison of lines and derivation methods, we also compare a variety of genetic markers and physiological functions indicative of differentiated RPE that may be used to represent the quality of the iPSC-RPE line to determine whether it is suitable for transplantation. Development of a release assay, a single test to determine quality of derived cells, will be important because many groups are planning to create human leukocyte antigen (HLA) matched super banks of iPSC. These banks will avoid the long derivation and testing time that it takes to create autologous patient specific cells [22]. It is thought that HLA matching will dampen any immune response following transplantation [23]. Determining a proper release assay will expedite the efficiency of creating quality transplant-ready HLA matched iPSC-RPE.

Methods

Cell Culture

Human Pluripotent Stem Cell Culture

Epstein-Barr vector (EBV)-derived iPSC lines DF4-3-7T and DF19-9-11T [24, 25] were both kindly donated from the James Thomson and David Gamm groups (WiCell Research Institute, Madison, WI), and the MyCell iPSC line (no. 1013.201) was acquired from Cellular Dynamics International's MyCell iPSC Cell Services (Madison, WI). The hESC lines used for comparison were obtained from J. Thomson (H9s) and the University of California, San Francisco (UCSF4s; NIH registry No. 0044). All iPSC and hESC lines were maintained on Matrigel (BD Biosciences, San Diego, CA) in mTeSR1 media (Stem Cell Technologies, Vancouver, BC, Canada). Cells were kept at 37°C 5% CO_2 in normoxic conditions and media was changed every other day.

Retinal Pigmented Epithelium: Spontaneous Continuously Adherent Culture (SCAC) Differentiation Method

Pluripotent stem cell lines were overgrown for 8-14 days; after which mTeSR1 medium was changed to XVIVO-10 medium without basic fibroblast growth factor (bFGF; Lonza, Walkersville, MD). XVIVO-10 medium was changed every other day for 90 days; pigmentation appeared approximately 1 month after medium switch. Following 90 days in culture, non-pigmented cells were manually dissected away from RPE pigmented spots. Cells were washed with phosphate buffered saline (PBS, Life Technologies, Carlsbad, CA), leaving only the pigmented patches adhering to the plate. Remaining pigmented cells were enzymatically digested using TrypLE Express (Life Technologies) for 5 minutes at 5% CO_2 37°C. Cells were collected, diluted in 1:10 volumes of XVIVO-10 and triturated, then spun at 1000 rpm for 5 minutes. The resulting pellet was resuspended in XVIVO-10, strained through at 30μM sieve and seeded onto Matrigel-coated plates at $1.0x10^5$cells/cm^2 creating a homogenous

population of enriched RPE cells. XVIVO-10 medium was changed every 2-3 days and cells were maintained at 5% CO_2 37°C in normoxic conditions. After RPE matured in culture for 30 days, they were passaged using TrypLE Express and plated again at $1.0x10^5$cells/cm^2 on a Matrigel-coated surface in XVIVO-10 medium as described above. Cells were passaged using this method until passage 2 when they were cryopreserved, generating intermediate cell banks (ICBs).

Retinal Pigmented Epithelium: 14-day Directed Differentiation Protocol

Pluripotent stem cells were directed to differentiate to RPE in 14 days as previously described [20, 21]. Briefly, iPSC and hESC were passaged with EDTA (Life Technologies) using the methods described by Beers et al. [26] and seeded onto Matrigel-coated 12-well plates in DMEM/F12 medium containing 1 X N2, 1 X B27, and 1 X NEAA (basal medium) (Life Technologies). From days 0-2 of differentiation, basal medium contained 10mM nicotinamide (NIC; Sigma-Aldrich, St. Louis, MO), 50ng/mL noggin, 10ng/mL Dkk1, and 10ng/mL IGF1 (R&D Systems Inc., Minneapolis, MN). From days 2-4, basal medium contained 10mM nicotinamide, 10ng/mL noggin, 10ng/mL Dkk1, 10ng/mL IGF1, and 5ng/mL bFGF. From days 4-6, 10ng/mL Dkk1, 10ng/mL IGF1, and 100ng/mL Activin A (Peprotech, Rocky Hill, NJ) was added to basal medium. From days 6-8, basal medium contained 100ng/mL Activin A and 10μM SU5402 (Santa Cruz Biotechnology Inc., Dallas, TX). From days 8-14, basal medium contained 100ng/mL Activin A, 10μM SU5402, and 3 μM CHIR99021 (Stemgent, Cambridge, MA). On day 14, cells lacking RPE morphology were manually scraped away using a pipette tip, leaving only RPE-like cells in the culture dish. The RPE left behind were enzymatically digested using TrypLE Express for 5min at 5% CO_2 37°C. Cells were

collected, strained, and seeded onto Matrigel-coated plates in XVIVO-10 medium at $1.0x10^5$cells/cm^2 using the methods described above for the SCAC method. XVIVO-10 medium was changed every 2-3 days and cells were maintained at 5% CO_2 37°C in normoxic conditions. 14-day-derived RPE cells were expanded by passaging every 30 days (as described above) and cryopreserved at passage 2 to generate ICBs.

Creation of Intermediate Cell Banks (ICBs)

Cells were frozen down prior to reaching confluence, 2-4 days following plating, at passage 2. Cells were lifted using TrypLE Express for 5 minutes at 5% CO_2 37°C, gently scraped, triturated and diluted in 1:10 volumes of XVIVO-10. Cells were spun down at 1000 rpm for 5 minutes and then resuspended in CryoStor CS10 freezing medium (Stem Cell Technologies), at $3\text{-}6x10^6$cells/ml. One ml aliquots were stored in cryovials and put into a slow rate freezing device and stored in the -80°C freezer for 24 hours, following which cells were moved to liquid nitrogen for long term storage. ICBs were created of each viable iPSC-RPE line (reference Supp. Table 1 for non-viable iPSC-RPE). HESC-RPE used for comparison were passaged and handled using the same methods as the iPSC-RPE. All cells used in analysis were thawed cells from ICBs, plated at passage 3 and seeded at $1.5x10^6$cells/cm^2. ICBs were created using at least 3 separate enrichments and expansions for each iPSC-RPE line. For all experiments and figures, three separate enrichments were performed and tested, n=3.

Real Time Quantitative Polymerase Chain Reaction (qRT-PCR)

iPSC-RPE and hESC-RPE ICB cells and human fetal RPE (fRPE, kindly provided by Lincoln Johnson (Center for the Study of Macular Degeneration, UCSB) and Dean Bok (Jules Stein Eye Institute, UCLA)) were thawed and plated on Matrigel and cultured for

30 days. fRPE were cultured using the medium and methods of Maminishkis et al. [27]. Cell lysates were collected using RLT Plus buffer with 1% β-mercaptoethanol and RNA was purified using Qiagen's RNeasy Plus Kit (Qiagen, Limberg, Austria). Photomicrographs were taken at day 30. The iScript cDNA Synthesis Kit (BioRad, California, USA) was used to create 1µg of cDNA. Expression of genes of interest was evaluated for three separate enrichments, per line, and with internal triplicates, using the same TaqMan gene expression assays as cited in Croze et al., 2014 [28]. The probes analyzed were as follows: RPE-specific protein 65kDa (RPE65) Hs01071462_m1; bestrophin 1 (BEST1) Hs00188249_ml; retinaldehyde binding protein 1 (RLBP1) Hs00165632_ml; microphthalmia-associated transcription factor (MITF2) isoform 2 AJD1S3G; premelanosome protein (PMEL) Hs00173854_m1; tyrosinase (TYR) Hs00165976_ml; paired box 6 (PAX6) Hs01088112_m1; marker of proliferation Ki-67 (MKI67) Hs01032443_m1; zinc finger protein 42 (REX1) Hs01124465_m1; spalt-like transcription factor 4 (SALL4) Hs00360675_m1; microtubule-associated protein 2 (MAP2) Hs00258900_m1; integrin, alpha 2 (ITGA2) Hs00158127_m1; platelet/endothelial cell adhesion molecule 1 (PECAM1) Hs00169777_m1; S100 calcium binding protein A4 (S100A4) Hs00243202_m1; and housekeepers: eukaryotic translation initiation factor 2B, subunit 2 beta (EIF2B2) Hs00204540_m1; ubiquitin-conjugating enzyme E2R 2 (UBE2R2) Hs00215107_m1; and small EDRK-rich factor 2 (SERF2) Hs00428481_m1 (Life Technologies). The relative level of expression for each gene was determined by normalizing to the geometric mean of the housekeeping gene set using CFX Manager (Bio-Rad) and Excel software. Student's t-test were run

comparing methods within each line, and then between two lines, same method, to determine statistical significance.

Immunocytochemistry (ICC)

Passage 3 iPSC-RPE and hESC-RPE were seeded onto Matrigel-coated 8-chambered slides. Thirty days after plating, the cells were washed with PBS and fixed with 4% paraformaldehyde in 0.1M sodium cacodylate buffer (pH 7.4) for 15 minutes at 4°C. The fixed cells were then washed with PBS and blocked with PBS containing 5% bovine serum albumin (BSA) and 0.2% Triton X-100 for 1 hour at 4°C. The cells were then probed with primary antibodies against MITF (1:100, Abcam, Cambridge, MA, USA), orthodenticle homeobox 2 (OTX2) (1:4000, Millipore, Billerica, MA, USA), RPE65 (1:100, Abcam), PMEL (1:100, Dako), zona occuldens 1 (ZO-1) (1:100, Life Technologies), or TRA1-81 (1:100, Millipore) in PBS with 5% BSA overnight at 4°C. Following 3 washes to remove the primary antibodies, cells were incubated with the appropriate Alexa Fluor conjugated secondary antibody (1:300, Life Technologies) for 1 hour at 4°C, washed with PBS and mounted using Prolong Gold Anti-fade (Life Technologies). Labeled cells were then washed with PBS and imaged using epifluorescent microscopy at 40X objective on a BX51 Olympus Microscope.

Rod Outer Segment (ROS) Phagocytosis Assay

IPSC-RPE, hESC-RPE, and fRPE were cultured using the medium and methods of Maminishkis et al. [27]. ARPE19 cells (ATCC, Virginia, USA) were cultured in Dulbecco's modified Eagle's medium with nutrient mix F12 and sodium pyruvate (DMEM/F12, Life Technologies), supplemented with GlutaMAX-I (1X, Life Technologies), 10% FBS (Atlas Biologicals, Colorado, USA) and 15mM HEPES (Life Technologies). Human umbilical

vein endothelial cells (HUVEC, ATCC) were grown in endothelial cell growth medium with supplement mix (EGM, PromoCell, Heidelberg, Germany). All cells were plated in quadruplicate onto 0.1% gelatin-coated wells and cultured for 30 days. The ROS phagocytosis assays were performed according to the methods of Croze et al. 2014 [28]. The fRPE and ARPE19 cells serve as positive controls and the HUVEC line was used as a negative control. All experiments were normalized to a single ARPE19 experimental data set. Following this normalization, the fRPE ROS values were set to 100% within each individual experiment and percent difference from this condition was determined. The anti-αVβ5 condition had significantly lower internalization then ROS and ROS+IgG in every cell line, except for the negative control HUVECs (Data not shown, $p \leq 0.05$). Student's t-tests were run to determine statistical significance.

Pigment Epithelium Derived Factor (PEDF) Enzyme-Linked Immunosorbent Assay (ELISA)

Thawed ICB iPSC-RPE, hESC-RPE, and fRPE were grown on gelatin coated wells in medium described in Maminishkis et al., plus 0.5X Normocin (InvivoGen, California, USA) [27]. On day 30, media was collected following a 24 hour exposure to the cells. The amount of human PEDF was determined by ELISA according to the manufacturer's instructions (BioProducts MD, LLC., Maryland, USA). All media volumes were kept constant and the growth area and volume were taken into consideration when calculating PEDF concentrations. Statistical significance was determined by an individual Student's t-test between two conditions at a time.

Results

RPE morphology and pigmentation differ between iPSC lines and derivation methods

Cells were thawed after undergoing 14-day directed or SCAC differentiation, expansion to passage 2, and intermediate cryopreservation (Fig. 3A); then RPE morphology was assessed at passage 3. Notably, we began this study with five iPSC lines, however two lines (DF6 and OAT) yielded insufficient quantities of RPE for characterization when differentiated using the SCAC method (Supp. Table 1).

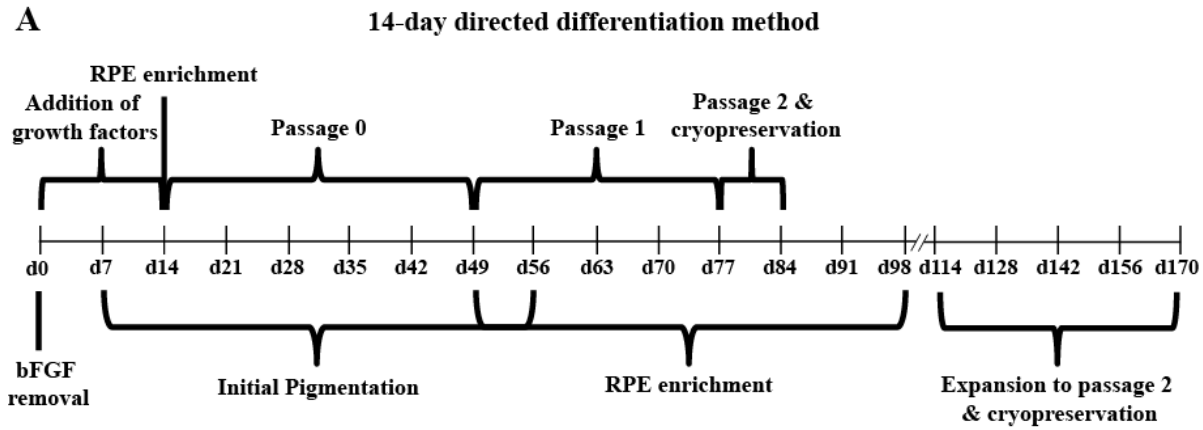

Spontaneous continuously adherent culture (SCAC) differentiation method

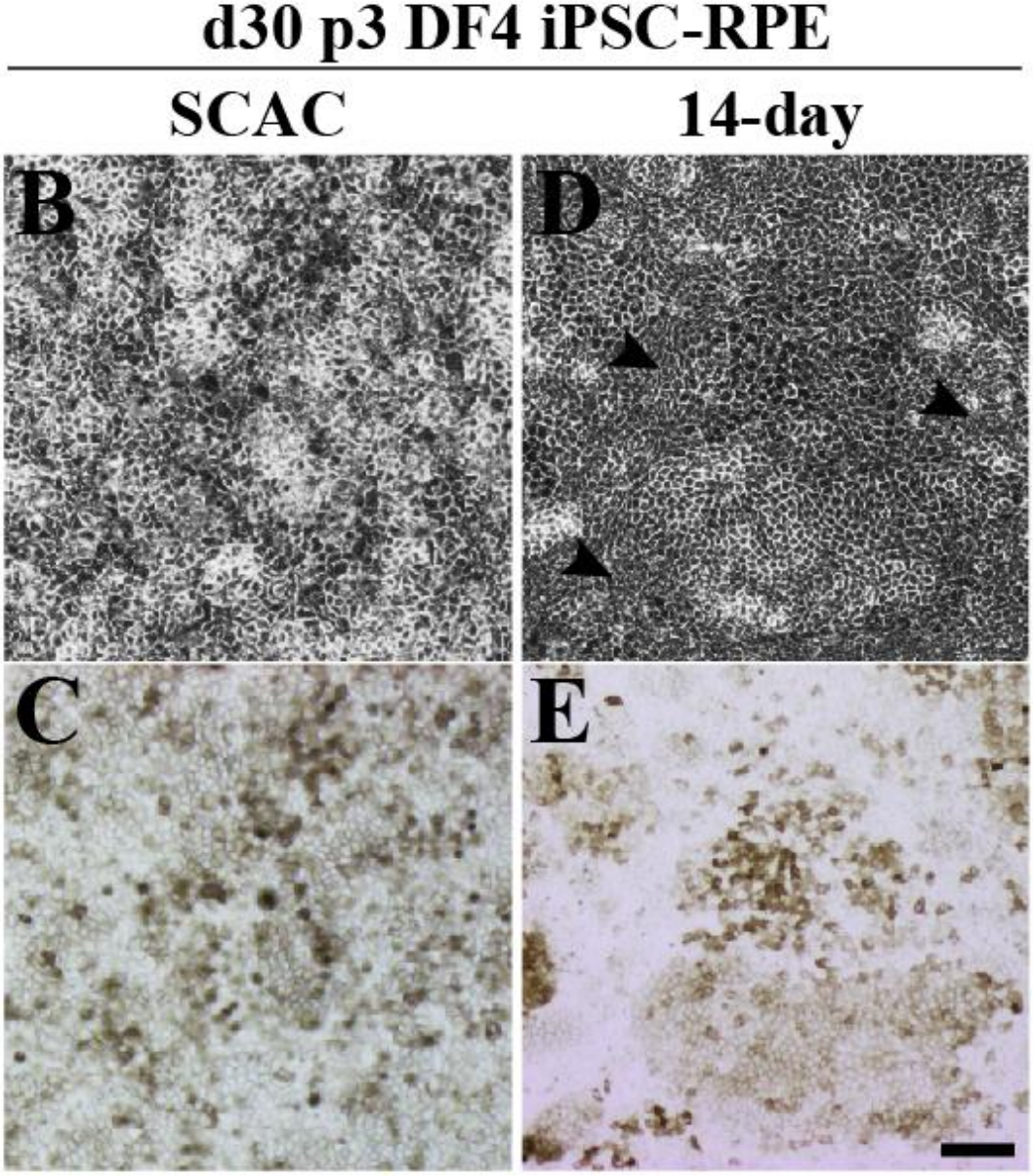
d30 p3 DF4 iPSC-RPE
SCAC
14-day
B
D
C
E

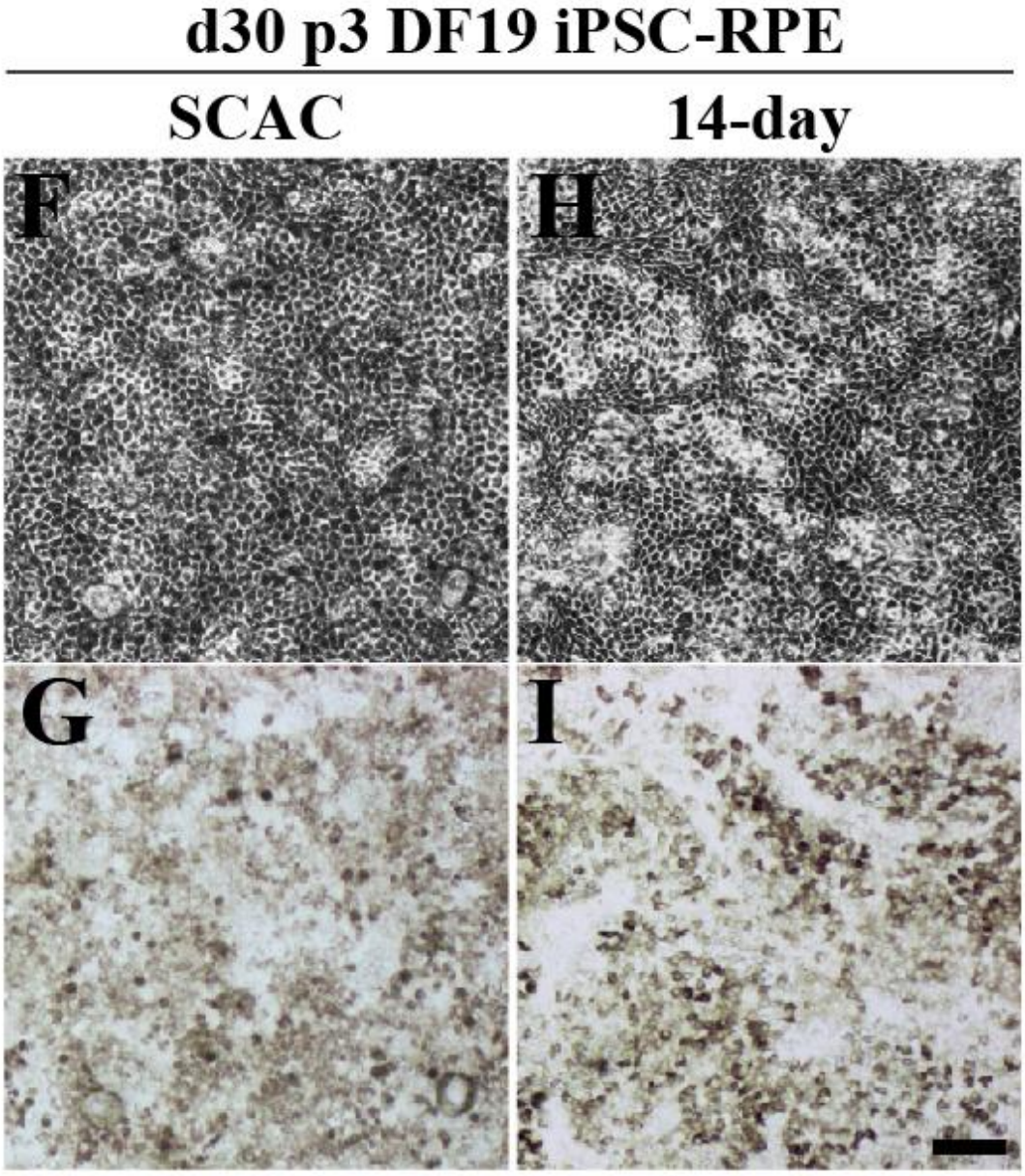
d30 p3 DF19 iPSC-RPE
SCAC
14-day
F
H
G
I

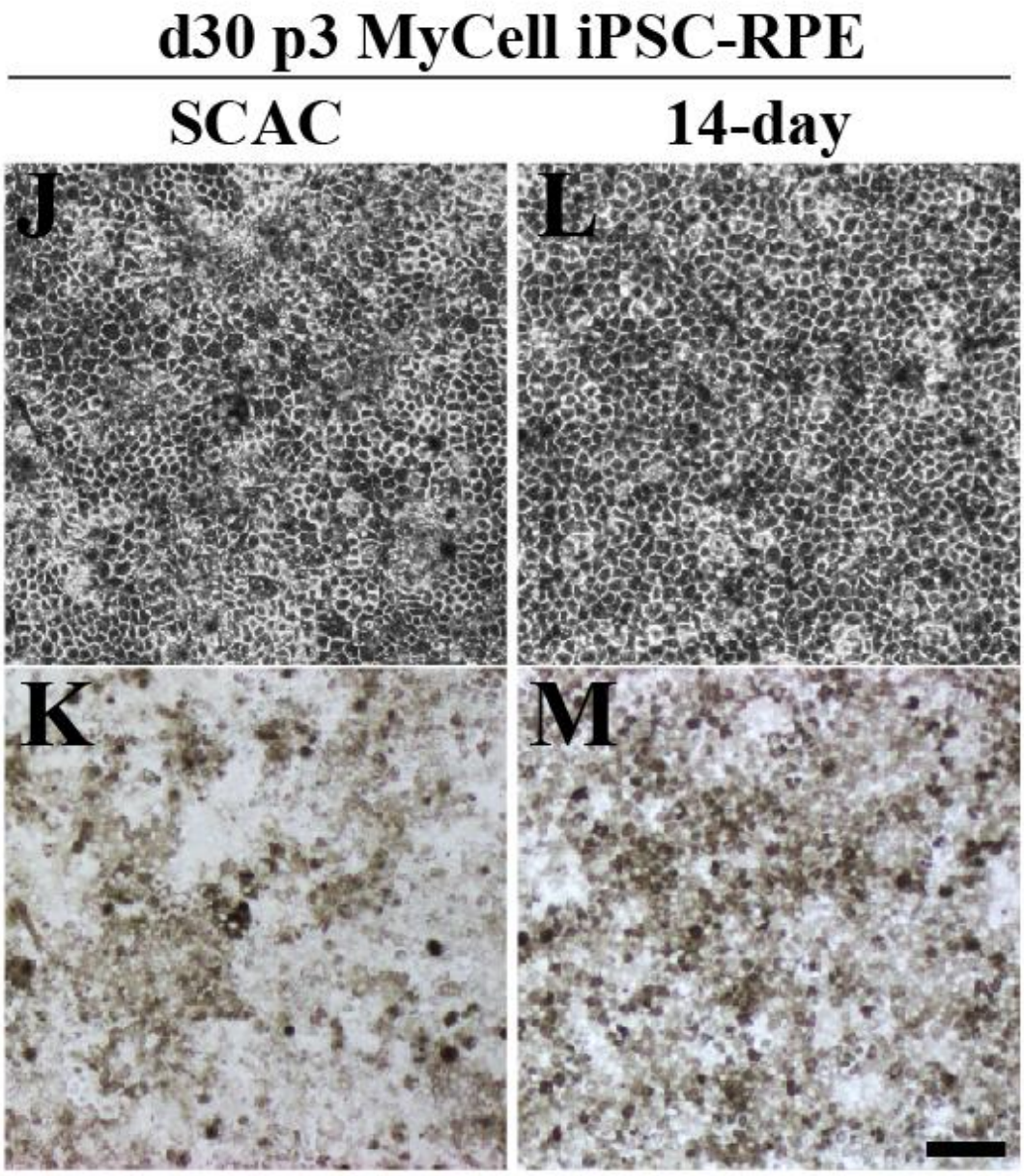

Figure 3. Morphology and degree of pigmentation in iPSC-RPE. (A) Schematic representation of 14-day directed (top) and spontaneous continuously adherent culture (SCAC, bottom) differentiation timelines. Phase contrast (B,D) and bright field (C,E) images of passage 3, day 30 DF4 iPSC-RPE derived by SCAC (B,C) or 14-day differentiation (D,E). (C) *Black arrowheads* indicate patches of cells lacking RPE morphology. Phase contrast (F,H) and bright field (G,I) images of passage 3, day 30 DF19 iPSC-RPE derived by SCAC (F,G) or 14-day differentiation (H,I). Phase contrast (J,L) and bright field (K,M) images of passage 3, day 30 MyCell iPSC-RPE derived by SCAC (J,K) or 14-day differentiation (L,M). Scale bar=100μm.

We found DF4, DF19, and MyCell iPSC-RPE lines yielded pigmented cells with cuboidal morphology by day 30 using both differentiation methods, but with varying efficiency (Fig. 3B-M). Comparison of RPE within the same iPSC line showed differences in cell morphology and pigmentation depending on the method of derivation, which were especially apparent for DF4 iPSC-RPE. The 14-day-derived DF4 iPSC-RPE were noticeably less pigmented (Fig. 3E) when compared to DF4 iPSC-RPE derived by the SCAC method (Fig. 3C). Additionally, 14-day-derived DF4 iPSC-RPE yielded patches of cells lacking defined tight junctions (Fig. 3D, arrowheads). DF19 iPSC-RPE derived by the 14-day method appeared slightly less pigmented (Fig. 3I) when compared to SCAC-derived DF19 iPSC-RPE (Fig. 3G), however cell morphology appeared normal (Fig. 3H) and similar to SCAC-derived DF19 iPSC-RPE (Fig. 3F). In contrast, 14-day-derived MyCell iPSC-RPE showed more uniform morphology (Fig. 3L) and appeared more pigmented (Fig. 3M) than SCAC-derived MyCell iPSC-RPE on day 30 (Fig. 3J, 3K).

Comparing line by line for each method, all three SCAC-derived iPSC-RPE lines were similarly pigmented (Fig. 3C, 3G, 3K), however DF19 iPSC-RPE had the best morphology (Fig. 3F) compared to DF4 and MyCell iPSC-RPE (Fig. 3B, 3J), showing clearly defined tight junctions and more homogenous cell size. MyCell iPSC-RPE were the most pigmented of the 14-day-derived iPSC-RPE lines (Fig. 3M) and were comparable with DF19 derived by the same method in terms of typical RPE morphology (Fig. 3H, 3L). DF4 iPSC were the least efficient at generating RPE with mature morphology and pigmentation when derived using the 14-day method (Fig. 3D, 3E).

Gene expression profiles change between iPSC-RPE lines and derivation methods

RNA from ICBs of iPSC-RPE was isolated on day 30 post thaw at passage 3 and was subjected to qRT-PCR examining a range of RPE (Fig. 4A) and non-RPE transcripts (Supp. Fig. 1A,B). fRPE were also thawed and grown for 30 days as a positive control comparison. Mature RPE marker BEST1 displayed lower levels in the 14-day-derived DF4 and DF9 iPSC-RPE when compared to the SCAC-derived lines. 14-day-derived DF4 iPSC-RPE had lower levels of RLBP1 from the DF4 SCAC line; however the 14-day-derived DF19 line showed an increase in this visual cycle transcript compared to the DF19 SCAC line. 14-day-derived DF4 iPSC-RPE also exhibited a decrease in PMEL and TYR expression (pigmentation markers) from SCAC-derived DF4 iPSC-RPE. 14-day-derived DF19 iPSC-RPE expressed less TYR than SCAC-derived DF19 iPSC-RPE. The Mycell iPSC-RPE line exhibited no significant differences between methods in RPE specific transcripts. However, PAX6, an immature RPE and neural retina marker was lower in 14-day-derived MyCell iSPC-RPE. RPE65 and MITF2 (specific RPE isoform) showed no changes between methods within lines (Fig. 4A).

14-day-derived DF4 iPSC-RPE exhibited statistically lower levels of BEST1, RLBP1, PMEL and TYR than the 14-day-derived DF19 iPSC-RPE ($p \leq 0.05$). 14-day-derived DF4 iPSC-RPE also showed a statistical decrease in RPE65, BEST1, RLBP1, PMEL and TYR expression compared to 14-day-derived MyCell iPSC-RPE ($p \leq 0.05$). 14-day-derived DF4 iPSC-RPE had increased levels of PAX6 compared to DF19 and Mycell iPSC-RPE within the 14-day-directed method ($p \leq 0.01$). Interestingly, RPE65 was increased in 14-day directed DF4 iPSC-RPE compared to 14-day directed DF19 iPSC-RPE ($p \leq 0.05$). In addition, 14-day-derived DF19 iPSC-RPE showed decreased levels in

RPE65, BEST and an increase in RLBP1 when compared to 14-day derived MyCell iPSC-RPE (Fig. 4A, $p \leq 0.05$).

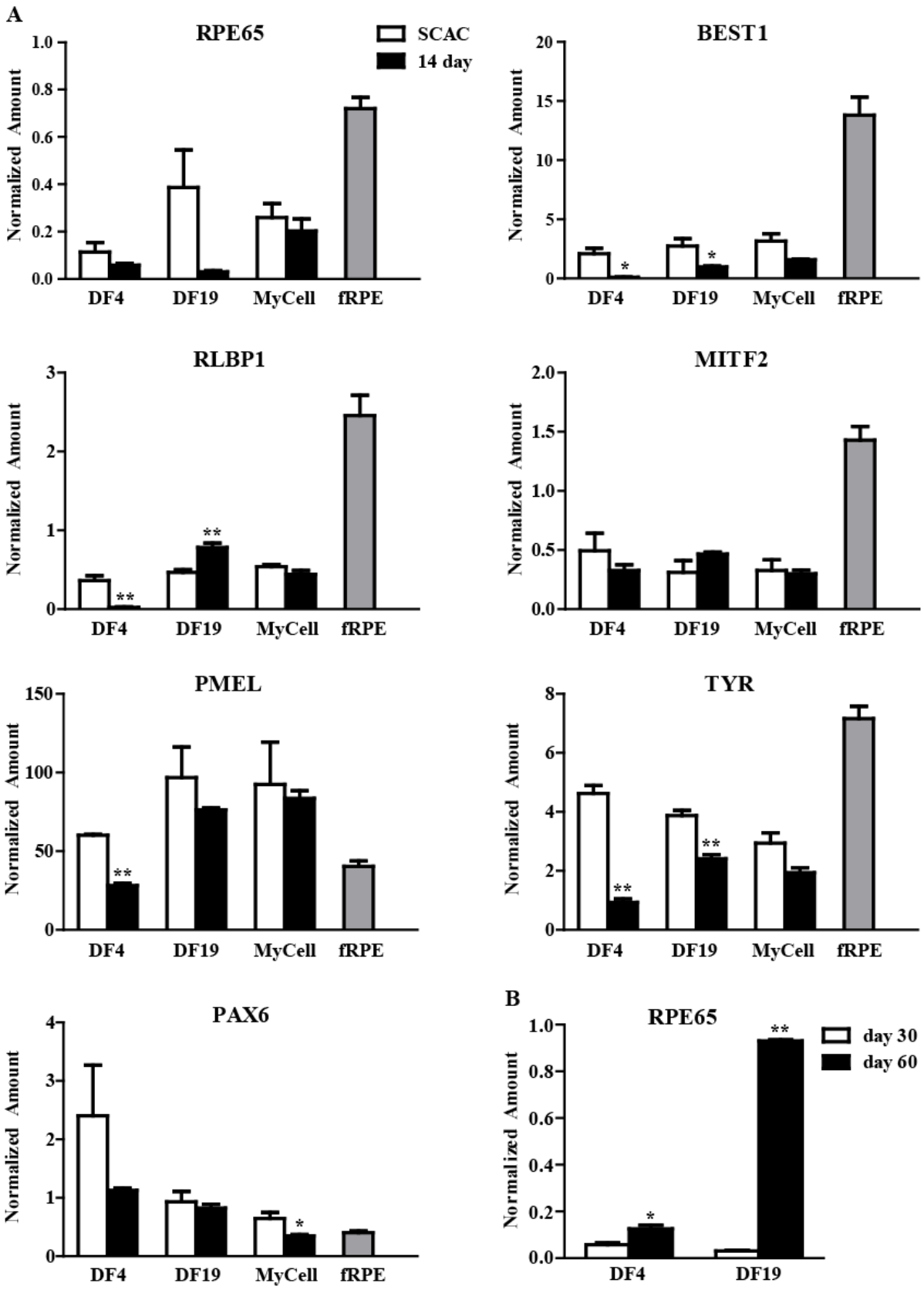
A
RPE65
SCAC
14 day
Normalized Amount
1.0
0.8
0.6
0.4
0.2
0.0
DF4
DF19
MyCell
fRPE
BEST1
20
15
10
5
0
*
RLBP1
3
2
1
0
**
MITF2
2.0
1.5
1.0
0.5
0.0
PMEL
150
100
50
0
TYR
8
6
4
2
0
PAX6
B
day 30
day 60

Figure 4. Gene expression in iPSC-RPE compared between methods and to fRPE. (A) RPE specific, pigmentation and neural retina/immature RPE expression was analyzed after thaw at passage 3, 30 days post-plating. All data was normalized to geometric mean of three housekeeper mRNAs. Error bars represent ± SEM. *p≤0.05 **p≤0.01 compared to same iPSC-RPE line, different method. n=3, separate enrichments for each line and method.

There was only one statistical difference between the lines within the SCAC-derived method. SCAC-derived DF4 iPSC-RPE had increased levels in TYR when compared to SCAC-derived MyCell iPSC-RPE (Fig. 4A, $p \leq 0.01$). Overall there was less variation between lines within the SCAC-derived method of differentiation. Within the 14-day-directed differentiation, the DF4 iPSC-RPE exhibited lower amounts of several critical RPE specific transcripts and showed an increase in the neural retina marker, PAX6. The 14-day directed cells may be less mature than SCAC-directed RPE when assessing statistics of critical RPE transcripts. However, this might be expected since the time to enrichment is 14 days versus 90 days as in the SCAC method. To examine whether the 14-day directed iPSC-RPE lines can mature if given longer time in culture, 14-day directed DF4 and DF19 iPSC-RPE cells were grown for 60 days following thaw. DF4 and DF19 lines were examined since they had the largest discrepancies in levels of RPE specific transcripts compared to the SCAC-directed method. RPE65 transcript levels, a mature RPE marker, were analyzed at 30 and 60 days post-thaw and a statistical increase of expression was examined for both 14-day directed DF4 and DF19 iPSC-RPE (Fig 4B).

Expression levels of contaminate markers and hESC-RPE derived cells from each method are shown in Supplemental Figures 1 and 2. All contaminate levels for all lines and methods were below background. See Supplemental Figure 1 legend for positive control contaminate marker levels.

<u>Protein localization remains similar between lines and methods, with DF4 iPSC-RPE as the exception</u>

Despite differences in morphology, pigmentation, and gene expression profiles, localization of RPE proteins appeared similar in all cell lines regardless of the differentiation method used, with the exception of 14-day derived DF4 iPSC-RPE. In all other cell lines, MITF and OTX2 transcription factors showed nuclear localization (Fig. 5A, 5B). Similarly, PMEL and RPE65 were localized to the cytoplasm (Fig. 5C, 5D), as expected, and ZO-1, a marker for tight junctions, showed positive staining at the perimeter of the cell (Fig. 5E). Protein expression and localization in DF19 and MyCell iPSC-RPE derived by either the 14-day or SCAC methods were analogous, and both cell lines were comparable to hESC-RPE (Supp. Fig. 3) derived using the respective differentiation protocol. The SCAC-derived DF4 iPSC-RPE also exhibited expected protein localization, which was comparable to other SCAC-derived iPSC- and hESC-RPE lines. Notably, ZO-1 staining in DF4 iPSC-RPE and DF19 iPSC-RPE derived by the SCAC method showed increased presence of larger cells and/or cells with abnormal morphology (Fig. 5E, arrows).

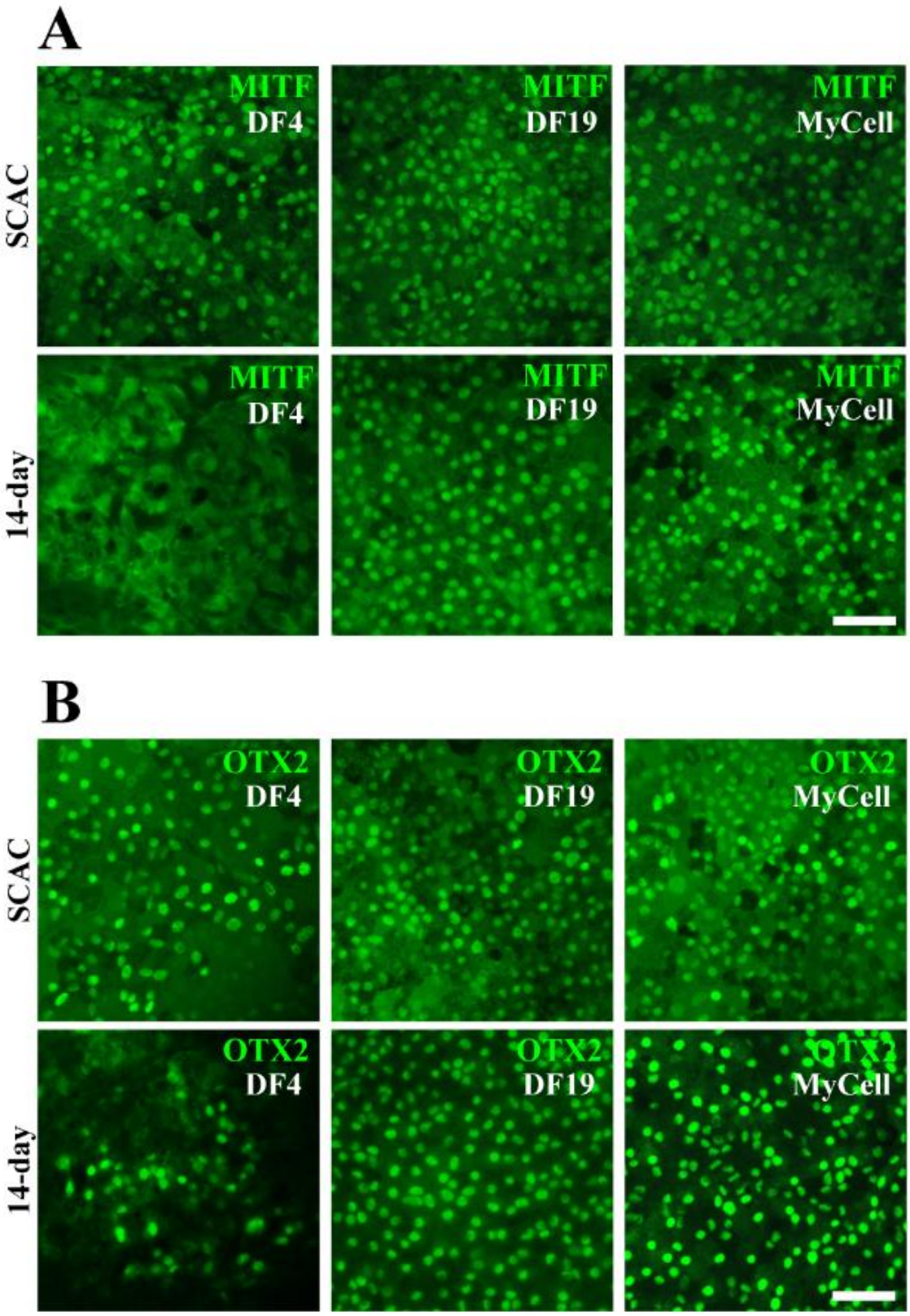
A
SCAC
14-day
MITF
DF4
MITF
DF19
MITF
MyCell
MITF
DF4
MITF
DF19
MITF
MyCell
B
SCAC
14-day
OTX2
DF4
OTX2
DF19
OTX2
MyCell
OTX2
DF4
OTX2
DF19
OTX2
MyCell

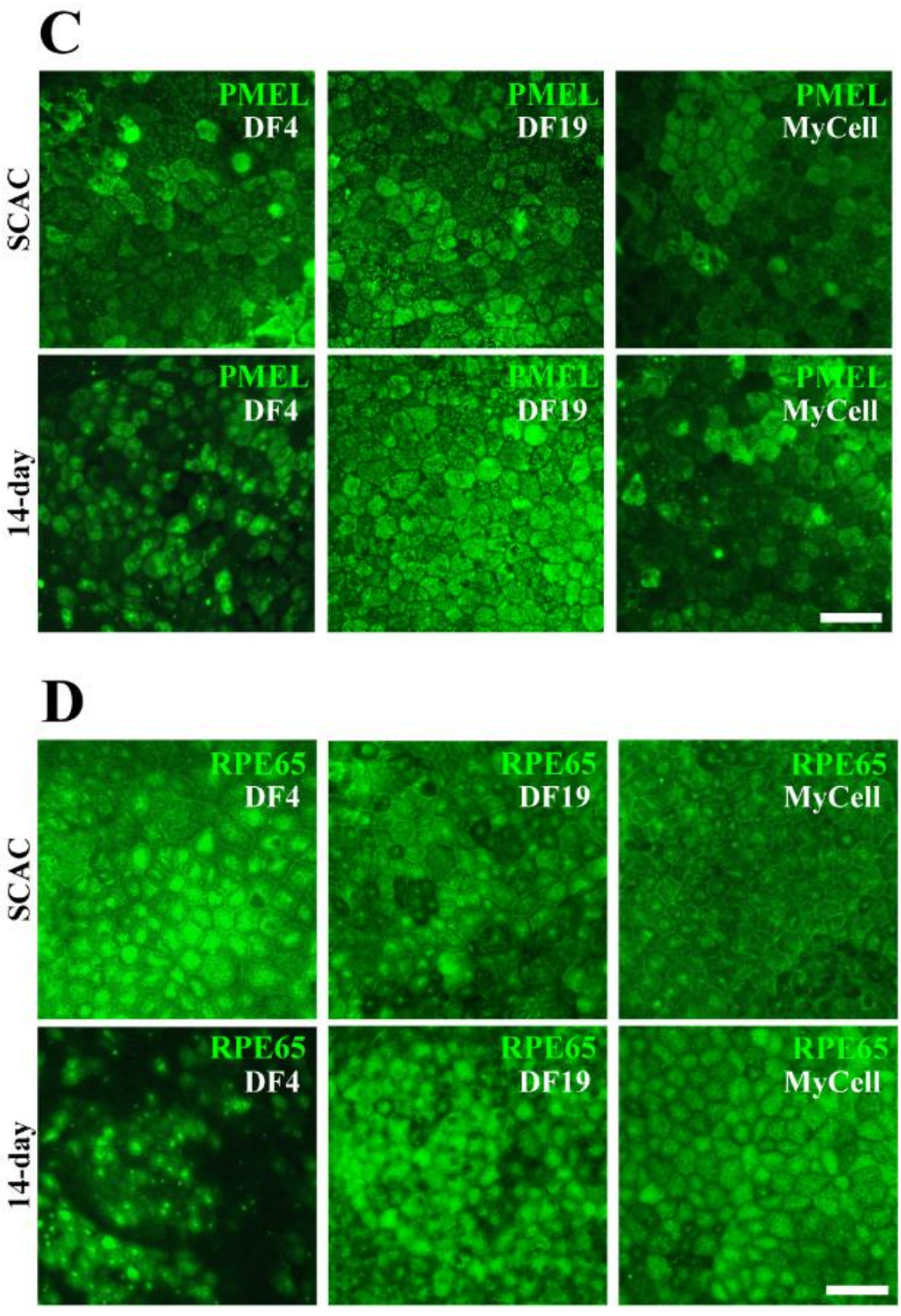
C
SCAC
14-day
PMEL
DF4
PMEL
DF19
PMEL
MyCell
PMEL
DF4
PMEL
DF19
PMEL
MyCell
D
SCAC
14-day
RPE65
DF4
RPE65
DF19
RPE65
MyCell
RPE65
DF4
RPE65
DF19
RPE65
MyCell

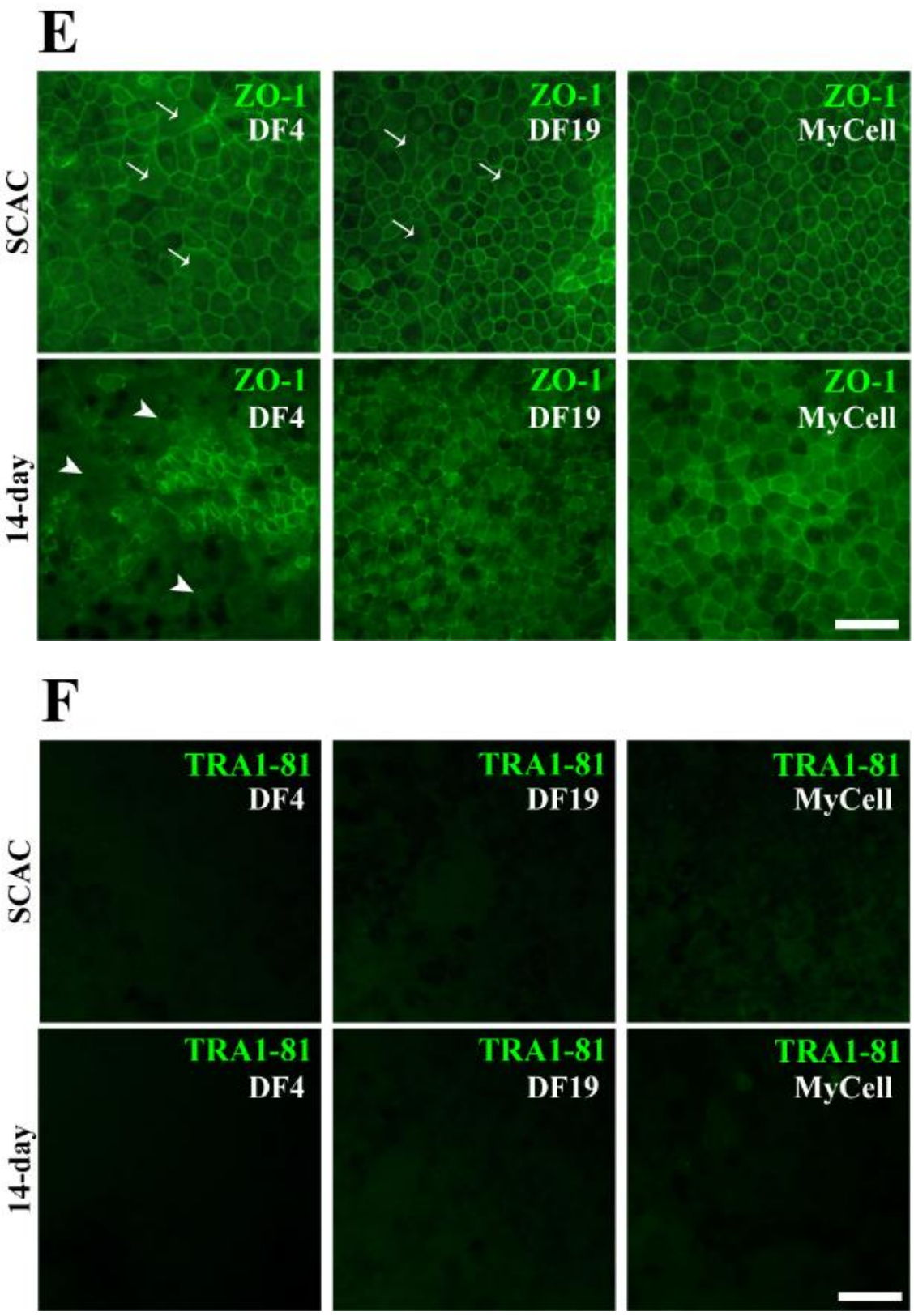
E
SCAC
14-day
ZO-1
DF4
ZO-1
DF19
ZO-1
MyCell
ZO-1
DF4
ZO-1
DF19
ZO-1
MyCell
F
SCAC
14-day
TRA1-81
DF4
TRA1-81
DF19
TRA1-81
MyCell
TRA1-81
DF4
TRA1-81
DF19
TRA1-81
MyCell

Figure 5. Protein localization and expression in iPSC-RPE. Immunofluorescence images of (A) OTX2, (B) MITF, (C) PMEL, (D) RPE65, (E) ZO-1, and (F) TRA1-81 are shown for passage 3, day 30 DF4, DF19, and MyCell iPSC-RPE derived by SCAC or 14-day directed differentiation. (E) *Arrows* indicate SCAC-derived DF4 and DF19 iPSC-RPE with abnormal morphology (large cells) based on ZO-1 expression. *White arrowheads* indicate patches of 14-day-derived DF4 iPSC-RPE lacking tight junctions (ZO-1 negative). Scale bar=50μm.

DF4 iPSC-RPE derived by the 14-day method showed abnormal non-nuclear staining of OTX2 and MITF (Fig. 5A, 5B). In some cells, ZO-1 was absent or localized to the cytoplasm (Fig. 5E, arrowheads), indicating a potential loss of junctional integrity, which has been previously observed in RPE cell lines after exposure to oxidative stressors [29] and EMT [30], and correlates with the poor morphology of these cells (Fig. 3C, arrowheads). Expression of PMEL and RPE65 localized as expected in 14-day-derived DF4 iPSC-RPE (Fig. 5C, 5D), however only patches of cells stained positive for RPE65 while others were devoid of signal (Fig. 5D). These findings parallel results depicted in Figure 3, showing the capacity of DF4 iPSC to generate and propagate mature RPE using the 14-day method is limited. Importantly, none of the cell lines expressed TRA1-81, a marker for pluripotent cells, when derived by the SCAC or 14-day methods (Fig. 5F).

Functional Comparison of SCAC and 14-day Differentiation Methods

RPE have numerous critical functions that maintain photoreceptor health [12]. To determine the functionality of the iPSC-RPE lines and elucidate any discrepancies between lines we performed two established tests to examine phagocytic abilities and PEDF secretion.

Phagocytosis was determined by internalization of FITC-labeled bovine-isolated ROS. Data were then calculated as a percent change from fRPE ROS treatment to statistically compare all lines and methods. Importantly, cells were also treated with a function blocking αVβ5 antibody, the critical integrin associated with phagocytosis in RPE. In all iPSC-RPE, fRPE and hESC-RPE lines, the anti-αVβ5 antibody significantly reduced phagocytosis compared to the ROS condition (Fig. 6A, $p \leq 0.05$). This

distinguished that the RPE were phagocytosing, not endocytosing ROS, and were using the same mechanism known in vivo [31]. DF4 and DF9 lines showed no differences in phagocytic abilities between SCAC and 14-day directed differentiation (Fig. 6A). However, the 14-day-derived MyCell iPSC-RPE line showed significantly more phagocytosis than the SCAC-derived MyCell line (Fig. 6A). There was no significant difference in phagocytosis between iPSC-RPE lines for either method. Fetal RPE were used as a positive control; many have published that their phagocytosis rate is low when compared to hESC-RPE, and the same phenomena was observed when compared to iPSC-RPE [20, 21, 28].

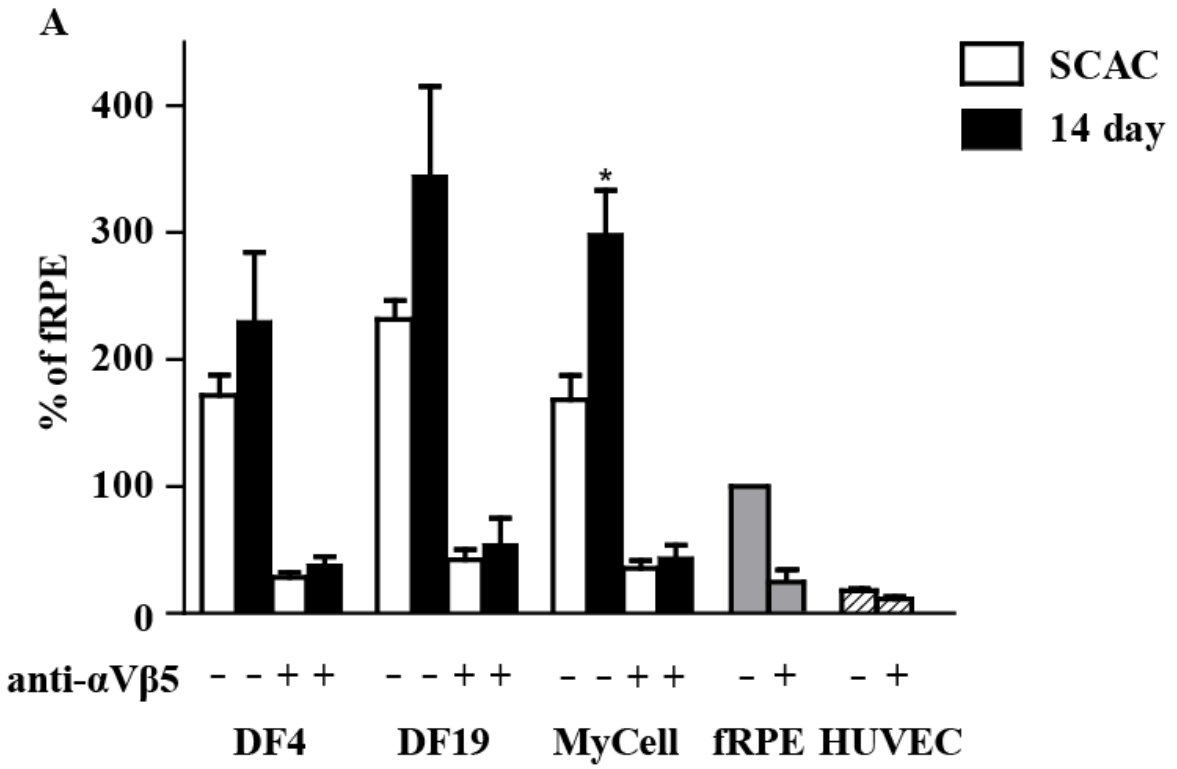
A
SCAC
14 day
% of fRPE
400
300
200
100
0
*
anti-αVβ5 - - + + - - + + - - + + - + - +
DF4
DF19
MyCell
fRPE
HUVEC

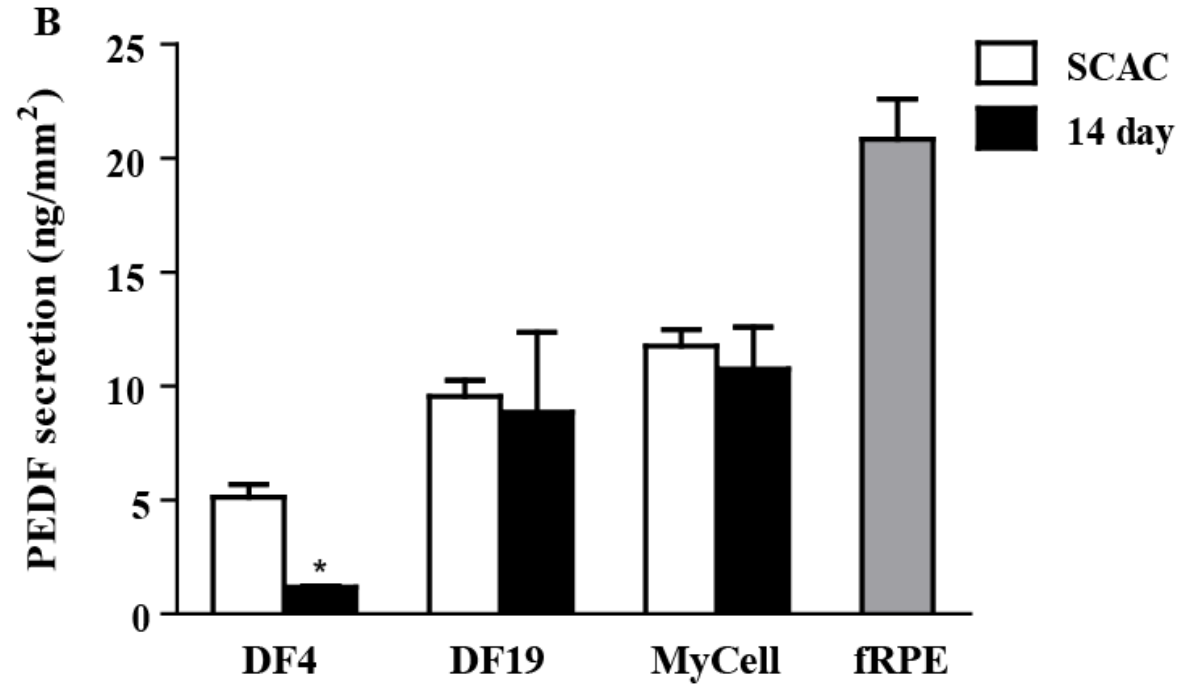
B
SCAC
14 day
PEDF secretion (ng/mm2)
25
20
15
10
5
0
*
DF4
DF19
MyCell
fRPE

Figure 6. Functional analysis of iPSC-RPE lines and fRPE. (A) RPE phagocytosis of bovine photoreceptor outer segments (ROS) as determined by pixel density percent change of fRPE ROS condition. ROS condition displayed with αVβ5 functional blocking antibody analysis. fRPE and HUVECs serve as positive and negative controls, respectively. All experiments are normalized to a single ARPE19 ROS experiment data set. 14-day-derived MyCell iPSC-RPE showed significantly more phagocytosis than SCAC-derived MyCell iPSC-RPE. All lines showed significantly decreased phagocytosis following anti- αvβ5 treatment. (B) ELISA analysis of PEDF. 14-day-derived DF4 iPSC-RPE secreted a lower level of PEDF than SCAC-derived DF4 iPSC-RPE. Error bars represent ± SEM. *$p \leq 0.05$, $n \geq 3$, separate enrichments for all experiments.

IPSC-RPE were also compared to hESC-RPE differentiated using the same method. DF4 and MyCell SCAC-derived iPSC-RPE phagocytosed less than H9 hESC-RPE (Supp. Fig. 4A). However, MyCell 14-day-derived iPSC-RPE showed an increase in phagocytosis from 14-day-derived differentiated UCSF4 hESC-RPE (Supp. Fig. 4B). It is important to note that H9 hESC-RPE and UCSF4 hESC-RPE cannot be directly compared. Overall, it appeared that all iPSC-RPE lines, independent of method, were phagocytosing significantly more than the HUVEC negative control line and were doing so using the known in vivo mechanism.

To detect for PEDF secretion, an ELISA was performed on medium collected following a 24 hour exposure to each iPSC-RPE line and was compared to fRPE PEDF levels (Fig. 6B). DF4 iPSC-RPE created using the 14-day method secreted significantly lower amounts of PEDF than the SCAC-derived DF4 iPSC-RPE. DF19 and MyCell lines displayed no difference in secretion between methods. SCAC-derived DF4 iPSC-RPE line was significantly lower than SCAC DF19 and MyCell iPSC-RPE ($p \leq 0.01$). PEDF secretion for the 14-day differentiated DF4 iPSC-RPE was significantly decreased compared to 14-day-derived MyCell iPSC-RPE ($p \leq 0.01$). PEDF levels in all lines, independent of method, were significantly lower than fRPE PEDF secretion ($p \leq 0.05$). (SCAC-derived H9 hESC-RPE secretion = 19.23±0.62ng/mm^2 and 14-day-derived UCSF4 hESC-RPE levels = 20.04±2.99 ng/mm^2).

Discussion

As iPSC technology continues to broaden in application for regenerative studies and more iPSC-derived cellular products move toward the clinic, establishing release analyses to assess quality and minimize variability between lines will be essential.

Using a multitude of assays to examine RPE maturity and function, this study provides an extensive comparison between multiple iPSC-RPE lines derived by established methods. Our results showed that all three iPSC lines characterized in this study generated RPE using the SCAC and 14-day directed differentiation methods; however, differences were found between derivation methods within the same iPSC-RPE line. Further, we observed line-by-line variation when using the same method, which has been previously reported with RPE [13, 18, 32], and other cell types derived from iPSC [32-36]. Overall, independent of differentiation method, the DF19 and MyCell lines produced the highest quality iPSC-RPE as determined by morphology, expression of RPE-specific genes, and functional analyses, while the DF4 line was the least robust.

A comparison to fRPE and hESC-RPE revealed iPSC-RPE derived by both methods secreted lower levels of PEDF and expressed lower levels of RPE genes related to visual cycle function (RPE65 and CRALBP), epithelial barrier function (BEST1), and RPE lineage (MITF2). These results are in agreement with other studies showing iPSC are not as efficient in generating RPE [20, 37, 38] and may take slightly longer to differentiate to retinal lineages than hESC [35, 39]. In contrast, however, iPSC-RPE derived by both methods expressed pigment-specific genes (PMEL and TYR) comparable to hESC-RPE (with some exceptions in 14-day-derived DF4 iPSC-RPE) and were able to outperform fRPE ROS phagocytosis in vitro. These discrepancies further underscore the need for standardized assays that accurately test RPE quality between lines. Since DF4 iPSC-RPE derived by the 14-day method showed the poorest performance in all assays except ROS phagocytosis, other analyses such as PEDF

secretion and expression of RPE function markers may be better indicative of a true RPE lineage.

Based on low expression levels of RPE65 in 14-day RPE (iPSC- and hESC-derived) compared to SCAC-derived cells, it is plausible that the 14-day RPE are not of lower quality, but are simply just immature, which may account for some of the differences we observed between differentiation methods. As more groups, including our own, develop protocols to push pluripotent cells toward RPE and other lineages in less time, it will be important to keep this question in mind - how fast can we speed up development in vitro? We showed that maturing 14-day-derived DF4 and DF19 iPSC-RPE for an additional 30 days significantly boosts expression of RPE65 (Fig. 4B), which is a critical regulator of visual cycle function, indicating longer time in culture may be essential for cells to develop properly. Importantly, we found all five iPSC lines originally used for this study could be induced to differentiate to RPE using the 14-day protocol, albeit with varying efficiencies, while two lines were unable to generate usable quantities of RPE with SCAC differentiation. These results indicate that some iPSC lines may require a more directed approach to produce enough cells for characterization and could be a case for using directed methods over a longer, spontaneous approach.

The original source of donor cells and the method of reprogramming are possible explanations for the differences seen in the quality of RPE differentiation between iPSC lines. MyCell iPSC were derived from T cells, while DF4 and DF19 iPSC were derived from foreskin fibroblasts [25]. Previous studies have shown RPE and neuroretinal cell types can be differentiated from T cell- and fibroblast-derived iPSC

[18, 20, 35, 38-42]; however characterized RPE have not been compared based on somatic cell origin. We found that DF19 and MyCell iPSC were broadly comparable in RPE derivation capability; thus it is unlikely, at least for the purposes of this study, that identity of the source cells contributed considerably to the ability of iPSC to differentiate to RPE. Further, DF4, DF19, and DF6 iPSC, all derived from the same foreskin fibroblast line [2, 25], showed substantial differences in RPE generation capacity. DF6 iPSC were unable to generate enough RPE for characterization using SCAC without contaminating cell types in the culture. This suggests that the method of reprogramming to iPSC may be more strongly contributing to RPE differentiation variability between lines. All three foreskin fibroblast-derived iPSC lines (DF4, DF19 and DF6) were reprogrammed using EBV-based episomal systems; however, different transgene arrangements and combinations of episomal vectors were used to induce pluripotency for each line [25]. It has been suggested that maintaining a balance between transgene expression levels is crucial for efficient reprogramming [43]. Thus it is possible that DF4 and DF6 iPSC lines may not be efficiently reprogrammed compared to DF19, and as a consequence, may have more limited differentiation and expansion capacity as RPE.

In summary, these data present a comparison between RPE differentiation methods for multiple iPSC lines, showing variability in RPE derivation capacity not only between methods, but also between iPSC lines within the same method. Furthermore, we showed that poorly differentiated iPSC-RPE (DF4) still performed ROS functional assays, that 14-day-derived RPE could be matured in culture for 30 days to improve RPE-specific marker expression, and that some iPSC lines may require directed

differentiation to generate enough RPE for characterization. As iPSC-RPE become more clinically applicable, these results have potentially important implications for developing standardized release assays, optimizing iPSC reprogramming methods, and developing superior iPSC lines as well as culture methods to use for patient therapy.

References

1. Takahashi, K. and S. Yamanaka, *Induction of pluripotent stem cells from mouse embryonic and adult fibroblast cultures by defined factors.* Cell, 2006. **126**(4): p. 663-76.
2. Yu, J., et al., *Induced pluripotent stem cell lines derived from human somatic cells.* Science, 2007. **318**(5858): p. 1917-20.
3. Walmsley, G.G., et al., *Induced pluripotent stem cells in regenerative medicine and disease modeling.* Curr Stem Cell Res Ther, 2014. **9**(2): p. 73-81.
4. Okano, H., et al., *Steps toward safe cell therapy using induced pluripotent stem cells.* Circ Res, 2013. **112**(3): p. 523-33.
5. Harding, J. and O. Mirochnitchenko, *Preclinical studies for induced pluripotent stem cell-based therapeutics.* J Biol Chem, 2014. **289**(8): p. 4585-93.
6. Kamao, H., et al., *Characterization of human induced pluripotent stem cell-derived retinal pigment epithelium cell sheets aiming for clinical application.* Stem Cell Reports, 2014. **2**(2): p. 205-18.
7. Kanemura, H., et al., *Tumorigenicity studies of induced pluripotent stem cell (iPSC)-derived retinal pigment epithelium (RPE) for the treatment of age-related macular degeneration.* PLoS One, 2014. **9**(1): p. e85336.
8. Carr, A.J., et al., *Protective effects of human iPS-derived retinal pigment epithelium cell transplantation in the retinal dystrophic rat.* PLoS One, 2009. **4**(12): p. e8152.
9. Klein, R., et al., *Prevalence of age-related macular degeneration in the US population.* Arch Ophthalmol, 2011. **129**(1): p. 75-80.
10. Friedman, D.S., et al., *Prevalence of age-related macular degeneration in the United States.* Arch Ophthalmol, 2004. **122**(4): p. 564-72.
11. Lim, L.S., et al., *Age-related macular degeneration.* Lancet, 2012. **379**(9827): p. 1728-38.
12. Strauss, O., *The retinal pigment epithelium in visual function.* Physiol Rev, 2005. **85**(3): p. 845-81.
13. Hu, Q., et al., *Memory in induced pluripotent stem cells: reprogrammed human retinal-pigmented epithelial cells show tendency for spontaneous redifferentiation.* Stem Cells, 2010. **28**(11): p. 1981-91.
14. Croze, R.H., *Differentiation of Pluripotent Stem Cells into Retinal Pigmented Epithelium*, in *Cell-Based Therapy for Retinal Degenerative Disease. Developmental Opthalmology*, Z.M. Casaroli-Marano RP, Editor. 2014, Karger: Basel. p. 81-96.
15. Klimanskaya, I., et al., *Derivation and comparative assessment of retinal pigment epithelium from human embryonic stem cells using transcriptomics.* Cloning Stem Cells, 2004. **6**(3): p. 217-45.
16. Lund, R.D., et al., *Human embryonic stem cell-derived cells rescue visual function in dystrophic RCS rats.* Cloning Stem Cells, 2006. **8**(3): p. 189-99.
17. Carr, A.J., et al., *Molecular characterization and functional analysis of phagocytosis by human embryonic stem cell-derived RPE cells using a novel human retinal assay.* Mol Vis, 2009. **15**: p. 283-95.
18. Buchholz, D.E., et al., *Derivation of functional retinal pigmented epithelium from induced pluripotent stem cells.* Stem Cells, 2009. **27**(10): p. 2427-34.

19. Vugler, A., et al., *Elucidating the phenomenon of HESC-derived RPE: anatomy of cell genesis, expansion and retinal transplantation.* Exp Neurol, 2008. **214**(2): p. 347-61.
20. Buchholz, D.E., et al., *Rapid and efficient directed differentiation of human pluripotent stem cells into retinal pigmented epithelium.* Stem Cells Transl Med, 2013. **2**(5): p. 384-93.
21. Leach, L.L., et al., *Canonical/beta-catenin Wnt pathway activation improves retinal pigmented epithelium derivation from human embryonic stem cells.* Invest Ophthalmol Vis Sci, 2015. **56**(2): p. 1002-13.
22. Gourraud, P.A., et al., *The role of human leukocyte antigen matching in the development of multiethnic "haplobank" of induced pluripotent stem cell lines.* Stem Cells, 2012. **30**(2): p. 180-6.
23. Taylor, C.J., et al., *Generating an iPSC bank for HLA-matched tissue transplantation based on known donor and recipient HLA types.* Cell Stem Cell, 2012. **11**(2): p. 147-52.
24. Hu, K., et al., *Efficient generation of transgene-free induced pluripotent stem cells from normal and neoplastic bone marrow and cord blood mononuclear cells.* Blood, 2011. **117**(14): p. e109-19.
25. Yu, J., et al., *Human induced pluripotent stem cells free of vector and transgene sequences.* Science, 2009. **324**(5928): p. 797-801.
26. Beers, J., et al., *Passaging and colony expansion of human pluripotent stem cells by enzyme-free dissociation in chemically defined culture conditions.* Nat Protoc, 2012. **7**(11): p. 2029-40.
27. Maminishkis, A., et al., *Confluent monolayers of cultured human fetal retinal pigment epithelium exhibit morphology and physiology of native tissue.* Invest Ophthalmol Vis Sci, 2006. **47**(8): p. 3612-24.
28. Croze, R.H., et al., *ROCK Inhibition Extends Passage of Pluripotent Stem Cell-Derived Retinal Pigmented Epithelium.* Stem Cells Transl Med, 2014. **3**(9): p. 1066-78.
29. Bailey, T.A., et al., *Oxidative stress affects the junctional integrity of retinal pigment epithelial cells.* Invest Ophthalmol Vis Sci, 2004. **45**(2): p. 675-84.
30. Chen, H.C., et al., *Wnt signaling induces epithelial-mesenchymal transition with proliferation in ARPE-19 cells upon loss of contact inhibition.* Lab Invest, 2012. **92**(5): p. 676-87.
31. Lin, H. and D.O. Clegg, *Integrin alphavbeta5 participates in the binding of photoreceptor rod outer segments during phagocytosis by cultured human retinal pigment epithelium.* Invest Ophthalmol Vis Sci, 1998. **39**(9): p. 1703-12.
32. Toivonen, S., et al., *Comparative analysis of targeted differentiation of human induced pluripotent stem cells (hiPSCs) and human embryonic stem cells reveals variability associated with incomplete transgene silencing in retrovirally derived hiPSC lines.* Stem Cells Transl Med, 2013. **2**(2): p. 83-93.
33. Streckfuss-Bomeke, K., et al., *Comparative study of human-induced pluripotent stem cells derived from bone marrow cells, hair keratinocytes, and skin fibroblasts.* Eur Heart J, 2013. **34**(33): p. 2618-29.

34. Trakarnsanga, K., et al., *Qualitative and quantitative comparison of the proteome of erythroid cells differentiated from human iPSCs and adult erythroid cells by multiplex TMT labelling and nanoLC-MS/MS.* PLoS One, 2014. **9**(7): p. e100874.
35. Meyer, J.S., et al., *Modeling early retinal development with human embryonic and induced pluripotent stem cells.* Proc Natl Acad Sci U S A, 2009. **106**(39): p. 16698-703.
36. Hu, B.Y., et al., *Neural differentiation of human induced pluripotent stem cells follows developmental principles but with variable potency.* Proc Natl Acad Sci U S A, 2010. **107**(9): p. 4335-40.
37. Osakada, F., et al., *In vitro differentiation of retinal cells from human pluripotent stem cells by small-molecule induction.* J Cell Sci, 2009. **122**(Pt 17): p. 3169-79.
38. Zhu, Y., et al., *Three-dimensional neuroepithelial culture from human embryonic stem cells and its use for quantitative conversion to retinal pigment epithelium.* PLoS One, 2013. **8**(1): p. e54552.
39. Hirami, Y., et al., *Generation of retinal cells from mouse and human induced pluripotent stem cells.* Neurosci Lett, 2009. **458**(3): p. 126-31.
40. Phillips, J., L.G. Zirkle, and R.A. Gosselin, *Achieving locked intramedullary fixation of long bone fractures: technology for the developing world.* Int Orthop, 2012. **36**(10): p. 2007-13.
41. Reichman, S., et al., *From confluent human iPS cells to self-forming neural retina and retinal pigmented epithelium.* Proc Natl Acad Sci U S A, 2014. **111**(23): p. 8518-23.
42. Singh, R., et al., *Functional Analysis of Serially Expanded Human iPS Cell-Derived RPE Cultures.* Invest Ophthalmol Vis Sci, 2013. **54**(10): p. 6767-78.
43. Yamanaka, S., *Elite and stochastic models for induced pluripotent stem cell generation.* Nature, 2009. **460**(7251): p. 49-52.

Chapter III

ROCK Inhibition Extends Passage of Human Embryonic Stem Cell Derived Retinal Pigmented Epithelium

Introduction

Human embryonic stem cells (hESC) offer a potentially unlimited supply of cells for emerging cell-based therapies. Unfortunately, the process of deriving distinct cell types can be time consuming and expensive. Furthermore, differentiated cells typically have a finite lifespan and can only be passaged a limited number of times. Expanding the propagation potential of stem cell-derived cells would be extremely useful for transplantation procedures and drug screening efforts.

Clinical trials are currently under way using hESC derived retinal pigmented epithelial cells (hESC-RPE) as a treatment for age related macular degeneration (AMD) [1, 2]. In the developed world, AMD is the leading cause of blindness in the elderly with over 7.2 million people afflicted in the US alone [3, 4]. AMD is a progressive disorder that eventually results in RPE cell death, photoreceptor death, and profound loss of central vision. It is generally agreed that AMD pathology is primarily linked to the dysfunction and death of the RPE, which acts to support and maintain the photoreceptors. When the RPE degenerates, the photoreceptors can no longer function and they eventually die [5, 6]. There are two clinically recognized forms of disease, exudative (wet) AMD and atrophic (dry) AMD. The neovascular genesis component of wet AMD can be successfully managed using anti-vascular endothelial growth factor drugs such as Lucentis, Avastin or Eylea [7]. However, these drugs do not act to inhibit the underlying RPE degeneration and patients with wet AMD can progress to more advanced stages of atrophic AMD characterized by macular regions devoid of RPE and photoreceptors [8, 9]. Outside of a vitamin cocktail which can only slow the progression

of AMD in 25% of patients taking the supplement, there is no effective treatment for dry AMD [10, 11].

Both hESC-RPE and induced pluripotent stem cell derived RPE (iPSC-RPE) [12] are being developed for AMD therapies by multiple groups, using either cell suspensions or differentiated monolayers on scaffolds [13]. The current preferred derivation process for RPE follows a spontaneous differentiation protocol involving the removal of fibroblastic growth factor 2 (FGF2) in continuously adherent cultures of pluripotent stem cells [1, 14]. This method can take up to 100 days before enrichment of the pigmented population followed by several months of additional culture to obtain relatively homogeneous, mature RPE ready for transplantation. hESC-RPE, iPSC-RPE and fetal RPE are passaged every 30 days and can only be maintained in culture for five to six passages before the cells display abnormal characteristics and are thought to undergo an epithelial-to-mesenchymal transition (EMT) [15-18]. Some reports have claimed an even more limited passage potential for iPSC-RPE, finding only one passage following enrichment was possible [19]. These late passage cells lose their pigmented, cobblestone morphology and appear more fibroblastic, and often senesce and die. Senescence in cultured primary somatic cells is commonly observed as telomeres shorten and the Hayflick limit is reached [20].

To attempt to overcome this passage limitation, we examined the involvement of Rho-associated, coiled-coil protein kinase (ROCK) in hESC-RPE and iPSC-RPE culture. Two distinct ROCK isoforms, ROCK1 and ROCK2, are activated by RHOA GTPase and initiate signal transduction cascades to modulate central cell functions, including proliferation, apoptosis, cytoskeletal rearrangements, and migration [21-23]. The

RHOA/ROCK pathway has been studied extensively for its downstream effects on stress fiber formation [24, 25] and actin filament stabilization [21, 26]. ROCK inhibition using synthetic compounds is currently being tested in clinical trials for pulmonary hypertension treatments with positive animal model results [23, 27, 28]. Current research suggests increasing roles for ROCK inhibitors, including ROCK1/2 inhibitor Y-27632, in regulating various cell processes [23, 29-31]. Previous studies have showed ROCK inhibition increased passage abilities of certain epithelial cell types [32-36], as well as the clonability of hESC [37, 38]. We have previously shown the beneficial effects of Y-27632 treatment following initial enrichment of RPE during directed differentiation from hESC [39].

Here we report that inhibiting ROCK1/2 with Y-27632 allows extended passage of hESC-RPE. Importantly, the resulting hESC-RPE cells maintain proper gene expression, protein localization, function, and karyotype. We also show evidence that iPSC-RPE extended passage is possible following ROCK1/2 inhibition as well. The simple culture methods described here allow a much greater yield of hESC-RPE and iPSC-RPE and can provide abundant cells for disease modeling, drug screening and further development of cellular therapies.

Materials and Methods

Cell Culture

Pluripotent Stem Cell Culture

H9 hESC were obtained from the WiCell Research Institute in Madison, WI. Vector free iPSC lines, DF 4.9, DF 19.11 and Mycell were obtained from David Gamm and James Thomson (University of Wisconsin, Cellular Dynamics International). hESC

and iPSC were maintained in mTeSR1 medium (STEMCELL Technologies, Vancouver, Canada) and grown on Matrigel coated plates (1:100 dilution, BD Biosciences, San Jose, CA, USA) at 37°C 5% CO_2 under normoxic conditions.

Continuously Adherent Retinal Pigmented Epithelium Differentiation and Enrichment

H9 hESC and iPSC were passaged onto Matrigel coated plates and allowed to overgrow for 8-14 days. mTeSR1 medium was then changed to X-VIVO 10 (Lonza, Basal, Switzerland), after which the X-VIVO 10 medium was changed every other day. X-VIVO 10 is a xeno-free medium that has been used with cells designed for therapeutic use and increases the efficiency of RPE differentiation [40]. Pigmented cells typically appeared after 4-6 weeks. After 90 days in X-VIVO 10, non-pigmented cells were removed via mechanical dissection and the remaining, mostly pigmented cells, were incubated with TrypLE Express (Life Technologies, Grand Island, NY, USA) for 5 minutes at 37°C. The resulting hESC-RPE or iPSC-RPE enriched cell suspension was passed through a 30μm strainer and replated on Matrigel coated plates using X-VIVO 10. Enriched RPE cultures were maintained at 5% CO_2 and 37°C in X-VIVO 10. The medium was changed every other day. Every 30 days the cells were harvested using TrypLE Express and replated at a density of 100,000 cells/cm^2. All passage 2 cells used in comparison to passage 13 Y-27632 treated cells were cultured following this method.

Extended Passage Protocol of hESC-RPE and iPSC-RPE

Directly following enrichment, hESC-RPE or iPSC-RPE were plated into four Matrigel coated wells at 25,000 cells/cm^2 in X-VIVO 10. Two wells were treated with Y-27632 (10μM, Tocris Bioscience, Bristol, UK) and the other two received an equal volume of water, as a control. One day post confluence (~4-5 days), one Y-27632

treated well and one control well were passaged and seeded again at 25,000 cells/cm^2. Passaging continued in this fashion until cells failed to reach confluence. The two wells not undergoing passaging continued to be supplemented with 10μM Y-27632 or water for 14 days. On day 30 RNA was harvested and images were taken on the Olympus CKX41 (Olympus, Center Valley, PA, USA). Passage 13 hESC-RPE used in all experiments were derived using this protocol. The extended passage experiment was performed with seven separate enrichment cultures of H9 hESC-RPE and three enrichments per iPSC-RPE line. Each 'n' represents a unique enrichment from a distinct H9 culture for every experiment.

MTT Assay

To determine the effect of ROCK inhibition on hESC-RPE cell proliferation, cells were plated into 96 well plates in X-VIVO 10 and allowed to attach for 2 hours. hESC-RPE are extremely adherent and we observe that following only 2 hours, most of the cells have attached. The medium was then removed and replaced with fresh X-VIVO 10 with or without 10μM Y-27632. The media were changed every two days for the duration of the experiment with continual Y-27632 supplementation. Cell proliferation was assessed by determining the number of viable cells using a MTT (3-(4,5-Dimethylthiazol-2-yl)-2,5-Diphenyltetrazolium Bromide) assay according to supplier instructions (Life Technologies, Carlsbad, CA, USA).

Quantitative Real Time PCR (QRT-PCR)

Total RNA was isolated using the Qiagen RNeasy Plus Extraction Kit (Qiagen, Valencia, CA, USA) and cDNA was generated using an iScript cDNA synthesis kit (BioRad). The extent of expression of genes of interest was then evaluated in triplicate

for using the following TaqMan gene expression assays (Life Technologies): RPE specific protein 65kDa (RPE65) Hs01071462_m1; bestrophin 1 (BEST1) Hs00188249_ml; retinaldehyde binding protein 1 (RLBP1) Hs00165632_ml; microphthalmia-associated transcription factor (MITF) isoform 2 AJD1S3G; premelanosome protein (PMEL) Hs00173854_m1; tyrosinase related protein 1 (TYRP1) Hs00167051_m1; tyrosinase (TYR) Hs00165976_ml; paired box 6 (PAX6) Hs01088112_m1; marker of proliferation Ki-67 (MKI67) Hs01032443_m1; zinc finger protein 42 (REX1) Hs01124465_m1; spalt-like transcription factor 4 (SALL4) Hs00360675_m1; microtubule-associated protein 2 (MAP2) Hs00258900_m1; integrin, alpha 2 (ITGA2) Hs00158127_m1; platelet/endothelial cell adhesion molecule 1 (PECAM1) Hs00169777_m1; S100 calcium binding protein A4 (S100A4) Hs00243202_m1; and housekeepers: eukaryotic translation initiation factor 2B, subunit 2 beta (EIF2B2) Hs00204540_m1; ubiquitin-conjugating enzyme E2R 2 (UBE2R2) Hs00215107_m1; and small EDRK-rich factor 2 (SERF2) Hs00428481_m1 (Life Technologies). The relative level of expression for each gene was determined by normalizing to the geometric mean of the housekeeping gene set using CFX Manager (Bio-Rad) and Excel software.

Immunocytochemistry (ICC)

Passage 2 hESC-RPE and passage 13 Y-27632 maintained hESC-RPE were seeded onto Matrigel coated 8-chambered slides at 100,000 cells/cm^2. The passage 13 hESC-RPE were treated with 10μM Y-27632 for 14 days in medium described in Maminishkis et al. [41]. Forty-five days after plating, the cells were washed with phosphate-buffered saline (PBS, Life Technologies) and fixed with 4% paraformaldehyde in 0.1M sodium

cacodylate buffer (pH 7.4) for 7 minutes at 4°C. The fixed cells were then washed with PBS and blocked with PBS containing 5% bovine serum albumin (BSA) and 0.2% Triton X-100 for 1 hour at 4°C. The cells were then probed with primary antibodies against MITFC5 (1:1000, Abcam, Cambridge, MA, USA), orthodenticle homeobox 2 (OTX2) (1:4000 Millipore, Billerica, MA, USA), RPE65 (1:100, Abcam), BEST1 (1:100, Abcam), PMEL (1:100, Abcam), tight junction protein ZO-1 (TJP1) (1:100, Life Technologies), or MKI67 (1:1000, Abcam), in PBS with 5% BSA overnight at 4°C. Following 3 washes to remove the primary antibodies, they were incubated with appropriate Alexa Fluor conjugated secondary antibody (1:300, Life Technologies) for 1 hour at 4°C. Following the incubation with secondary antibody, cellular DNA was labeled by the addition of Hoescht (2μg/ml, Life Technologies) to the medium for 5 minutes at room temperature. The labeled cells were then washed with PBS and mounted with Prolong Gold Anti-fade and imaged using epifluorescent microscopy at 40X objective on a BX51 Olympus Microscopy. For both passages, five enrichments of hESC-RPE were probed with this panel of primary antibodies.

Karyotype analysis

Karyotyping of passage two and passage 13 hESC-RPE, from the same enrichment, was performed by Cell Line Genetics. Cells were analyzed prior to reaching confluence.

Rod Outer Segment (ROS) Phagocytosis Assay

hESC-RPE and human fetal RPE (fRPE, kindly provided by Lincoln Johnson (Center for the Study of Macular Degeneration, UCSB) and Dean Bok (Jules Stein Eye Institute, UCLA)) were cultured using the medium and methods of Maminishkis et al.

[41]. ARPE19 cells were cultured in Dulbecco's modified eagle medium with nutrient mix F12 and sodium pyruvate (DMEM/F12, Life Technologies), supplemented with GlutaMAXI (1X, Life Technologies), 10% FBS (Atlas Biologicals) and 15mM HEPES (Life Technologies). Human umbilical vein endothelial cells (HUVEC) were grown in endothelial cell growth medium with supplement mix (EGM, PromoCell, Heidelberg, Germany). All cells were plated in quadruplicate at 100,000 cells/cm^2 onto 0.1% gelatin-coated wells and cultured for 30 days. hESC-RPE passage 13 were treated with 10μM Y-27632 for 14 days.

Rod outer segments (ROS) were isolated from bovine retinas [42] (Sierra for Medical Science, Whittier, CA, USA) and fluorescently labeled with FluoReporter FITC Protein Labeling Kit (Life Technologies). The cultured cells were treated with or without αVβ5 function blocking antibody (62.5μg/ml, Abcam) or IgG (62.5μg/ml Abcam) isotype control for 30 minutes at 37°C 5% CO_2. Following the initial antibody incubation, the cells were challenged with $1x10^6$ FITC-ROS/well for 5 hours at 37°C 5% CO_2 [39, 43] in media supplemented with a fresh aliquot of antibody. After ROS incubation, the wells were washed 6X with PBS and then 0.4% trypan blue was added for 20 minutes to quench any fluorescence originating from residual extracellular ROS. Each well was imaged using epifluorescent microscopy and integrated pixel density of photomicrographs were generated with Image J software (National Institute of Health, Bethesda, MD, USA) using a rolling pixel radius of 50. The phagocytosis assay was performed with three independent enrichments of hESC-RPE. The fRPE and ARPE19 cells serve as positive controls and the HUVEC line was used as a negative control. All experiments were normalized to a single ARPE19 ROS experimental data set.

Pigment Epithelium Derived Factor (PEDF) and Vascular Endothelial Growth Factor (VEGF) Enzyme-Linked Immunosorbent Assay (ELISA)

Passage two hESC-RPE and passage 13 Y-27632 treated hESC-RPE were grown on Matrigel coated 0.45μm HA inserts (0.6cm^2, Millipore) seeded at 100,000 cells/cm^2 in medium described in Maminishkis et al. [41]. The hESC-RPE passage 13 cells were treated with 10 □M Y-27632 for 14 days. On day 30, media was collected from both the apical and basal chambers following a 72 hour exposure to the cells. The amount of pigment epithelium derived factor (PEDF) and vascular endothelial growth factor (VEGFA) in the basal and apical compartments were determined by ELISA according to the manufacturer's instructions (PEDF: BioProducts MD, LLC., Middletown, MD, USA; VEGFA: Life Technologies). All media volumes were kept constant and the growth area and volume were taken into consideration when calculating data.

Agilent Whole Human Genome Microarray

hESC-RPE were cultured following the extended passage protocol. At passage 5, control and Y-27632 lysates were collected two days after plating, prior to reaching confluence. RNA from four separate biological replicates was isolated using the Qiagen miRNeasy Kit (Qiagen) for each treatment group. Global transcriptome analysis was performed with the Agilent Whole Human Genome 4 × 44K in situ oligonucleotide array platform (G4112F, Agilent Technologies, Inc., Santa Clara, CA, USA) using the reagents and methods of the manufacturer and a 2-color experimental design, pairing the control and Y-27632 samples. After background and Lowess correction, the 200 replicate probe sets were averaged and the entire array data set was quantile normalized. Array data are reported as normalized net intensity levels.

Results

ROCK inhibition allows extended passage of hESC-RPE and iPSC-RPE

hESC-RPE or iPSC-RPE can typically only be passaged five to six times before undergoing a switch in phenotype suggestive of an epithelial-to-mesenchymal transition (EMT) and eventually senescing [15-18]. We sought to determine if inhibition of the Rho kinases, ROCK1 and ROCK2, could extend the effective passaging of hESC-RPE and iPSC-RPE. To test the role of ROCK1/2 in this process, the synthetic compound, Y-27632, which is a competitive inhibitor of the ATP binding domain of both ROCK1 and ROCK2 isoforms [23], was added to the culture medium, and cells were continuously passaged, plating at a fourth of the usual seeding density. For each passage, a portion of cells were grown for 30 days to allow them to mature and reach confluence, with removal of the ROCK inhibitor at day 14. Phase contrast images of the resulting cultures are shown in Figure 7. In contrast to untreated hESC-RPE, which underwent an EMT and failed to become confluent following five passages, Y-27632 treated cells were able to assume their typical RPE cobblestone morphology up to passage 14. However, after 15 passages, patches of larger cells displaying a mesenchymal morphology (examples shown by arrows) were intermixed with areas of cells with epithelial morphology. By passage 18, cells failed to reach confluence following 30 days in culture and never regained the typical RPE morphology. All iPSC-RPE lines acted in a similar fashion as hESC-RPE, but were not passaged beyond passage 13 (images not shown). Brightfield images of control passage 2 and Y-27632 treated passage 13 hESC-RPE, depicted in Supplemental Figure 5, show similar pigmentation patterns.

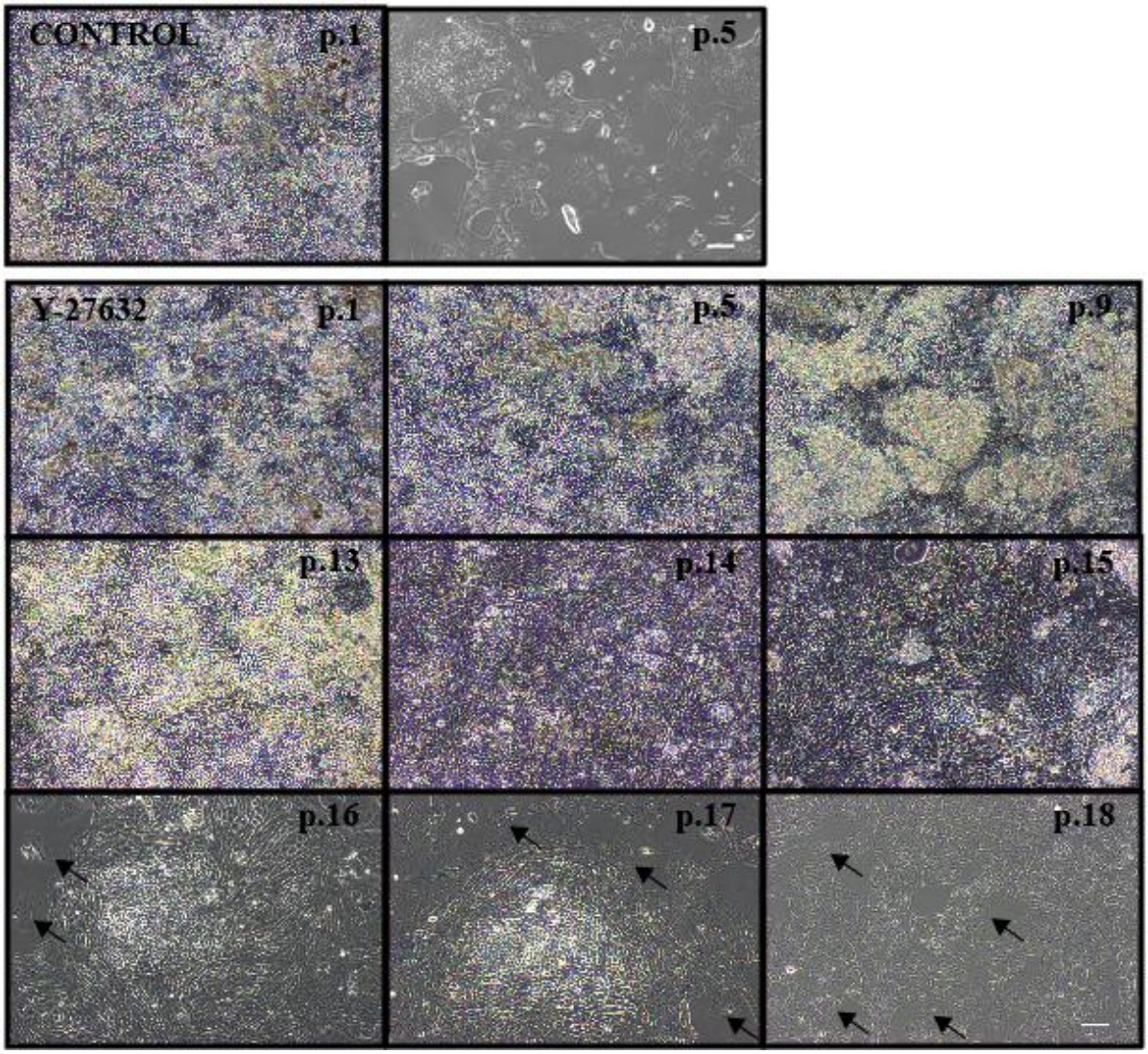

Figure 7. Effect of ROCK inhibition on hESC-RPE passage. Control hESC-RPE and Y-27632 treated hESC-RPE were serially passaged and cultured as detailed in *Methods*. Phase contrast images are shown of control and Y-27632-treated hESC-RPE, with passage number indicated in the upper right. All images were collected on day 30. Images are from a single experiment that is representative of nine experiments. Arrows indicate examples of cells with mesenchymal-like phenotype at passage 16, 17 and 18**.** Seeding density: 25,000 cells/cm^2. Scale bar=100μm.

To determine the effect of Y-27632 on the rate of proliferation cell counts were taken at each passage as hESC-RPE and iPSC-RPE underwent the extended passage protocol. Cells treated with Y-27632 showed a substantial increase in population doublings, allowing an average of 30 doublings compared to only 9 doublings in control cultures for both hESC-RPE and iPSC-RPE (Fig. 8A, B). In the presence of the ROCK inhibitor, cell numbers increase exponentially, with an average doubling time of 2.4 days, whereas the control doubling time was significantly longer with an average of 3.8 days, for hESC-RPE. There was some line to line variation in iPSC-RPE; however the average Y-27632 treated cell doubling time was 2.1 days compared to 3.6 days in control cells. All control cultures could not be propagated beyond 5 passages, suggesting that they had senesced.

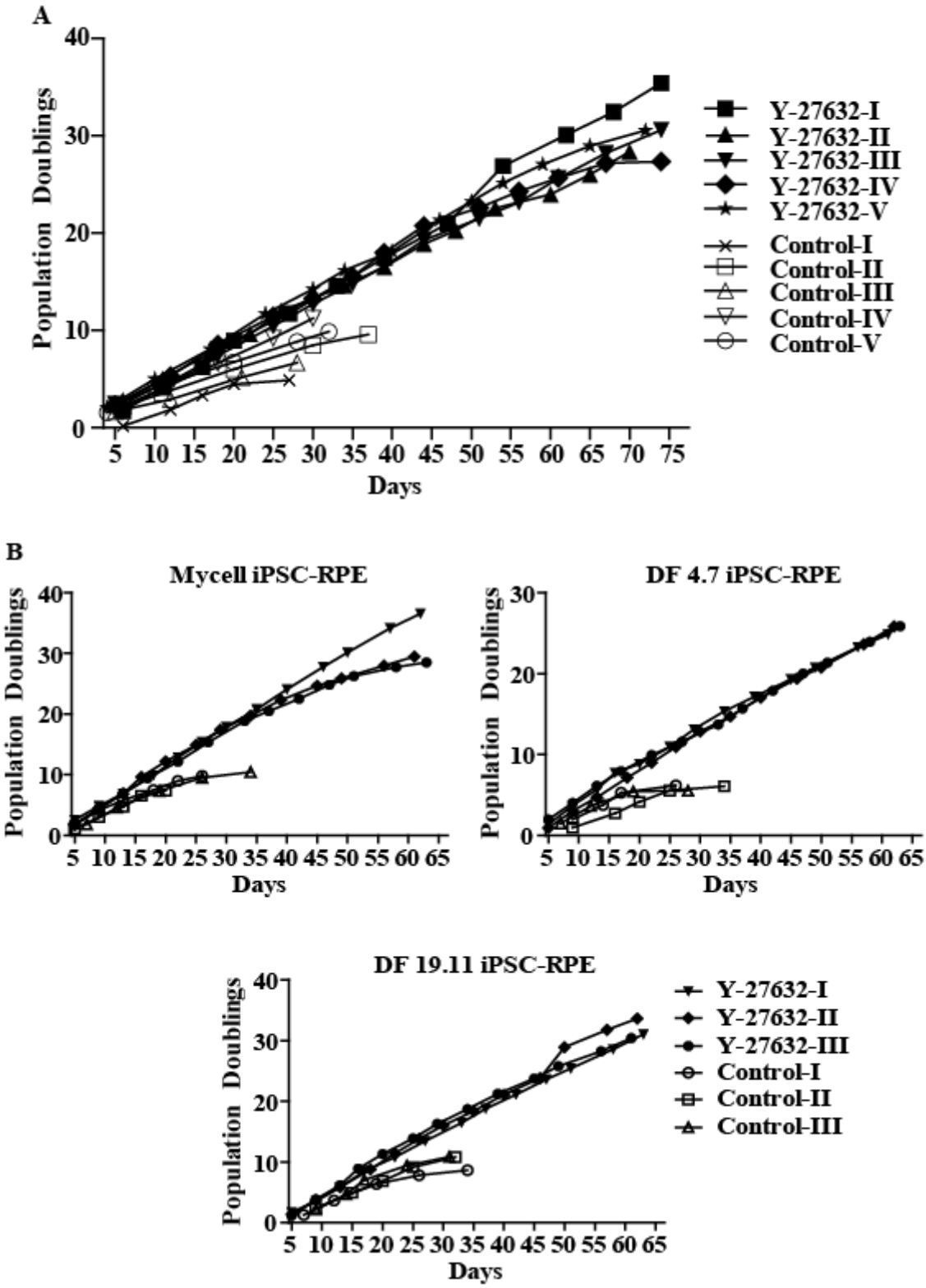
A
Population Doublings
Days
Y-27632-I
Y-27632-II
Y-27632-III
Y-27632-IV
Y-27632-V
Control-I
Control-II
Control-III
Control-IV
Control-V
B
Mycell iPSC-RPE
DF 4.7 iPSC-RPE
DF 19.11 iPSC-RPE
Population Doublings
Days
Y-27632-I
Y-27632-II
Y-27632-III
Control-I
Control-II
Control-III

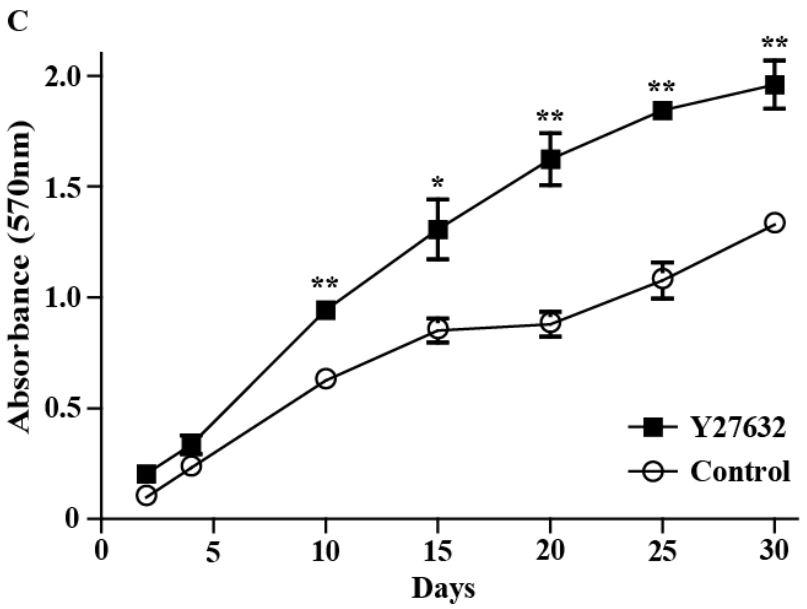

Figure 8. ROCK inhibition affects hESC-RPE proliferation. (A) Population doubling (PD) is plotted versus time in cultures with and without addition of Y-27632. Each point represents a passage, n=5. PD=$\log_2$(number of cells counted at time of passage/number of cells plated) (B) Population doubling of three iPSC-RPE lines throughout the extended passage protocol. n=3 per line. (C) Passage 4 hESC-RPE grown in the presence or absence of Y-27632 and cell number was quantified by measuring MTT reduction. Error bars represent ± SEM. *p≤0.05 **p≤0.01 compared to control for the same time point. n=3 (same enrichment).

In addition to monitoring cell expansion at the time of each passage, over numerous passages, cell proliferation was measured more directly within a single passage. Similar effects of Y-27632 on hESC-RPE growth rate were observed when the number of living cells within a single passage was monitored as a function of time using a MTT assay (Fig. 8C). When passage 4 hESC-RPE were grown in the continual presence or absence of Y-27632, a significant increase in the number of cells was detected by 10 days in the Y-27632 treated cells which persisted to at least day 30. Both control and Y-27632 treated passage 4 cells retained RPE morphology at day 30; however the characteristics of these particular cells at higher passages was not examined. This experiment shows that ROCK inhibition speeds up the rate of proliferation of hESC-RPE.

Gene expression during extended passage of hESC-RPE

In an effort to assess the effects of Y-27632 on gene expression we determined the relative amounts of a select set of RPE and non-RPE marker transcripts. As shown in Figure 9, control hESC-RPE showed a decrease in the abundance of RPE RNAs (RPE65, BEST1 RLBP1, and MITF) as a function of passage, with significant differences being observed at passage 5 (Fig. 9). Interestingly, levels of pigment related mRNAs, PMEL, TYRP1, and TYR, remained constant in untreated hESC-RPE. PAX6, a neural retina and immature RPE marker, increased over passage, but not significantly. In contrast, in Y-27632 treated hESC-RPE, all seven RPE marker RNA levels remained relatively stable over the course of 13 passages, and PAX6 mRNA levels did not increase. We believe that the larger error bars for several control passage 3 and passage 5 transcripts is due to the mixed population of cells arising within the well as the RPE begin to undergo EMT.

In addition, although Y-27632 treatment preserves the mitotic potential of hESC-RPE, there is no evidence for increased expression of MKI67, a marker of mitosis, in confluent 30 day old cultures of Y-27632 treated cells relative to that seen with untreated cells. This would imply that while cells proliferate more rapidly in the presence of Y-27632 (Fig. 8), the effects of Y-27632 are not lasting (Fig. 9). After removal of ROCK inhibition, cells reach confluence and exit from the cell cycle.

We also examined markers for pluripotency, and potential contaminating or transdifferentiated cell types. The level of the pluripotent mRNAs, REX1 and SALL4, remained negligible with extended passage, as did the neuronal marker MAP2, the smooth muscle marker ITGA2, the endothelial marker PECAM, and the fibroblastic marker S100A4. (See figure legend for positive control cell values for non-RPE gene markers).

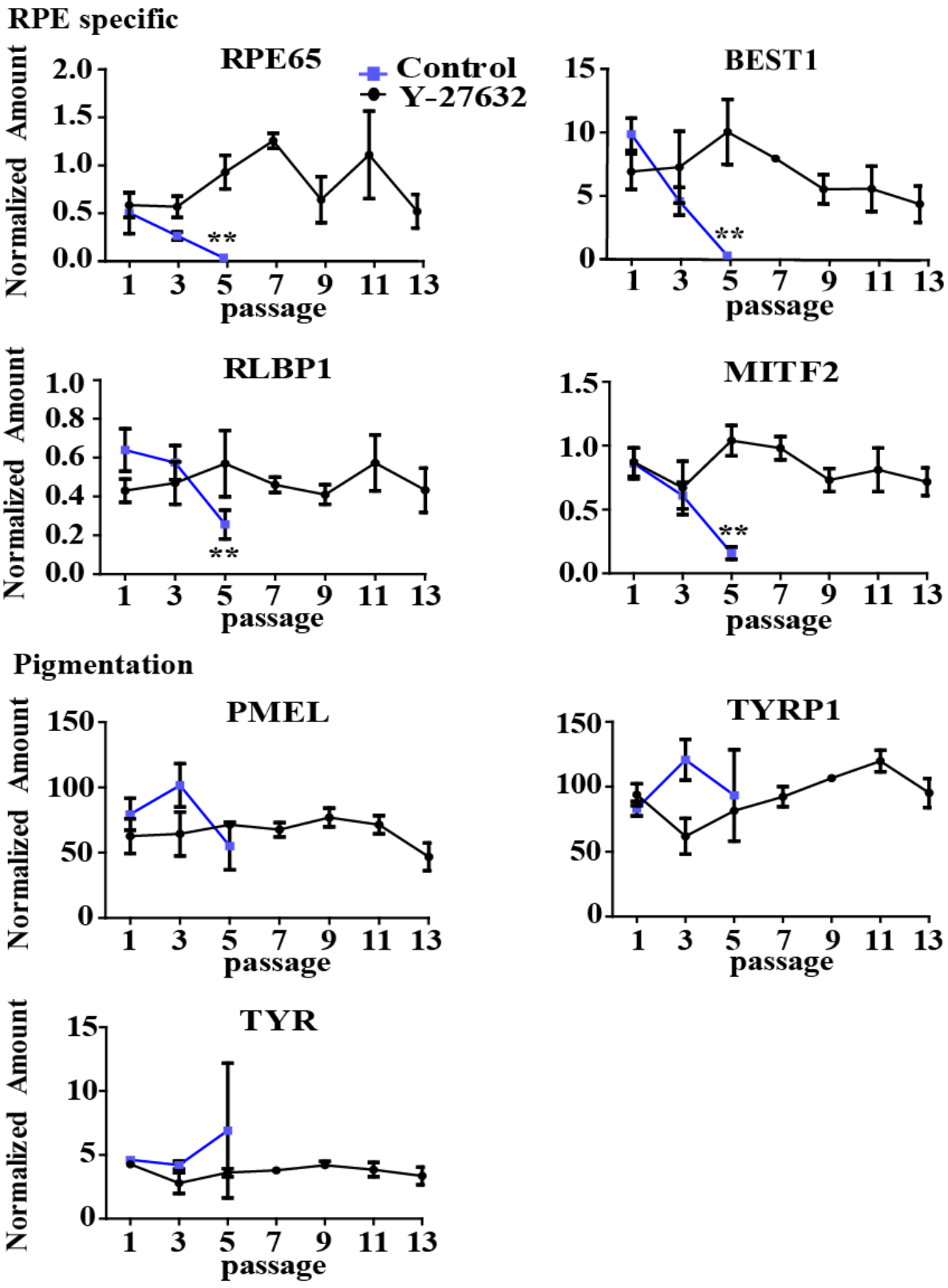
RPE specific
RPE65
Control
Y-27632
Normalized Amount
2.0
1.5
1.0
0.5
0.0
**
1 3 5 7 9 11 13
passage
BEST1
15
10
5
0
**
1 3 5 7 9 11 13
passage
RLBP1
1.0
0.8
0.6
0.4
0.2
0.0
**
1 3 5 7 9 11 13
passage
MITF2
1.5
1.0
0.5
0.0
**
1 3 5 7 9 11 13
passage
Pigmentation
PMEL
150
100
50
0
1 3 5 7 9 11 13
passage
TYRP1
150
100
50
0
1 3 5 7 9 11 13
passage
TYR
15
10
5
0
1 3 5 7 9 11 13
passage

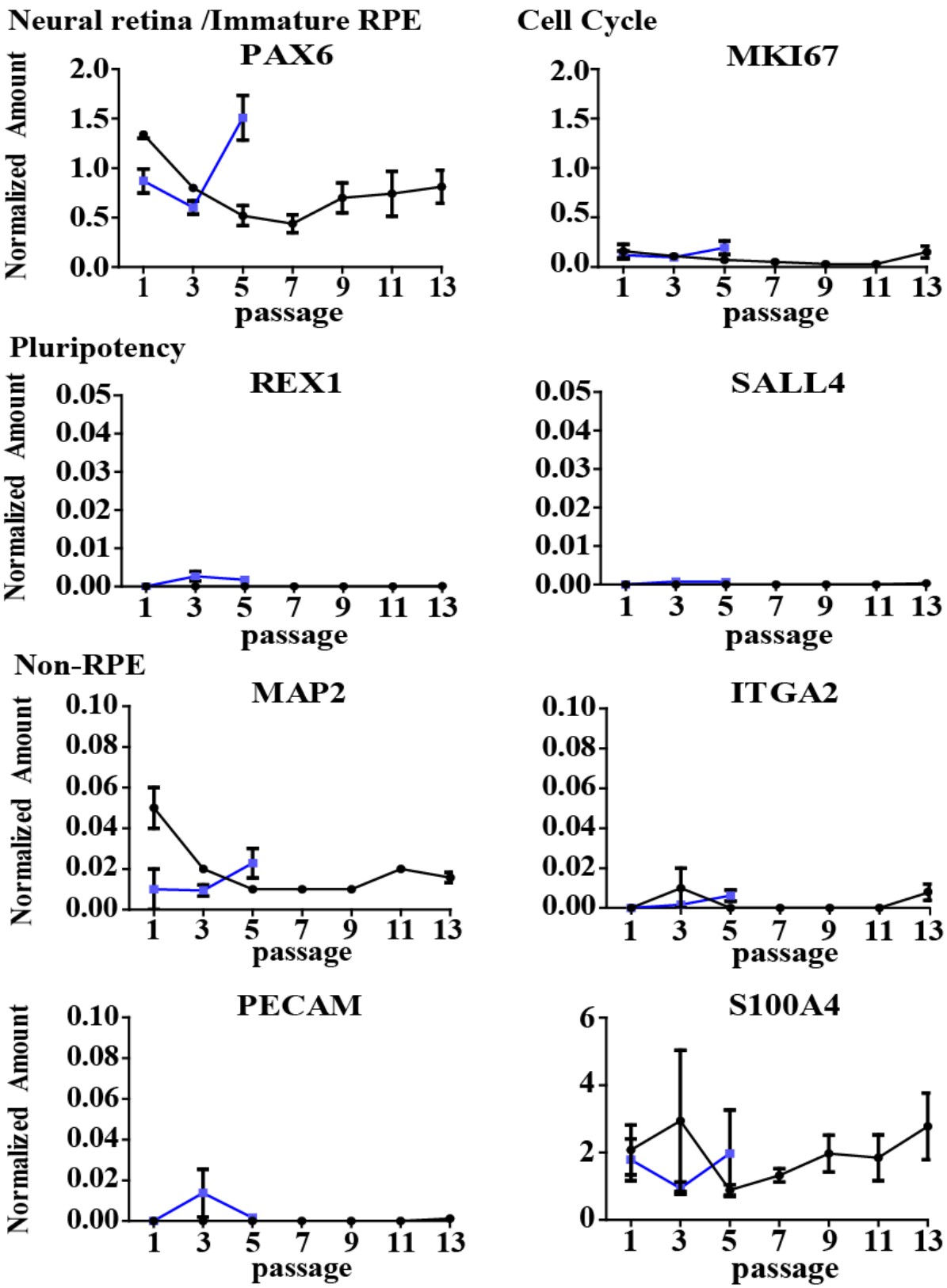
Neural retina /Immature RPE
PAX6
Normalized Amount
2.0
1.5
1.0
0.5
0.0
1 3 5 7 9 11 13
passage
Cell Cycle
MKI67
2.0
1.5
1.0
0.5
0.0
1 3 5 7 9 11 13
passage
Pluripotency
REX1
Normalized Amount
0.05
0.04
0.03
0.02
0.01
0.00
1 3 5 7 9 11 13
passage
SALL4
0.05
0.04
0.03
0.02
0.01
0.00
1 3 5 7 9 11 13
passage
Non-RPE
MAP2
Normalized Amount
0.10
0.08
0.06
0.04
0.02
0.00
1 3 5 7 9 11 13
passage
ITGA2
0.10
0.08
0.06
0.04
0.02
0.00
1 3 5 7 9 11 13
passage
PECAM
Normalized Amount
0.10
0.08
0.06
0.04
0.02
0.00
1 3 5 7 9 11 13
passage
S100A4
6
4
2
0
1 3 5 7 9 11 13
passage

Figure 9. Gene expression in extended passage hESC-RPE. RPE specific, pigmentation, neural retina/immature RPE, cell cycle, pluripotent and non-RPE gene expression was analyzed as a function of passage at 30 days post-plating. All data was normalized to geometric mean of three housekeeper mRNAs. Positive control cell values for non-RPE genes: H9 hESC, Rex 1 (4.09±0.09), Sall4 (10.93±0.45); SH-SY5Y, MAP2 (0.78±0.29); SMC, ITGA2 (2.02±0.24); HUVEC, PECAM (15.7±0.53); Hs27, S100A4 (20.13±1.09). Error bars represent ± SEM. *p≤0.05 **p≤0.01 compared to passage one within the same treatment group. n=3.

Protein expression and localization during extended passage of hESC-RPE

To assess whether there were any gross differences in protein localization between differentiated cultures of Y-27632 treated, extended passage cells versus minimally passaged control cells, 30 day cultures of each condition were evaluated using immunocytochemistry. Cells were probed with antibodies directed against the RPE marker proteins MITF, OTX2, RPE65, BEST1, PMEL, and ZO-1 (TJP1) as well as an antibody against the mitosis associated antigen, MK167 (Fig. 10). In all cases the pattern of protein localization was indistinguishable between control cells at passage 2 and Y-27632 treated cells at passage 13. The mature RPE markers BEST1 and RPE65 were both localized to the cytoplasm with additional localization of BEST1 to the plasma membrane being evident in passage 2. The pigmentation associated protein PMEL was found to be co-localized with distinct melanosomes and the tight junction protein ZO-1 (TJP1) to cell borders. Consistent with the lack of evidence for the presence of MKI67 mRNA in 30 day control passage 2 or Y-27632 treated passage 13 cells, no MIK67 immunoreactivity was detected.

Normal chromosomal arrangement was observed following karyotype analysis of control passage 2 and Y-27632 treated passage 13 cells (Supp. Fig. 6).

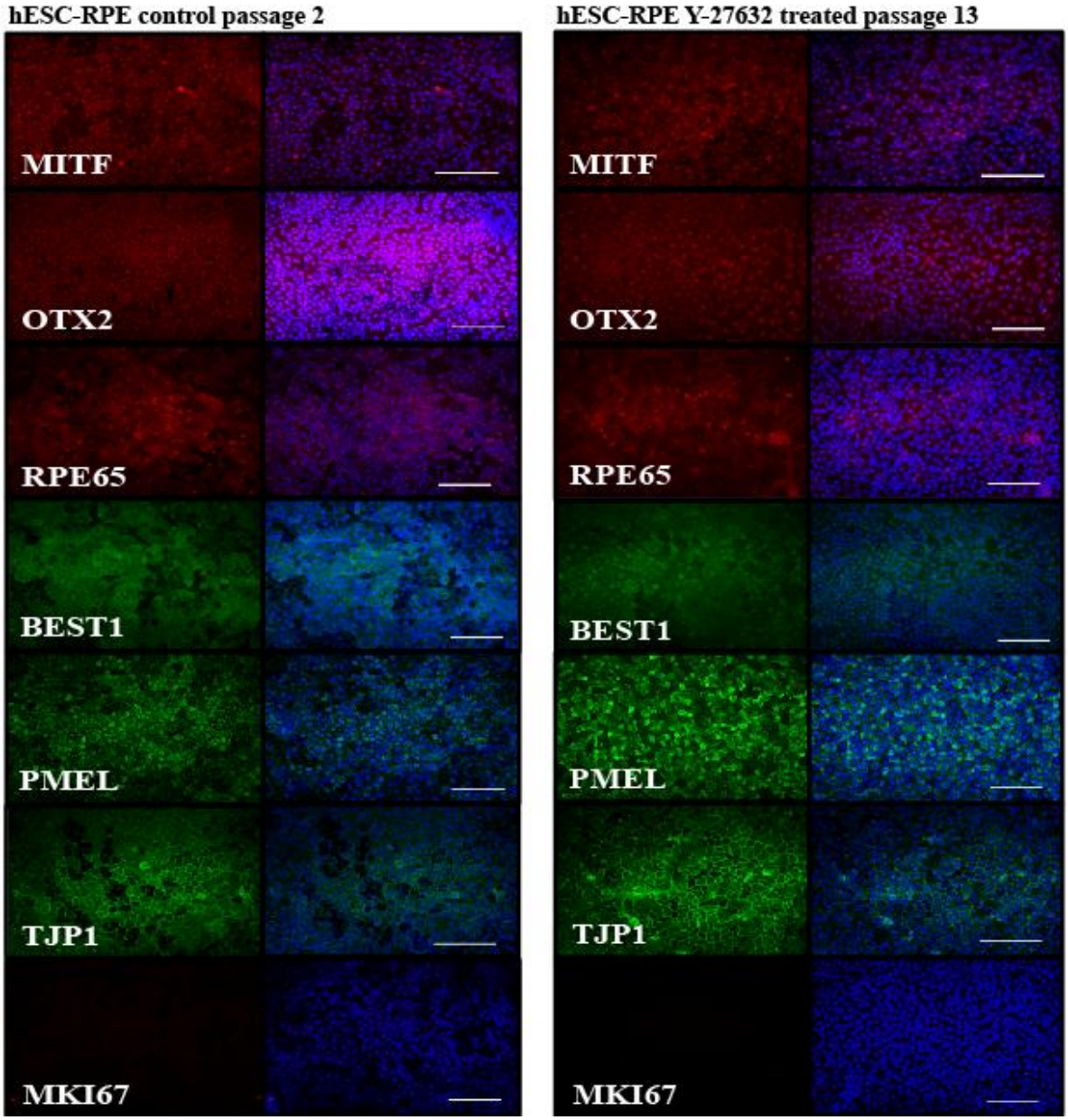

Figure 10. Protein expression and localization in extended passage hESC-RPE. Control passage 2 (left panel) and Y-27632 treated passage 13 (right panel) cells were stained for RPE markers and a mitotic marker after reaching confluence at day 30. Scale bars=100μm. Images shown are representatives of four experiments for each passage. Primary antibody stain is shown in left column and merged image with Hoescht (blue) is depicted in right column.

Functional analysis of extended passage hESC-RPE

The diurnal phagocytosis of photoreceptor outer segments, the apical secretion of PEDF, and basal VEGF secretion are critical RPE functions [44]. To examine these functions in extended passage hESC-RPE treated with the ROCK inhibitor, phagocytosis assays and ELISAs were performed. For the phagocytosis assays, hESC-RPE passage 2 and hESC-RPE passage 13 cells, as well as negative and positive control cells were challenged with FITC labeled bovine rod outer segments (ROS) and the extent ROS uptake was measured using quantitative immunofluorescence microscopy. Passage 13 Y-27632 treated hESC-RPE showed levels of phagocytosis similar to that seen in passage 2 control cells (Fig. 11A). To test whether phagocytosis occurred through the receptor-dependent mechanism utilized by RPE *in vivo*, cells were incubated with an integrin αVβ5 function blocking antibody prior to challenging with FITC labeled ROS. This integrin has been shown to be important for RPE phagocytosis [45]. There was a significant decrease in the amount of ROS internalization compared to IgG control treated cells (*$p \leq 0.05$) for fRPE, hESC-RPE passage 2 and hESC-RPE passage 13 cells after αVβ5 activity was blocked. This showed that phagocytosis requires the same integrin receptor after extended passage, and that passage 13 hESC-RPE retain normal phagocytosis activity.

For the determination of apical and basal growth factor secretion, media was collected from the inner and outer chambers of transwell hESC-RPE cultures and the amount of the PEDF and VEGF in the two media compartments was quantified. There was no significant difference for either apical or basal PEDF release between passage 2 and passage 13 hESC-RPE (Fig. 11B). The amount of basal VEGF secretion also

remained unchanged following extended passage in the presence of Y-27632, however there was 2-fold decrease in amount the apical VEGF in the passage 13 cultures compared to passage 2, but this did not reach significance (Fig. 11C).

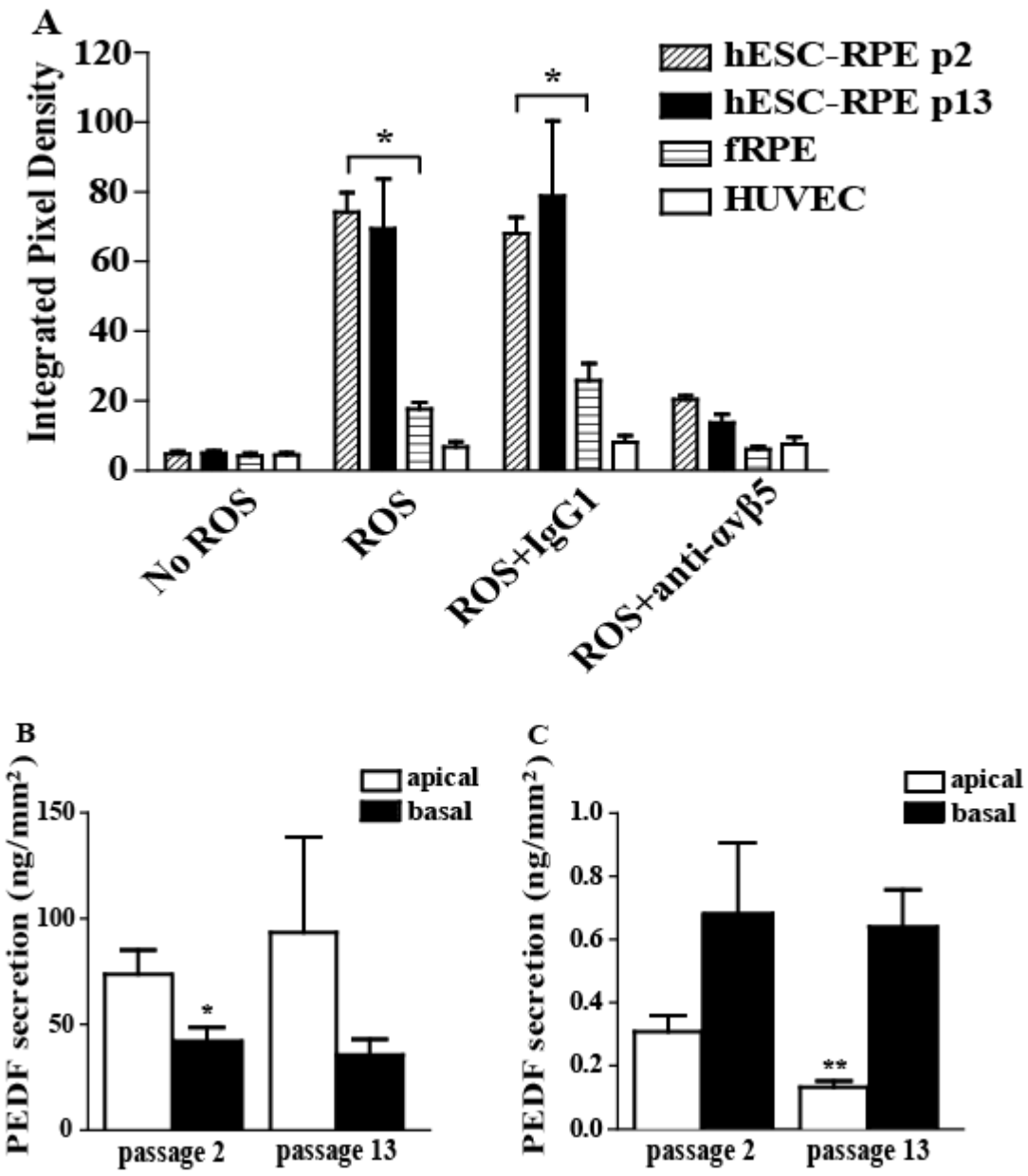

Figure 11. Function of extended passage hESC-RPE. (A) RPE phagocytosis of bovine photoreceptor outer segments, as determined by pixel density analysis of photomicrographs, is shown. fRPE and HUVECs serve as positive and negative controls, respectively. All experiments are normalized to a single ARPE19 ROS experiment data set. Isotype matched IgG was added as a negative control for the αVβ5 function blocking antibody. (B, C) ELISA analysis of PEDF and VEGF. Polarized hESC-RPE showed a higher level of apical PEDF and basal VEGF secretion, consistent between passages. Error bars represent ± SEM. *p≤0.05 **p≤0.01 (A) compared to samples treated with anti-αVβ5 (B, C) compared to secretion from opposite cell side. n=3 for all experiments.

ROCK inhibition affects transcript levels within many cell pathways

ROCK is known to be involved in numerous pathways within the cell, but its effect on gene transcription has not been fully examined. To gain more insight into how ROCK inhibition allows for extended passage of hESC-RPE, we assessed the global transcription patterns using cDNA microarray analysis in passage 5 control and Y-27632 treated cells, two days post-plating. Microarray analysis revealed that around 12,200 probes had above background signals. From those, just over 700 transcripts had at least a 1.5 fold change in each pairwise comparison and an average fold change of two or greater for all experiments. Three hundred and sixty nine genes decreased after treatment and 356 increased.

Our microarray data reiterates the published literature that ROCK plays a role in several different pathways that all could contribute to the ability of hESC-RPE to undergo extended passage (Table 1) [22, 26, 46, 47]. Table 1 summarizes the microarray data using a pathway centric organization based on the Kyoto Encyclopedia of Genes and Genomes (KEGG) pathways containing ROCK. These pathways include: Actin Cytoskeleton Rearrangements, Adherens Junctions, Tight Junctions, Cell Adhesion Molecules, ECM Receptor Interactions/Focal Adhesions, Vascular Smooth Muscle Contraction, Axon Guidance, Chemokine Guidance, HIPPO Signaling, TGFβ Signaling, Wnt Signaling and the Cell Cycle. This analysis reveals a decreased expression of genes encoding proteins involved in tight junctions, cell adhesion molecules, ECM-receptor interactions, and focal adhesion, at day two, prior to cell confluence, following ROCK inhibition. In addition, examination of the HIPPO, TGFβ and Wnt signaling pathways showed lower levels of transcripts encoding key ligands as a result of ROCK inhibition.

No changes in SMADs were detected, however they are activated through phosphorylation, therefore more work is needed to uncover whether ROCK inhibition affects SMAD function. In addition, transcripts tied to progression through the cell cycle increased substantially after Y-27632 treatment. These data were also analyzed using the gene ontology enrichment analysis software DAVID [48, 49]. This analysis revealed several significant gene groups, many of which overlap the KEGG pathway analysis (Supp. Fig. 7).

Table 1. Microarray: KEGG pathways (passage 5, day 2; control vs. Y-27632)

Control	Y-27632	Gene name	Gene symbol	$\log_2$(Y-27632/control)
Actin cytoskeleton rearrangements				
13.99	51.64	Fibroblast growth factor receptor 3	FGFR3	1.88
94.35	341.02	Fibroblast growth factor 18	FGF18	1.85
41.57	137.16	Fibroblast growth factor 13	FGF13	1.72
32.15	94.53	Bradykinin receptor B1	BDKRB1	1.56
9.61	21.97	Fibroblast growth factor receptor 2	FGFR2	1.19
65.78	23.11	Fibroblast growth factor 5	FGF5	−1.51
430.48	131.35	Coagulation factor II (thrombin) receptor	F2R	−1.71
Adherens junction				
22.91	6.78	Snail homolog 2 (Drosophila)	SNAI2	−1.76
Tight junctions				
280.66	669.95	Myeloid/lymphoid or mixed-lineage leukemia (trithorax homolog, Drosophila); translocated to, 4	MLLT4	1.26
19.73	8.71	Erythrocyte membrane protein band 4.1-like 3	EPB41L3	−1.18
1066.10	407.49	RAB3B, member RAS oncogene family	RAB3B	−1.39
36.13	13.29	Junctional adhesion molecule 2	JAM2	−1.44
Cell adhesion molecules				
504.89	207.34	Cadherin 2, type 1, N-cadherin (neuronal)	CDH2	−1.28
8426.36	3299.04	Integrin, β 1 (fibronectin receptor, β polypeptide, antigen CD29 incldes MDF2, MSK12)	ITGB1	−1.35
30.51	10.57	Netrin G1	NTNG1	−1.53
3747.97	1253.88	Integrin, α V (vitronectin receptor, α polypeptide, antigen CD51)	ITGAV	−1.58
259.28	81.80	Versican	VCAN	−1.66
15.13	4.47	Neuronal growth regulator 1	NEGR1	−1.76
50.13	14.81	Contactin associated protein-like 2	CNTNAP2	−1.76
ECM receptor interactions/focal adhesion				
117.69	330.94	Laminin, α 3	LAMA3	1.49
7.61	17.64	Vitronectin	VTN	1.21
1109.78	510.39	Collagen, type IV, α 1	COL4A1	−1.12
9372.90	4219.15	Collagen, type IV, α 2	COL4A2	−1.15
131.05	57.75	Integrin, β 3 (platelet glyoprotein IIIa, antigen CD61)	ITGB3	−1.18
64.56	27.53	Integrin, α 2 (CD49B, α 2 subunit of VLA-2 receptor)	ITGA2	−1.23
2477.12	991.35	Collagen, type V, α 2	COL5A2	−1.32
3106.25	1228.04	Collagen, type I, α 1	COL1A1	−1.34
57.31	22.50	Tenascin C	TNC	−1.35
714.71	260.49	Laminin, γ 2	LAMC2	−1.46
4299.60	1453.43	Laminin, β 1	LAMB1	−1.56
946.84	315.71	Collagen, type V, α 1	COL5A1	−1.58
549.68	124.46	Secreted phosphoprotein 1	SPP1	−2.14
1261.40	74.09	Integrin, α 11	ITGA11	−4.09
Vascular smooth muscle contraction				
791.61	1875.15	Natriuretic peptide B	NPPB	1.24
200.72	72.18	Phospholipase C, β 4	PLCB4	−1.48
849.62	291.19	Potassium large conductance calcium-activated channel, subfamily M, α member 1	KCNMA1	−1.54
28.61	9.73	Phospholipase A2, group IVC (cytosolic, calcium-independent)	PLA2G4C	−1.56
150.17	47.68	Receptor (G protein-coupled) activity modifying protein 1	RAMP1	−1.66

Table 1. (*Cont'd*)

Control	Y-27632	Gene name	Gene symbol	$\log_2$(Y-27632/control)
Axon guidance				
30.57	104.89	Sema domain, immunoglobin domain (Ig), short basic domain, secreted, (semaphorin) 3E	SEMA3E	1.78
156.69	357.84	Dihydropyrimidinase-like 5	DPYSL5	1.19
852.85	388.05	Netrin 4	NTN4	−1.14
127.79	53.10	Sema domain, immunoglobin domain (Ig), short basic domain, secreted, (semaphorin) 3C	SEMA3C	−1.27
302.93	114.09	Ephrin-A1	EFNA1	−1.41
39.14	14.51	EPH receptor B2	EPHB2	−1.43
Chemokine signaling				
277.50	1617.19	Chemokine (C-X-C motif) ligand 14	CXCL14	2.54
Hippo signaling				
5.01	14.93	Ras association (Ra1GDS/AF-6) domain family member 6	RASSF6	1.58
2354.57	1142.33	Connective tissue growth factor	CTGF	−1.04
21.60	9.80	Discs, large homolog 4 (Drosophila)	DLG4	−1.14
311.31	111.11	FERM domain containing 6	FRMD6	−1.49
TGFβ signaling				
152.52	466.58	Bone morphogenetic protein 7	BMP7	1.61
920.43	379.19	Inhibin, β A	INHBA	−1.28
19.39	7.67	Transforming growth factor, β 1	TGFB1	−1.34
202.25	31.08	Growth differentiation factor 6	GDF6	−2.70
Wnt signaling				
1091.07	3320.85	Secreted frizzled-related protein 1	SFRP1	1.61
21.54	59.10	Secreted frizzled-related protein 5	SFRP5	1.46
108.17	51.86	Prickle homolg 2 (Drosophila)	PRICKLE2	−1.06
140.28	66.06	Frizzled family receptor 7	FZD7	−1.09
502.34	234.90	Protein phosphatase 3, catalytic subunit, α isozyme	PPP3CA	−1.10
64.97	21.82	Wingless-type MMTV integration site family, member 5B	WNT5B	−1.57
604.38	112.49	Wingless-type MMTV integration site family, member 5A	WNT5A	−2.43
Cell cycle				
22.04	90.57	TTK protein kinase	TTK	2.04
24.56	98.55	Cyclin-dependent kinase inhibitor 2C (p18, inhibits CDK4)	CDKN2C	2.00
100.34	349.01	Cell division cycle 45 homolog (S. cerevisiae)	CDC45	1.80
79.48	270.73	E2F transcription factor 2	E2F2	1.77
49.17	166.34	Cell division cycle 7 homolog (S. cerevisiae)	CDC7	1.76
19.90	62.77	Cell division cycle 25 homolog A (S. pombe)	CDC25A	1.66
137.68	407.45	Cyclin-dependent kinase 1	CDK1	1.57
7.8	22.7	Antigen identified by monoclonal antibody Ki-67	MKI67	1.53
476.30	1324.63	Polo-like kinase 1	PLK1	1.48
48.86	120.50	Cyclin A2	CCNA2	1.30
516.13	1169.81	Proliferating cell nuclear antigen	PCNA	1.18
61.82	127.52	Extra spindle pole bodies homolg 1 (S. cerevisiae)	ESPL1	1.04
3249.66	1190.42	Cyclin-dependent kinase 6	CDK6	−1.45
566.19	96.50	Cyclin-dependent kinase inhibitor 2B (p15, inhibits CDK4)	CDKN2B	−2.55

Table 1. Changes in gene expression resulting from ROCK inhibition. Microarray data comparing gene expression differences between control and Y-27632 treated hESC-RPE at day two passage five. The KEGG pathways containing ROCK and those affected by Y-27632 addition are represented. Control and Y-27632 numerical values on the left represent the mean quantile normalized data of four biological replicates. Color coded ratio on the right represents $\log_2$(Y-27632/Control), 1=2 fold change. n=4. GEO link: http://www.ncbi.nlm.nih.gov/geo/query/acc.cgi?token=kxynoswinzslrgj&acc=GSE56618

Discussion

RPE were first noted in differentiated hESC cultures in 2001 [50] and then expanded and characterized in a landmark paper by Klimanskaya et al. in 2004 [51]. Since then groups have been attempting to optimize the process for derivation of RPE from hESC or iPSC [14, 51]. The main obstacles of culturing pluripotent cell derived RPE have always been long derivation time and limited potential for expansion once differentiated. Recently, progress has been made in developing more rapid methods for differentiation of hESC into RPE [39, 52-54]. For example, Buchholz et al. [39] described a method to direct differentiation using a series of growth factors known to play a role in RPE differentiation in vivo. However, once RPE are obtained, they still have a limited functional lifespan.

We report here a novel passaging strategy that relies on inhibition of ROCK that results in an increased rate of proliferation and extended passage of both hESC-RPE and iPSC-RPE, with retention of function. This phenomenon occurs even when the cells are plated at a fourth of the seeding density that is typically used. Thus, one can employ less starting material, and passage cells longer, leading to an exponential increase in number of cells produced from a single culture of hESC or iPSC.

Extended passage hESC-RPE maintained appropriate morphology and gene expression of key RPE markers without an increase in pluripotent, fibroblastic or endothelial transcripts. Immunocytochemistry of passage 13 hESC-RPE exhibited proper localization of RPE transcription factors, proteins involved in pigmentation, tight junctions, and proteins important for RPE-specific functions. Importantly, from a therapeutic application perspective, no aberrant proliferation was detected at day 30.

Functional analysis demonstrated that passage 13 hESC-RPE were normal with respect to ROS phagocytosis and polarized secretion of PEDF and VEGF. In addition, no gross genomic abnormalities were detected following ROCK inhibition and repeated passage.

How does ROCK inhibition lead to extended passage? Microarray analysis suggests that ROCK inhibition could be suppressing an epithelial-to-mesenchymal transition (EMT) through various pathways. These include inhibition of key ligands of the TGFβ pathway (TGFβ1 and GDF6) [55] and Wnt signaling (WNT5A and WNT5B) [56, 57]; along with decreasing levels of collagens 1A1, 4A2 [58, 59], and SNAI2, known biomarkers of EMT [60]. RPE are thought to undergo EMT after repeated passages in culture, a main reason why hESC-RPE have a finite ability to expand, limiting their production for use in transplantation [17, 61]. TGFβ signaling has been shown to be the implicated in activating EMT in RPE [17, 55, 62-64]. Furthermore, several investigations have predicted the RHO/ROCK pathway is involved in regulating EMT in multiple cell types [65-68] , possibly through TGFβ signaling [69]. There has also been evidence linking Wnt activation and β-catenin accumulation to the increased expression of EMT related genes [56, 70]. Inhibition of ROCK, through addition of Y-27632 or other synthetic compounds has already been shown in some cases to reverse this transition [71, 72]. Our results are consistent with the idea that decreased expression of TGFβ and Wnt signaling transcripts lead to the suppression of EMT. In addition, there could be novel, undocumented pathways contributing to the maintenance and increased expansion rate of hESC-RPE, which lead to the persistence of RPE identity.

Overall, two important processes are affected allowing for an increase in hESC-RPE expansion. First, ROCK inhibition promotes proliferation by inducing multiple

components that are involved in cell cycle progression. This allows RPE to quickly reform tight junctions, which is critical to RPE health [73]. Second, ROCK inhibition affects many pathways that could be converging to suppress RPE-to-mesenchymal transition. This allows hESC-RPE to remain functional for an extended, but finite, period in culture.

The prevalence of AMD for individuals over the age of 40 in the US alone was calculated to be 7.2 million people; that number is projected to increase 50% by 2020 [4]. Assuming that a 3 by 5 mm patch of a hESC-RPE monolayer on a scaffold might be developed as a dry AMD therapy, it is estimated that 300,000 hESC-RPE cells will be required for each patient transplant [13, 74]. Based on this number, 3.3 trillion cells would be required to treat all patients affected in 2020. Following the extended passage protocol, a single well of a 6 well plate will generate enough cells in 55 days to treat all those calculated to be affected by the disease in 2020. This does not include the additional cells that would be required for release assays, quality control and cell loss, but the protocol can easily be scaled up. Compared to the current method of derivation, the extended passage protocol using ROCK inhibition can exponentially increase the yield of mature hESC-RPE to 49 billion from 9 million within the first 60 days in culture, over a 5000 fold increase; in addition to using a fourth of the starting cell number.

From a cell engineering perspective, it is clear that these discoveries have the potential to greatly facilitate the production of functional hESC-RPE and iPSC-RPE for both therapeutic and research applications. It is even possible that these findings may also be transferable to other epithelial cells derived from pluripotent stem cells. Currently, minimally passaged hESC-RPE are being employed in clinical trials.

Transitioning to the usage of more highly passaged cells deserve further experimentation to characterize their efficacy and potential tumorigenicity in animal studies; including a full transcriptome analysis of day 30 Y-27632 treated passage 13 hESC-RPE to ensure complete restoration of the gene profile to a passage two like state. In addition, defining the mechanisms of increased proliferation and suppressed EMT, and devising methods to manipulate these processes, could be extremely beneficial in developing therapeutics for other RPE dysfunction diseases such as geographic atrophy and proliferative vitreal retinopathy, a complication of retinal detachment characterized by RPE-to-mesenchymal transition that can lead to loss of vision [64, 75].

Inhibition of ROCK activity by the synthetic compound Y-27632 allows extended passage of hESC-RPE and iPSC-RPE. Extended passage, in part, seems to be achieved by increased proliferation and through the prevention of gene expression that promotes and contributes to the mesenchymal phenotype. We have shown that inhibiting ROCK allows hESC-RPE and iPSC-RPE to be seeded at a fourth the normal density and grow for up to 13 passages. The extended passaged hESC-RPE were comparable to untreated early passage hESC-RPE by all parameters tested. This simple technique, in combination with the published rapid differentiation protocols, could lead to a faster and more efficient way of producing hESC-RPE and iPSC-RPE for clinical trials, basic disease research and drug screening.

References

1. Croze, R.H., *Differentiation of Pluripotent Stem Cells into Retinal Pigmented Epithelium*, in *Cell-Based Therapy for Retinal Degenerative Disease. Developmental Opthalmology*, Z.M. Casaroli-Marano RP, Editor. 2014, Karger: Basel. p. 81-96.
2. Schwartz, S.D., et al., *Embryonic stem cell trials for macular degeneration: a preliminary report.* Lancet, 2012. **379**(9817): p. 713-20.
3. Klein, R., et al., *Prevalence of age-related macular degeneration in the US population.* Arch Ophthalmol, 2011. **129**(1): p. 75-80.
4. Friedman, D.S., et al., *Prevalence of age-related macular degeneration in the United States.* Arch Ophthalmol, 2004. **122**(4): p. 564-72.
5. Curcio, C.A., N.E. Medeiros, and C.L. Millican, *Photoreceptor loss in age-related macular degeneration.* Invest Ophthalmol Vis Sci, 1996. **37**(7): p. 1236-49.
6. Young, R.W., *Pathophysiology of age-related macular degeneration.* Surv Ophthalmol, 1987. **31**(5): p. 291-306.
7. Gehrs, K.M., et al., *Age-related macular degeneration--emerging pathogenetic and therapeutic concepts.* Ann Med, 2006. **38**(7): p. 450-71.
8. Bird, A.C., *Therapeutic targets in age-related macular disease.* J Clin Invest, 2010. **120**(9): p. 3033-41.
9. Ferris, F.L., 3rd, et al., *Clinical classification of age-related macular degeneration.* Ophthalmology, 2013. **120**(4): p. 844-51.
10. Age-Related Eye Disease Study Research, G., *A randomized, placebo-controlled, clinical trial of high-dose supplementation with vitamins C and E, beta carotene, and zinc for age-related macular degeneration and vision loss: AREDS report no. 8.* Arch Ophthalmol, 2001. **119**(10): p. 1417-36.
11. Bowes Rickman, C., et al., *Dry age-related macular degeneration: mechanisms, therapeutic targets, and imaging.* Invest Ophthalmol Vis Sci, 2013. **54**(14): p. ORSF68-80.
12. Buchholz, D.E., et al., *Derivation of functional retinal pigmented epithelium from induced pluripotent stem cells.* Stem Cells, 2009. **27**(10): p. 2427-34.
13. Bharti, K., et al., *Developing cellular therapies for retinal degenerative diseases.* Invest Ophthalmol Vis Sci, 2014. **55**(2): p. 1191-202.
14. Rowland, T.J., D.E. Buchholz, and D.O. Clegg, *Pluripotent human stem cells for the treatment of retinal disease.* J Cell Physiol, 2012. **227**(2): p. 457-66.
15. Burke, J.M., *Epithelial phenotype and the RPE: is the answer blowing in the Wnt?* Prog Retin Eye Res, 2008. **27**(6): p. 579-95.
16. Grisanti, S. and C. Guidry, *Transdifferentiation of retinal pigment epithelial cells from epithelial to mesenchymal phenotype.* Invest Ophthalmol Vis Sci, 1995. **36**(2): p. 391-405.
17. Lee, S.C., et al., *Epitheliomesenchymal transdifferentiation of cultured RPE cells.* Ophthalmic Res, 2001. **33**(2): p. 80-6.
18. Singh, R., et al., *Functional Analysis of Serially Expanded Human iPS Cell-Derived RPE Cultures.* Invest Ophthalmol Vis Sci, 2013. **54**(10): p. 6767-78.
19. Feng, Q., et al., *Hemangioblastic derivatives from human induced pluripotent stem cells exhibit limited expansion and early senescence.* Stem Cells, 2010. **28**(4): p. 704-12.

20. Shay, J.W. and W.E. Wright, *Hayflick, his limit, and cellular ageing.* Nat Rev Mol Cell Biol, 2000. **1**(1): p. 72-6.
21. Riento, K. and A.J. Ridley, *Rocks: multifunctional kinases in cell behaviour.* Nat Rev Mol Cell Biol, 2003. **4**(6): p. 446-56.
22. Amano, M., Y. Fukata, and K. Kaibuchi, *Regulation and functions of Rho-associated kinase.* Exp Cell Res, 2000. **261**(1): p. 44-51.
23. Liao, J.K., M. Seto, and K. Noma, *Rho kinase (ROCK) inhibitors.* J Cardiovasc Pharmacol, 2007. **50**(1): p. 17-24.
24. Leung, T., et al., *The p160 RhoA-binding kinase ROK alpha is a member of a kinase family and is involved in the reorganization of the cytoskeleton.* Mol Cell Biol, 1996. **16**(10): p. 5313-27.
25. Somlyo, A.P. and A.V. Somlyo, *Signal transduction by G-proteins, rho-kinase and protein phosphatase to smooth muscle and non-muscle myosin II.* J Physiol, 2000. **522 Pt 2**: p. 177-85.
26. Street, C.A. and B.A. Bryan, *Rho kinase proteins--pleiotropic modulators of cell survival and apoptosis.* Anticancer Res, 2011. **31**(11): p. 3645-57.
27. Doggrell, S.A., *Rho-kinase inhibitors show promise in pulmonary hypertension.* Expert Opin Investig Drugs, 2005. **14**(9): p. 1157-9.
28. Pankey, E.A., et al., *The Rho kinase inhibitor azaindole-1 has long-acting vasodilator activity in the pulmonary vascular bed of the intact chest rat.* Can J Physiol Pharmacol, 2012. **90**(7): p. 825-35.
29. Zhou, Q., C. Gensch, and J.K. Liao, *Rho-associated coiled-coil-forming kinases (ROCKs): potential targets for the treatment of atherosclerosis and vascular disease.* Trends Pharmacol Sci, 2011. **32**(3): p. 167-73.
30. Okumura, N., et al., *Enhancement on primate corneal endothelial cell survival in vitro by a ROCK inhibitor.* Invest Ophthalmol Vis Sci, 2009. **50**(8): p. 3680-7.
31. Koizumi, N., N. Okumura, and S. Kinoshita, *Development of new therapeutic modalities for corneal endothelial disease focused on the proliferation of corneal endothelial cells using animal models.* Exp Eye Res, 2012. **95**(1): p. 60-7.
32. Liu, X., et al., *ROCK inhibitor and feeder cells induce the conditional reprogramming of epithelial cells.* Am J Pathol, 2012. **180**(2): p. 599-607.
33. Horani, A., et al., *Rho-associated protein kinase inhibition enhances airway epithelial Basal-cell proliferation and lentivirus transduction.* Am J Respir Cell Mol Biol, 2013. **49**(3): p. 341-7.
34. Miyashita, H., et al., *Long-term maintenance of limbal epithelial progenitor cells using rho kinase inhibitor and keratinocyte growth factor.* Stem Cells Transl Med, 2013. **2**(10): p. 758-65.
35. van den Bogaard, E.H., et al., *Rho kinase inhibitor Y-27632 prolongs the life span of adult human keratinocytes, enhances skin equivalent development, and facilitates lentiviral transduction.* Tissue Eng Part A, 2012. **18**(17-18): p. 1827-36.
36. Chapman, S., et al., *Human keratinocytes are efficiently immortalized by a Rho kinase inhibitor.* J Clin Invest, 2010. **120**(7): p. 2619-26.
37. Ohgushi, M., et al., *Molecular pathway and cell state responsible for dissociation-induced apoptosis in human pluripotent stem cells.* Cell Stem Cell, 2010. **7**(2): p. 225-39.

38. Ohgushi, M. and Y. Sasai, *Lonely death dance of human pluripotent stem cells: ROCKing between metastable cell states.* Trends Cell Biol, 2011. **21**(5): p. 274-82.
39. Buchholz, D.E., et al., *Rapid and efficient directed differentiation of human pluripotent stem cells into retinal pigmented epithelium.* Stem Cells Transl Med, 2013. **2**(5): p. 384-93.
40. Diniz, B., et al., *Subretinal implantation of retinal pigment epithelial cells derived from human embryonic stem cells: improved survival when implanted as a monolayer.* Invest Ophthalmol Vis Sci, 2013. **54**(7): p. 5087-96.
41. Maminishkis, A., et al., *Confluent monolayers of cultured human fetal retinal pigment epithelium exhibit morphology and physiology of native tissue.* Invest Ophthalmol Vis Sci, 2006. **47**(8): p. 3612-24.
42. Molday, R.S., D. Hicks, and L. Molday, *Peripherin. A rim-specific membrane protein of rod outer segment discs.* Invest Ophthalmol Vis Sci, 1987. **28**(1): p. 50-61.
43. Rowland, T.J., et al., *Differentiation of human pluripotent stem cells to retinal pigmented epithelium in defined conditions using purified extracellular matrix proteins.* J Tissue Eng Regen Med, 2013. **7**(8): p. 642-53.
44. Strauss, O., *The retinal pigment epithelium in visual function.* Physiol Rev, 2005. **85**(3): p. 845-81.
45. Lin, H. and D.O. Clegg, *Integrin alphavbeta5 participates in the binding of photoreceptor rod outer segments during phagocytosis by cultured human retinal pigment epithelium.* Invest Ophthalmol Vis Sci, 1998. **39**(9): p. 1703-12.
46. Duong-Quy, S., et al., *Role of Rho-kinase and its inhibitors in pulmonary hypertension.* Pharmacol Ther, 2013. **137**(3): p. 352-64.
47. Amano, M., M. Nakayama, and K. Kaibuchi, *Rho-kinase/ROCK: A key regulator of the cytoskeleton and cell polarity.* Cytoskeleton (Hoboken), 2010. **67**(9): p. 545-54.
48. Huang da, W., B.T. Sherman, and R.A. Lempicki, *Systematic and integrative analysis of large gene lists using DAVID bioinformatics resources.* Nat Protoc, 2009. **4**(1): p. 44-57.
49. Huang da, W., B.T. Sherman, and R.A. Lempicki, *Bioinformatics enrichment tools: paths toward the comprehensive functional analysis of large gene lists.* Nucleic Acids Res, 2009. **37**(1): p. 1-13.
50. Odorico, J.S., D.S. Kaufman, and J.A. Thomson, *Multilineage differentiation from human embryonic stem cell lines.* Stem Cells, 2001. **19**(3): p. 193-204.
51. Klimanskaya, I., et al., *Derivation and comparative assessment of retinal pigment epithelium from human embryonic stem cells using transcriptomics.* Cloning Stem Cells, 2004. **6**(3): p. 217-45.
52. Idelson, M., et al., *Directed differentiation of human embryonic stem cells into functional retinal pigment epithelium cells.* Cell Stem Cell, 2009. **5**(4): p. 396-408.
53. Zahabi, A., et al., *A new efficient protocol for directed differentiation of retinal pigmented epithelial cells from normal and retinal disease induced pluripotent stem cells.* Stem Cells Dev, 2012. **21**(12): p. 2262-72.
54. Zhu, Y., et al., *Three-dimensional neuroepithelial culture from human embryonic stem cells and its use for quantitative conversion to retinal pigment epithelium.* PLoS One, 2013. **8**(1): p. e54552.

55. Lee, S.C., et al., *TGF-betas synthesized by RPE cells have autocrine activity on mesenchymal transformation and cell proliferation.* Yonsei Med J, 2001. **42**(3): p. 271-7.
56. Son, H. and A. Moon, *Epithelial-mesenchymal Transition and Cell Invasion.* Toxicol Res, 2010. **26**(4): p. 245-52.
57. Xiao, L., et al., *A Glimpse of the Pathogenetic Mechanisms of Wnt/ -Catenin Signaling in Diabetic Nephropathy.* Biomed Res Int, 2013. **2013**: p. 987064.
58. Billings, P.C., et al., *The transforming growth factor-beta-inducible matrix protein (beta)ig-h3 interacts with fibronectin.* J Biol Chem, 2002. **277**(31): p. 28003-9.
59. Kim, J.E., et al., *Molecular properties of wild-type and mutant betaIG-H3 proteins.* Invest Ophthalmol Vis Sci, 2002. **43**(3): p. 656-61.
60. Scanlon, C.S., et al., *Biomarkers of epithelial-mesenchymal transition in squamous cell carcinoma.* J Dent Res, 2013. **92**(2): p. 114-21.
61. Tamiya, S., L. Liu, and H.J. Kaplan, *Epithelial-mesenchymal transition and proliferation of retinal pigment epithelial cells initiated upon loss of cell-cell contact.* Invest Ophthalmol Vis Sci, 2010. **51**(5): p. 2755-63.
62. Stocks, S.Z., S.M. Taylor, and I.A. Shiels, *Transforming growth factor-beta1 induces alpha-smooth muscle actin expression and fibronectin synthesis in cultured human retinal pigment epithelial cells.* Clin Experiment Ophthalmol, 2001. **29**(1): p. 33-7.
63. Gamulescu, M.A., et al., *Transforming growth factor beta2-induced myofibroblastic differentiation of human retinal pigment epithelial cells: regulation by extracellular matrix proteins and hepatocyte growth factor.* Exp Eye Res, 2006. **83**(1): p. 212-22.
64. Lee, J., M. Ko, and C.K. Joo, *Rho plays a key role in TGF-beta1-induced cytoskeletal rearrangement in human retinal pigment epithelium.* J Cell Physiol, 2008. **216**(2): p. 520-6.
65. Hu, Y.B., et al., *Roles of Rho/Rock signaling pathway in silica-induced epithelial-mesenchymal transition in human bronchial epithelial cells.* Biomed Environ Sci, 2013. **26**(7): p. 571-6.
66. Wei, J., et al., *Rho kinase pathway is likely responsible for the profibrotic actions of aldosterone in renal epithelial cells via inducing epithelial-mesenchymal transition and extracellular matrix excretion.* Cell Biol Int, 2013. **37**(7): p. 725-30.
67. Clay, M.R. and M.C. Halloran, *Rho activation is apically restricted by Arhgap1 in neural crest cells and drives epithelial-to-mesenchymal transition.* Development, 2013. **140**(15): p. 3198-209.
68. Zhang, H., et al., *Epithelial-mesenchymal transition of rat peritoneal mesothelial cells via Rhoa/Rock pathway.* In Vitro Cell Dev Biol Anim, 2011. **47**(2): p. 165-72.
69. Cho, H.J. and J. Yoo, *Rho activation is required for transforming growth factor-beta-induced epithelial-mesenchymal transition in lens epithelial cells.* Cell Biol Int, 2007. **31**(10): p. 1225-30.
70. Azar, K.M., L. Xiao, and J. Ma, *Baseline obesity status modifies effectiveness of adapted diabetes prevention program lifestyle interventions for weight management in primary care.* Biomed Res Int, 2013. **2013**: p. 191209.
71. Gu, L., et al., *Fasudil inhibits epithelial-myofibroblast transdifferentiation of human renal tubular epithelial HK-2 cells induced by high glucose.* Chem Pharm Bull (Tokyo), 2013. **61**(7): p. 688-94.

72. Das, S., et al., *Complete reversal of epithelial to mesenchymal transition requires inhibition of both ZEB expression and the Rho pathway.* BMC Cell Biol, 2009. **10**: p. 94.
73. Rizzolo, L.J., *Development and role of tight junctions in the retinal pigment epithelium.* Int Rev Cytol, 2007. **258**: p. 195-234.
74. Tribukait, A., U. Rosenhall, and B. Osterdahl, *Morphological characteristics of the human macula sacculi.* Audiol Neurootol, 2005. **10**(2): p. 90-6.
75. Chen, H.C., et al., *Wnt signaling induces epithelial-mesenchymal transition with proliferation in ARPE-19 cells upon loss of contact inhibition.* Lab Invest, 2012. **92**(5): p. 676-87.

Chapter IV

ROCK Inhibition Promotes Wound Closure and Attachment in Human Embryonic Stem Cell Derived Retinal Pigmented Epithelium

Introduction

Age-related macular degeneration (AMD) is a progressive disease that is the leading cause of blindness in the aged population of the developed world [1]. AMD initially affects a region in the back of the eye responsible for fine acuity vision called the macula. The disease presents when a monolayer of cells called the retinal pigmented epithelium (RPE) begin to degrade. The RPE are the critical cell type responsible for maintaining the function and viability of the photoreceptors, the main light sensing neuron. Therefore when the RPE degrade, the photoreceptors in turn begin to die and vision is lost [2, 3].

There are two forms of the disease, wet or exudative, and dry AMD. Wet AMD is characterized by neovascularization, which disrupts the RPE monolayer. This form, although rapidly progressive, can be treated with intraocular injections of anti-VEGF antibodies to suppress the overactive blood vessel formation [1]. The dry form, affecting 90% of patients diagnosed with AMD, can only be treated with a vitamin cocktail and antioxidant supplements, which merely slows disease progression in 25% of patients [4, 5]. Geographic atrophy (GA), areas devoid of RPE and subsequently photoreceptors, often occurs in late stage AMD patients and is extremely devastating to vision. Unfortunately, RPE have limited proliferative abilities to fill in areas affected by GA prior to photoreceptor death [6, 7]. Therefore, a human embryonic stem cell (hESC) RPE cellular replacement therapy is a promising candidate for a novel, effective treatment for ocular diseases that affect RPE [8, 9]; and is currently in clinical trials for both AMD and Stargardt's disease [10, 11].

Rho-GTPase coiled coil kinase (ROCK) has been known for over ten years to affect cytoskeletal rearrangement through the regulation LIMK/cofilin activity [12] and is increasingly being studied in a variety of diseases [13]. ROCK inhibition, using synthetic inhibitors, is being examined as a treatment option for pulmonary hypertension [14], cancer [15], glaucoma [16], and certain neurological diseases [17, 18]. ROCK inhibition also boosts proliferation rates of hESC-RPE and allows hESC-RPE and iPSC-RPE to be continually passaged in culture for over ten passages prior to senescence [19]. Based on the known effects of ROCK inhibition on proliferation and the cytoskeleton, we hypothesized that ROCK inhibition would affect wound healing and substrate attachment in hESC-RPE. More recently groups have been identifying a range of distinct functions for the two isoforms, ROCK1 and ROCK2 [20-24]. Therefore we have examined the effects of a pan ROCK inhibitor as well as a ROCK2 isoform-specific inhibitor to elucidate differences in function.

ROCK inhibition, using synthetic inhibitors, could provide a combinational therapy together with cellular replacement to help promote attachment of transplanted cells or could serve as a stand-alone therapy to increase proliferation of endogenous RPE to fill in areas affected by GA. This chapter will show that ROCK inhibition promotes wound healing and attachment.

Methods

Cell Culture

Pluripotent Stem Cell Culture

H9 human embryonic stem cells (hESC) were acquired from the Thomson group and were cultured on Matrigel in mTESR1. Medium was changed every other day and cells were kept at 37°C in 5% CO_2 in normoxic conditions.

Retinal Pigmented Epithelium Derivation and Maintenance

H9 hESC were overgrown for 8-14 days, followed by the removal of basic fibroblastic growth factor and a medium change to XVIVO-10. Cells were cultured for 90-120 days with a medium change every 2-3 days. After 90-120 days, the non-pigmented cell patches were manually excised and washed away using phosphate buffered saline (PBS). Pigmented patches were lifted from the plate following a 5 minute incubation at 37°C with TrypLE Express. Cells were then diluted in XVIVO-10, spun for 5 minutes at 1000 rpm, and plated at $1.0x10^5$ cells/cm^2 on Matrigel-coated 6-well plates. Every 30 days, these enriched RPE were again enzymatically passaged using TrypLE Express. Medium was changed every 2-3 days. Cells used in experiments were between passages 1-4. At least three individual enrichments derived from distinct H9 cultures were used for all analyses; each enrichment equals an 'n.' Statistical significance was determined by Student's t-tests for all experiments, comparing two experimental data sets at a time.

Scratch Assay

hESC-RPE were grown for 30 days in XVIVO-10. Using a P200 pipet tip, a scratch was created down the center of the well from the top to the bottom on day 30. Cells were washed 3 times with PBS. 10μM of Y-27632 (ROCK1/2 inhibitor), 10μM of ROCKIV (ROCK2 inhibitor), or an equal volume of water as a control was added to cells in fresh XVIVO-10 for 14 days post scratch. Immediately following the scratch, cells

were imaged along the wound and will be identified as day 0. Three, 7 and 30 days post scratch, the cells were imaged again. Quantification of the area of the wound closure was determined using the polygonal tool within Image J software to outline the area devoid of cells at day 0, and subsequently at days 3, 7 and 30. The areas were then subtracted from day 0 area and divided by day 0 area, then made into a percent to represent percent wound closure.

Immunoctyochemistry (ICC)

On day 5 and 30 after scratch, cells were fixed with 4% paraformaldehdye in 0.1M cacodylate buffer for 15 minutes at 4°C. Cells were then blocked with 5% bovine serum albumin plus 0.2% Triton X-100 for 1 hour at 4°C. Primary antibody MKI67 was diluted in block at (1:1000, Abcam) and incubated at 4°C overnight. The next day, the cells were washed 3 times with PBS. The corresponding 488 Alexa Fluor secondary antibody (1:300) and Phalloidin conjugated to Tetramethylrhodamine (TRITC, 220μM) were added to the cells in PBS for 45 minutes at 4°C (Life Technologies). Hoescht dye (2μg/ml) was then added and incubated at 25°C for 5 minutes to stain cellular DNA. Cells were washed 3 times and mounted using Prolong Gold Anti-fade. Fluorescent microscopy was used to analyze expression patterns at 40X objective on an Olympus BX51 Microscope. Fiji and Microsoft Excel software were used to quantify the integrated pixel density of MKi67 fluorescence within scratched region and cell area was determined by outlining cells within the scratched region using the polygonal tool within Fiji and quantifying the area. Twenty cells were analyzed per image using internal triplicates and three separate experiments (independent enrichments).

Attachment Assay

hESC-RPE were passaged as described above, and seeded at $1.0x10^5$ cells/cm^2 on Matrigel-coated slides in XVIVO-10. At the time of plating, cells were treated with 10μM Y-27632, 10μM ROCKIV or an equal volume of water as a control. Cells were allowed to attach for 1, 2, 4, 6 and 24 hours. At each time point, attached living cells were stained with Calcein AM according to manufacturer's instructions using a LIVE/DEAD Cytotoxicity Kit (Life Technologies). Cells were then fixed for 1 hour at 25°C in 4% paraformaldehyde (PFA) in PBS. Fluorescent microscopy was used to image attached cells. Fluorescent quantification was performed with Image J and Microsoft Excel software. Each treatment was represented as the percent of the sum total fluorescence for the corresponding time point to eliminate the variability of dye intensity between experiments, but preserving the change between treatments.

Cell Spreading Determination

hESC-RPE were plated and treated as described in the attachment assay. Cells were allowed to attach for 1, 2 and 4 hours. Cells were then fixed in 4% PFA in 0.1M cacodylate buffer for 15 minutes at 4°C. Cells were blocked and permeabilized in 5% bovine serum albumin plus 0.2% Triton X-100 for 1 hour at 4°C. Phalloidin-TRITC and Hoescht were added as described in *Immunoctyochemistry*. F-actin was visualized through fluorescent microscopy at 60X on a BX51 Olympus microscope and cell area was analyzed using the Fiji software polygonal tool to outline cells, 20 cells per image in internal triplicate.

Results

ROCK inhibition promotes wound closure

hESC-RPE were grown for 30 days and then scratched to mimic a wound and monitored for an additional 30 days. ROCK1/2 inhibition, added at the time of the scratch, significantly enhanced wound closure compared to control by day 3 (Fig. 12A). ROCK2 inhibition alone showed significant wound closure by day 3 as well; however the cell morphology within the scratched area was large and mesenchymal, not typical of the RPE. By day 30, the ROCK1/2-inhibited cells completely closed the wound, while the control cells failed to regain a confluent monolayer in the scratched space. ROCK2-inhibited cells showed significantly more wound closure than control at day 30; however the larger cells seen in the earlier time points persisted. The amount of wound closure was calculated from photomicrographs and quantified (Fig. 12B).

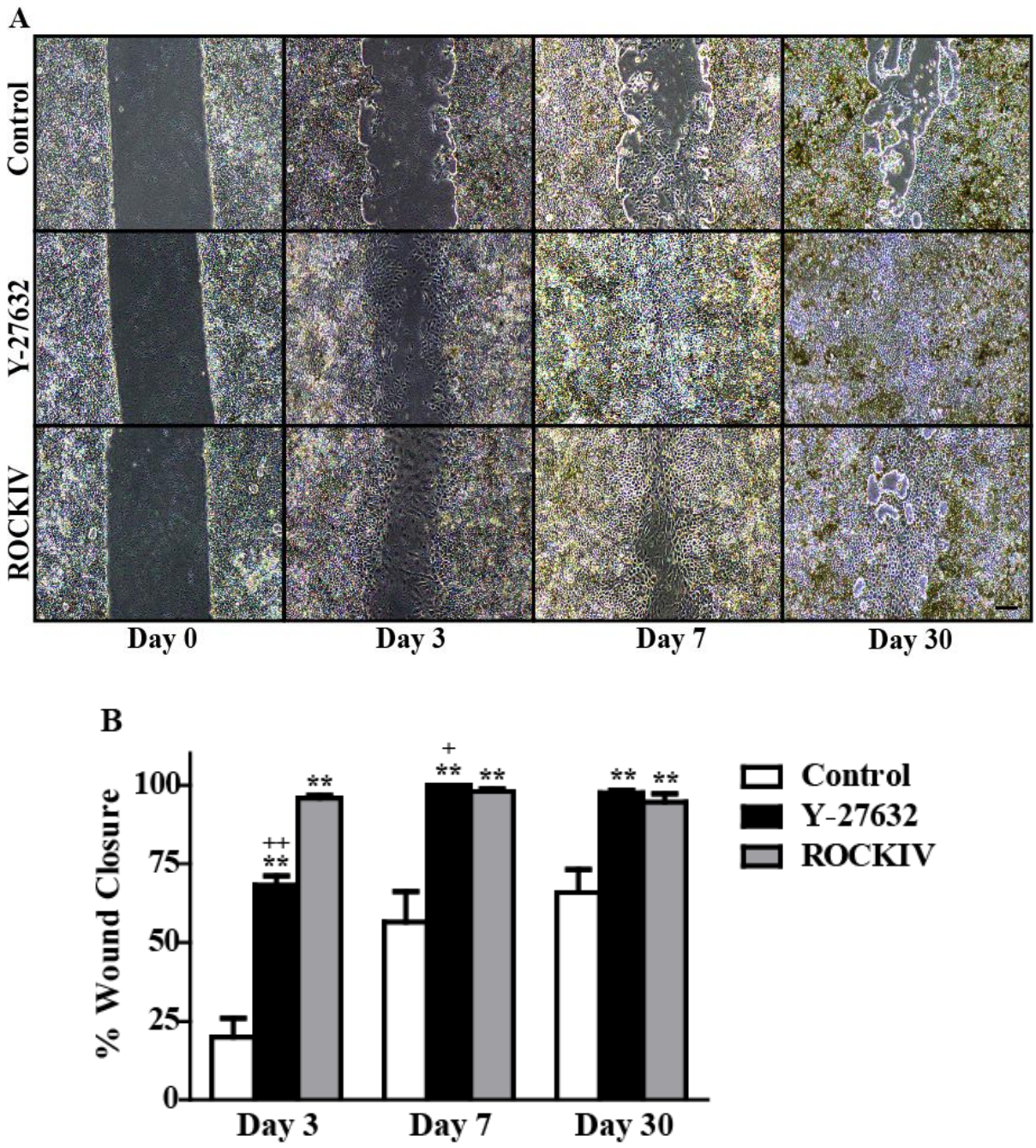

Figure 12. ROCK inhibition enhances wound closure. (A) hESC-RPE were scratched following 30 days in culture and treated with either Y-27632 (ROCK1/2 inhibitor) or ROCKIV (ROCK2 inhibitor) and wound closure was monitored over an additional 30 days. Control and ROCKIV-treated cells failed to completely close the wounded area. (B) Quantification of wound closure at each time point imaged. Scale bar (A)=200μm (B) **p<0.01 compared to control at that time point. +p≤0.05 ++p≤0.01 compared to ROCKIV at that time point. Error bars represent ± SEM. n=3.

Interestingly, most of the cells treated with Y-27632 regained their epithelial morphology by day 7. Although control cells failed in fill in the entire scratched area, the cells present in the wounded space have mainly recovered their epithelial morphology by day 30. In contrast, ROCKIV treated cells, although fast to close the wounded area, still had larger and more mesenchymal looking cells compared to control and Y-27632 treated cells at day 30.

ROCK1/2 inhibition promotes proliferation at wound site

A general concept of epithelium wound healing is that cells undergo an epithelial to mesenchymal transition (EMT) that allows them to migrate into the area devoid of cells and form scar tissue [25]. We hypothesized in our wound healing system, based on ROCK inhibition's known effects on proliferation, that the increase in wound closure was in part due to an increase in proliferation [19]. Five days after the scratch, cells were subjected to immunocytochemistry and probed with MKI67, a proliferation marker, and phalloidin, an F-actin probe, to analyze cytoskeletal arrangements (Fig. 13A). There was a significant increase in MKI67 staining within the wounded area following ROCK1/2 inhibition (Fig. 13B). Surprisingly, ROCK2 inhibition showed no changes from control in MKI67 expression patterns. However, ROCK2 inhibition significantly increased the individual cell size within the scratched region compared to both control and ROCK1/2 inhibition treatments, similarly seen in the day 30 images of ROCK2 inhibited cells from Figure 12A (Fig. 13C). Importantly, there was no MKI67 expression detected 30 days post scratch in any of the treatment groups; therefore the increase in proliferation due to ROCK1/2 inhibition did not aberrantly continue after

treatment was stopped at 14 days after scratch (Supp. Fig. 8). In addition, F-actin staining at 30 days post scratch also shows the persistent larger cell size morphology of ROCKIV treated cells (Supp. Fig. 8).

A

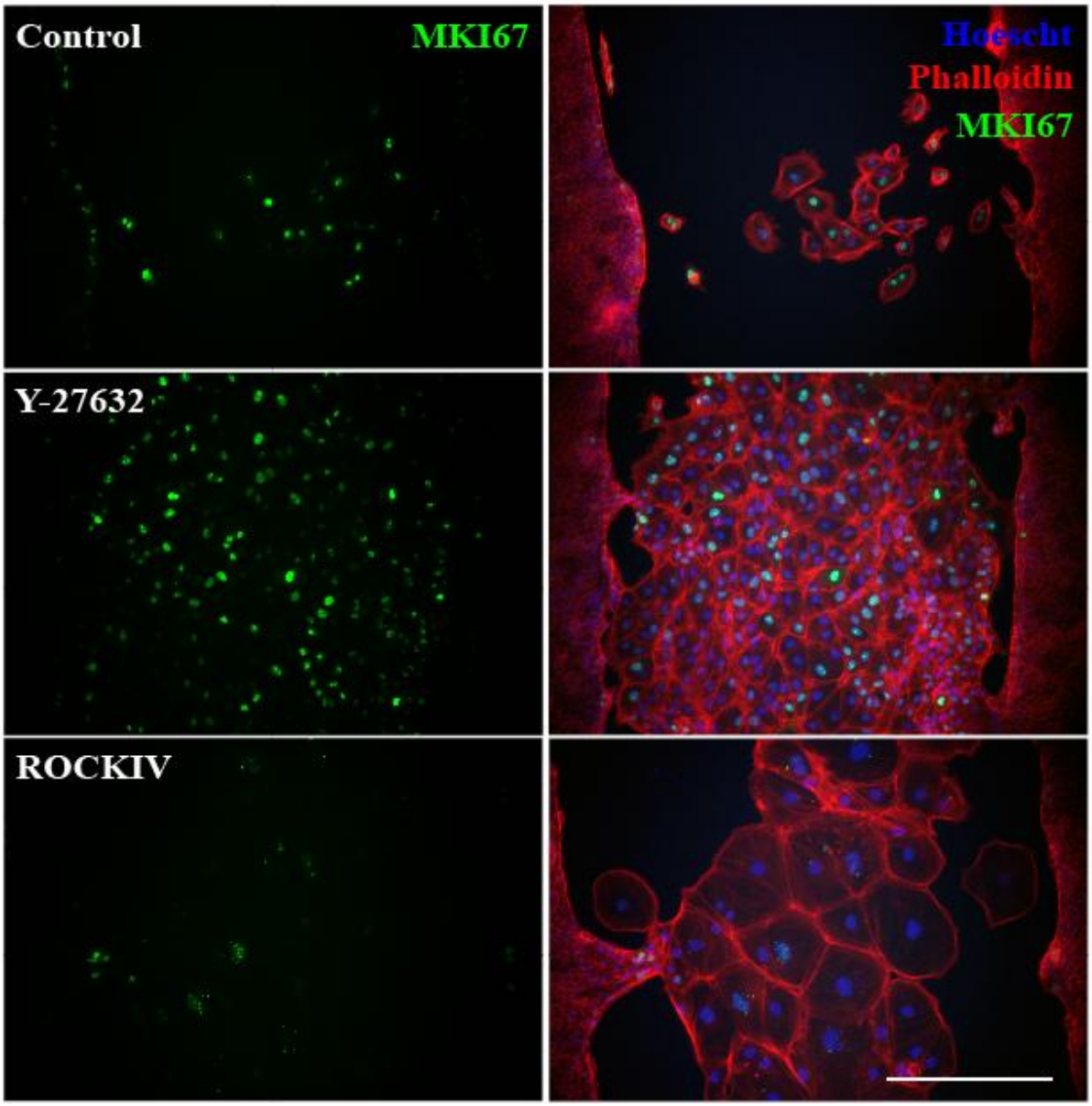

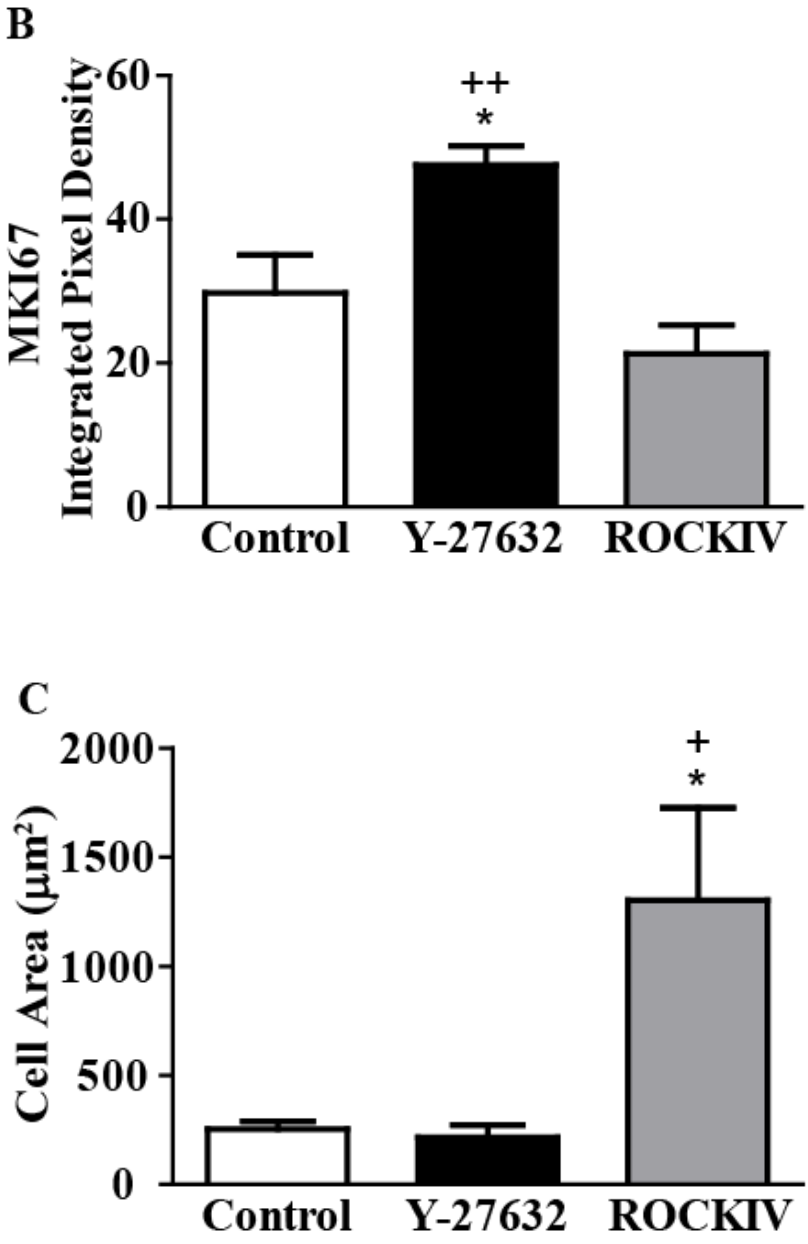

Figure 13. ROCK1/2 inhibition promotes proliferation in wounded area. (A) Five days after scratch, MKI67, a marker of proliferation (green), Phalloidin (F-actin, red), and Hoescht (blue) were examined. (B) MKI67 fluorescence in wounded area was quantified and was significantly higher when cells were treated with 10μM of Y-27632. (C) ROCKIV increased cell size compared to Control and Y-27632 treatments. Scale bar (A)=100μM. (B) *p≤0.05 to control, ++p≤0.01 to ROCKIV. (C) *p≤0.05 to control, +p≤0.05 to Y-27632. Error bars represent ± SEM. n=3.

ROCK inhibition promotes attachment through an increase in cell spreading

ROCK activates LIMK, which inactivates cofilin leading to actin stabilization [12]. ROCK is also known to affect cytoskeletal rearrangements through the regulation of myosin light chain [26]. Therefore inhibition of ROCK should lead to actin depolymerization and the release of actin monomers for the reorganization of the cytoskeleton, which could affect cell attachment. hESC-RPE were examined at 1, 2, 4, 6 and 24 hours after equal-density plating and Calcein AM dye fluorescence was determined, which was indicative of the number of attached cells (Fig. 14A, 6 hour image representation). ROCK1/2 and ROCK2 inhibition significantly promoted attachment of cells as early as 1 hour after plating, and maintained this effect at all time points examined (Fig. 14B). ROCK inhibition had a quick acting and significant role in hESC-RPE attachment.

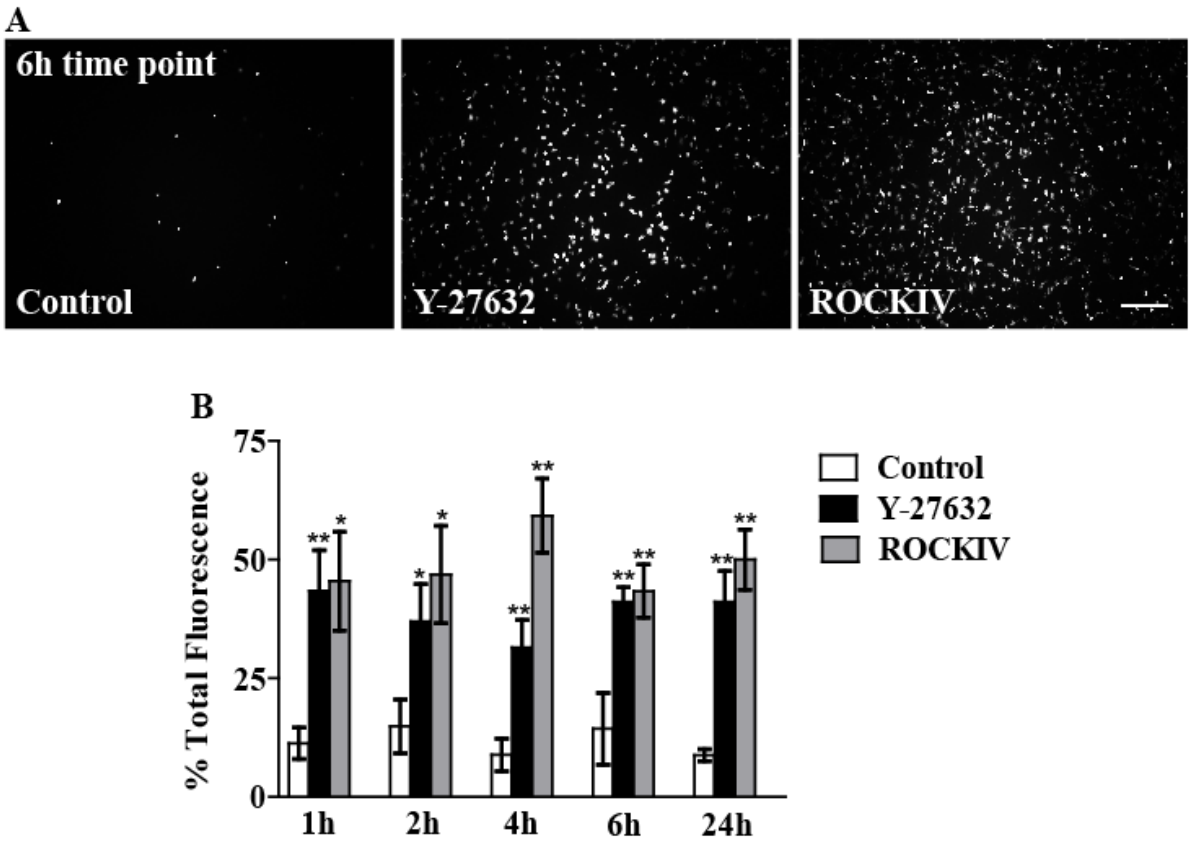

Figure 14. ROCK inhibition increases cell attachment. (A) At various time points after plating, cells were stained with a Calcein AM dye to detect adherent and living cells. Fluorescent images at the 6 hour time point are shown for all three treatments. (B) Quantification of the percent of the sum total fluorescence for each time point and treatment. ROCK inhibition drastically increased cell attachment as early as 1 hour after plating. Scale bar (A)=200μm. (B) *p≤0.05 **p≤0.01 compared to control within each time point. Error bars represent ± SEM. n≥6.

To examine cytoskeletal organization during cell attachment immunoctyochemisty was performed using phalloidin-TRITC (F-actin probe) (Fig. 15A). ROCK inhibition significantly increased cell spreading 1 hour after plating when compared to control cells, as determined by the calculation of cell area outlined from the F-actin fluorescence (Fig. 15B). This effect persisted at 2 and 4 hours after plating. ROCK 2-specific inhibition further increased cell spreading at all time points examined compared to ROCK1/2 inhibition, distinguishing a specific ROCK2 isoform role in cell spreading.

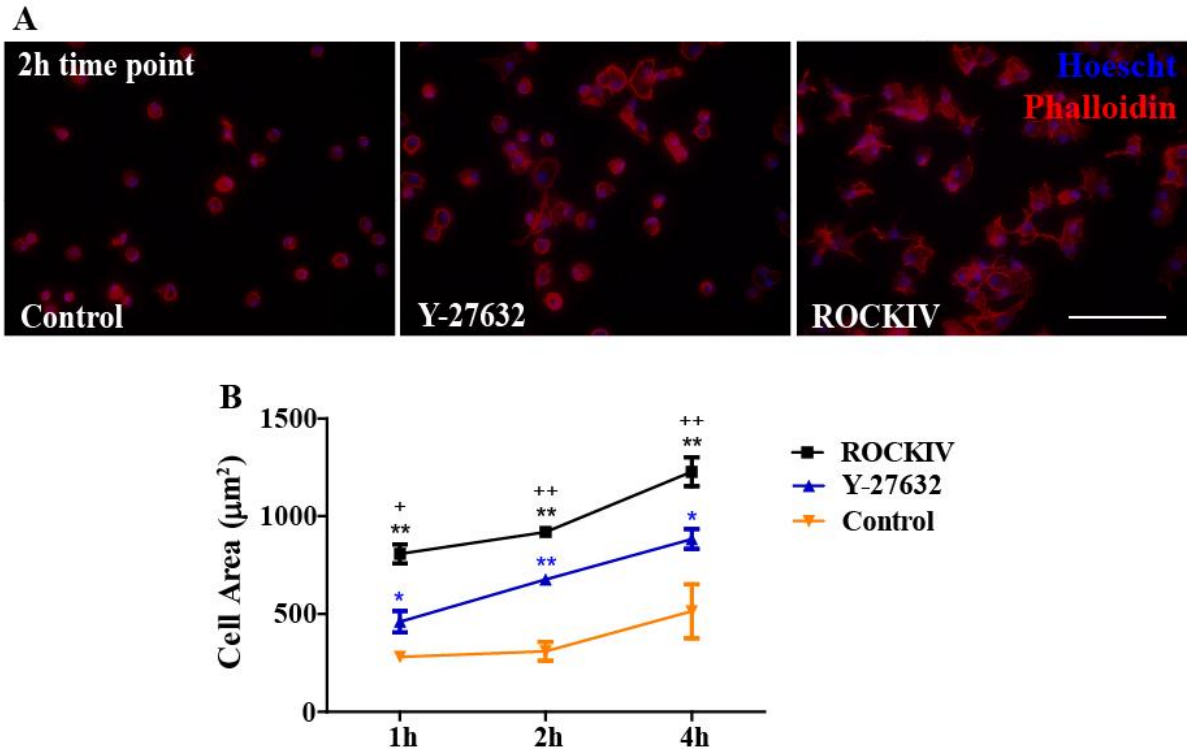

Figure 15. ROCK inhibition promotes cell spreading. (A) Fluorescent images taken 2 hours after plating and stained with phalloidin-TRITC (red) to visualize F-actin and Hoescht (blue) to label cellular DNA. (B) Quantification of cell area from phalloidin fluorescence. Scale bar (A)=100µm. (B) *p≤0.05 **p≤0.01 compared to control within each time point. +p≤0.05 ++p≤0.01 compared to Y-27632 within each time point. Error bars represent ± SEM. n=5.

Discussion

ROCK inhibition, using synthetic inhibitors, is currently in several clinical trials for various diseases [27]. ROCK inhibition is thought to prevent the EMT, perhaps through inhibition of TGF-β signaling, which often contributes to scarring following a wound [19, 25]. In a naïve model of in vitro wound healing, ROCK1/2 inhibition, but not ROCK2 inhibition alone, promotes proliferation to fill in the area devoid of cells. Typical cobblestone epithelial morphology was quickly regained and the wound was closed faster than control when cells were treated with a ROCK1/2 inhibitor. These data could distinguish a specific role for ROCK1 in proliferation. Importantly, this increase in proliferation was not predominating elsewhere in the culture and cells exited the cell cycle after the wound was closed and treatment was stopped (Fig. 13, Supp. Fig. 8).

Interestingly, ROCK2 inhibition initiates wound closure the fastest however did not show an increase in proliferation within the scratched area, perhaps pointing towards a role for ROCK2 in cell migration and EMT. This would be consistent with the change in cell morphology observed in ROCK2-inhibited cultures; away from the traditional epithelial cell characteristics, towards a larger, flatter, more mesenchymal-like cell. ROCK2 treated cells were significantly larger cells within the scratched region at day 5 compared to control and ROCK1/2 treated cells. ROCK1/2 inhibition has been shown to inhibit major players in the TGFβ and EMT pathways [19], however these data suggest that ROCK2 inhibition alone might promote EMT. This could point towards opposing and specific roles for ROCK1 and ROCK2; ROCK2 in inhibiting EMT, while ROCK1 may promote EMT, in this system. Unfortunately, at this time there are no ROCK1 specific inhibitors; therefore, hESC-RPE siRNA knockouts of ROCK1 and ROCK2

need to be examined to fully test this theory. A closer examination of ROCK inhibition in wound healing could prompt a novel therapeutic for GA, a devastating progression of AMD.

ROCK has been known for years to stabilize actin fibers and promote stress fiber formation through its regulation of LIMK and MLC [12]. Current literature has repeatedly shown that ROCK inhibition destabilizes actin polymerization [28]; however here, we found that ROCK inhibition increases cell attachment. We believe this is due to the reorganization of actin fibers. LIMK is activated by ROCK1/2 and inactivates cofilin, stabilizing actin [29]. ROCK inhibition therefore activates cofilin and initiates the depolymerization of actin fibers. This creates a pool of F-actin monomers that by a mechanism not yet known, could be contributing to the creation of new F-actin fibers and focal adhesion complexes, promoting attachment. In contrast to other ROCK inhibition data, we found an increase in cell spreading within the first hour after plating following ROCK inhibition compared to control [30]. Interestingly, there was a significantly greater effect in cell spreading with ROCK2 inhibition alone, perhaps correlating to the wound assay hypothesize that ROCK2 inhibition promotes larger mesenchymal cells through the initiation of EMT.

The effects of ROCK inhibition on attachment could be extremely beneficial in hESC-RPE cellular therapies involving bolus injections of cells, as in the ACT clinical trial for AMD [10, 11]. It also provides a new, fast acting role for ROCK inhibition in attachment of hESC-RPE. hESC-RPE are generally plated at a high seeding density, but through the use of ROCK inhibition, we can combine the beneficial effects of an increase

in cell attachment with the known effects of increased proliferation to seed RPE at a lower density to save time, money and amount of these precious cells. ROCK inhibition's role in attachment should also be examined for other cellular therapies with poor integration to try to overcome this obstacle.

Although at the beginning stages, this work provides valuable insight into the effects of specific isoform ROCK functions on hESC-RPE and could lead to the formation of a novel treatment to be used alone or in combination with cellular therapies to help restore the RPE in various ocular diseases. Furthermore, ROCK inhibition treatment could cross over to other diseases where epithelial layers are compromised, or be used to help prevent post-operative scarring as is common in glaucoma surgeries [27].

Aside from the implications in ocular disease, ROCK inhibition is under investigation as an anti-metastatic agent to prevent migration in various cancers [31]. Most researchers have examined the effect of ROCK inhibition on migration, however the data presented here should open up research avenues to elucidate ROCK inhibition's role in attachment of tumor cells and EMT, a characteristic of metastatic tumor cells [32]. It was recently published that ROCK inhibition can promote the reattachment of breast cancer cells in circulation, which correlates with our conclusions [33]. The role of ROCK inhibition in attachment and EMT described in this chapter warrant further examination in a cancer-based system for the possible development of a cancer therapeutic.

References

1. Gehrs, K.M., et al., *Age-related macular degeneration--emerging pathogenetic and therapeutic concepts.* Ann Med, 2006. **38**(7): p. 450-71.
2. Curcio, C.A., N.E. Medeiros, and C.L. Millican, *Photoreceptor loss in age-related macular degeneration.* Invest Ophthalmol Vis Sci, 1996. **37**(7): p. 1236-49.
3. Young, R.W., *Pathophysiology of age-related macular degeneration.* Surv Ophthalmol, 1987. **31**(5): p. 291-306.
4. Bowes Rickman, C., et al., *Dry age-related macular degeneration: mechanisms, therapeutic targets, and imaging.* Invest Ophthalmol Vis Sci, 2013. **54**(14): p. ORSF68-80.
5. Age-Related Eye Disease Study Research, G., *A randomized, placebo-controlled, clinical trial of high-dose supplementation with vitamins C and E, beta carotene, and zinc for age-related macular degeneration and vision loss: AREDS report no. 8.* Arch Ophthalmol, 2001. **119**(10): p. 1417-36.
6. Bird, A.C., *Therapeutic targets in age-related macular disease.* J Clin Invest, 2010. **120**(9): p. 3033-41.
7. Ferris, F.L., 3rd, et al., *Clinical classification of age-related macular degeneration.* Ophthalmology, 2013. **120**(4): p. 844-51.
8. Ramsden, C.M., et al., *Stem cells in retinal regeneration: past, present and future.* Development, 2013. **140**(12): p. 2576-85.
9. Croze, R.H., *Differentiation of Pluripotent Stem Cells into Retinal Pigmented Epithelium*, in *Cell-Based Therapy for Retinal Degenerative Disease. Developmental Opthalmology*, Z.M. Casaroli-Marano RP, Editor. 2014, Karger: Basel. p. 81-96.
10. Schwartz, S.D., et al., *Embryonic stem cell trials for macular degeneration: a preliminary report.* Lancet, 2012. **379**(9817): p. 713-20.
11. Schwartz, S.D., et al., *Human embryonic stem cell-derived retinal pigment epithelium in patients with age-related macular degeneration and Stargardt's macular dystrophy: follow-up of two open-label phase 1/2 studies.* Lancet, 2015. **385**(9967): p. 509-16.
12. Vardouli, L., A. Moustakas, and C. Stournaras, *LIM-kinase 2 and cofilin phosphorylation mediate actin cytoskeleton reorganization induced by transforming growth factor-beta.* J Biol Chem, 2005. **280**(12): p. 11448-57.
13. Pan, P., et al., *Advances in the development of Rho-associated protein kinase (ROCK) inhibitors.* Drug Discov Today, 2013. **18**(23-24): p. 1323-33.
14. Shaw, D., et al., *Novel ROCK inhibitors for the treatment of pulmonary arterial hypertension.* Bioorg Med Chem Lett, 2014. **24**(20): p. 4812-7.
15. Rath, N. and M.F. Olson, *Rho-associated kinases in tumorigenesis: re-considering ROCK inhibition for cancer therapy.* EMBO Rep, 2012. **13**(10): p. 900-8.
16. Harrison, B.A., et al., *Discovery and Development of LX7101, a Dual LIM-Kinase and ROCK Inhibitor for the Treatment of Glaucoma.* ACS Med Chem Lett, 2015. **6**(1): p. 84-8.
17. Alokam, R., et al., *Design of dual inhibitors of ROCK-I and NOX2 as potential leads for the treatment of neuroinflammation associated with various neurological diseases including autism spectrum disorder.* Mol Biosyst, 2015. **11**(2): p. 607-17.

18. Lu, Q., et al., *Signaling through Rho GTPase pathway as viable drug target.* Curr Med Chem, 2009. **16**(11): p. 1355-65.
19. Croze, R.H., et al., *ROCK Inhibition Extends Passage of Pluripotent Stem Cell-Derived Retinal Pigmented Epithelium.* Stem Cells Transl Med, 2014. **3**(9): p. 1066-78.
20. Zandi, S., et al., *ROCK-Isoform-Specific Polarization of Macrophages Associated with Age-Related Macular Degeneration.* Cell Rep, 2015. **10**(7): p. 1173-86.
21. Surma, M., et al., *ROCK1 deficiency enhances protective effects of antioxidants against apoptosis and cell detachment.* PLoS One, 2014. **9**(3): p. e90758.
22. Lee, S.H., et al., *ROCK1 isoform-specific deletion reveals a role for diet-induced insulin resistance.* Am J Physiol Endocrinol Metab, 2014. **306**(3): p. E332-43.
23. Mertsch, S. and S. Thanos, *Opposing signaling of ROCK1 and ROCK2 determines the switching of substrate specificity and the mode of migration of glioblastoma cells.* Mol Neurobiol, 2014. **49**(2): p. 900-15.
24. Hahmann, C. and T. Schroeter, *Rho-kinase inhibitors as therapeutics: from pan inhibition to isoform selectivity.* Cell Mol Life Sci, 2010. **67**(2): p. 171-7.
25. Wynn, T.A., *Common and unique mechanisms regulate fibrosis in various fibroproliferative diseases.* J Clin Invest, 2007. **117**(3): p. 524-9.
26. Kosako, H., et al., *Rho-kinase/ROCK is involved in cytokinesis through the phosphorylation of myosin light chain and not ezrin/radixin/moesin proteins at the cleavage furrow.* Oncogene, 2000. **19**(52): p. 6059-64.
27. Wang, S.K. and R.T. Chang, *An emerging treatment option for glaucoma: Rho kinase inhibitors.* Clin Ophthalmol, 2014. **8**: p. 883-90.
28. Amin, E., et al., *Rho-kinase: regulation, (dys)function, and inhibition.* Biol Chem, 2013. **394**(11): p. 1399-410.
29. Pritchard, C.A., et al., *B-Raf acts via the ROCKII/LIMK/cofilin pathway to maintain actin stress fibers in fibroblasts.* Mol Cell Biol, 2004. **24**(13): p. 5937-52.
30. Ye, N., et al., *Direct observation of alpha-actinin tension and recruitment at focal adhesions during contact growth.* Exp Cell Res, 2014. **327**(1): p. 57-67.
31. Kale, V.P., et al., *The regulatory roles of ROCK and MRCK kinases in the plasticity of cancer cell migration.* Cancer Lett, 2015. **361**(2): p. 185-196.
32. Tsubaki, M., et al., *Activation of NF-kappaB by the RANKL/RANK system up-regulates snail and twist expressions and induces epithelial-to-mesenchymal transition in mammary tumor cell lines.* J Exp Clin Cancer Res, 2013. **32**: p. 62.
33. Bhandary, L., et al., *ROCK inhibition promotes microtentacles that enhance reattachment of breast cancer cells.* Oncotarget, 2015.

Chapter Five

Monitoring Stem Cell Transplants in Ocular Disease: Creating a Molecular Tool Basket

Introduction

Current research for development of an Age-related Macular Degeneration (AMD) therapeutic focuses on using human embryonic stem cells (hESC) derived cells as a cellular replacement therapy [1, 2]. hESCs spontaneously differentiate into retinal pigmented epithelium (RPE) after the removal of basic fibroblastic growth factor and can be enriched to create a homogenous population of cells [3, 4]. In the US, clinical trials are already underway using a bolus injection of hESC-RPE into the eye [1, 5]. In addition, a second transplantation approach is being studied [6, 7] that involves culturing hESC-RPE on a synthetic substrate [8] and transplanting the monolayer into the eye. It has been shown that transplantation as a monolayer improves cell survival and decreases cell dispersion from site of implantation and allows for better graft control and traceability [9, 10]. However all these studies have been done using end point analyses.

Stem cell transplantation does have potential caveats, including transplanted cell migration [11], proliferation [12, 13], death [14, 15], immune rejection [16-18], and teratoma formation [13, 19]. There is potential for devastating effects if these events occur [20]. Surprisingly, these behaviors have yet to be sufficiently studied in either method of hESC-RPE transplantation in real time [1, 21].

To address these issues we have created molecular tools to examine parameters of cell identity, function, proliferation, migration, and population homogeneity post-transplantation. This will provide a more complete view of cell behavior after implantation and further compare transplantation methods. Key characteristics of hESC-RPE cells can be monitored using a reporter system, where fluorescent color

indicates a specific cell process. We have created four reporters to monitor migration, identity, maturity and mitosis (Table 2). Through the use of fundus autofluorescence and optical coherence tomography imaging techniques, we would be able to follow these reporters after transplantation within the same animal in real time. This will elucidate novel data about how the hESC-RPE responds to the retinal environment, how cells are incorporated, and how the hESC-RPE behaves at multiple time points. In addition, the two transplantation methods can be extensively compared to bring the best strategy to the clinics to ensure optimal surgical outcome for patients.

Process Monitored	Promoter	Reporter
Migration/Survival	EF1α	eGFP
RPE function/identity	BEST1	copGFP
RPE function/maturity	RPE65	copGFP
Mitosis	MKI67	eGFP

Table 2. A list of the processes monitored by the reporter system (left column). The promoter region of a specific gene (middle column) has been cloned to drive expression of the reporter gene (right column). All reporters were cloned using a lentiviral supporting backbone. EF1α=elongation factor 1α, BEST1=bestrophin-1, RPE65=retinal pigmented epithelium 65kDa, MKi67=marker of proliferation Ki-67 eGFP=enhanced green fluorescent protein, copGFP=copepod green fluorescent protein

Methods

Reporter Cloning

The elongation factor 1α-enhanced green fluorescent protein (EF1α-eGFP) reporter was obtained from Addgene (Plasmid #12247). The marker of proliferation Ki-67(MKi67)-eGFP reporter was kindly donated from Alexander Zambon from the University of California, San Diego [22]. The bestrophin-1 (BEST1) promoter region was donated by Noriko Esumi at the Nagoya University School of Medicine, Japan [23]. The BEST1 promoter was subcloned into the multiple cloning site of the pGreenFire Lenti-Reporter plasmid from Systems Biosciences (SBI), to drive copepod GFP (copGFP), positioned directly downstream (SBI, California, USA). The retinal pigmented epithelium 65kDa (RPE65) promoter region was annotated in [24] and primers were created around this region (Forward: 5' AT GCC CTC ACT GTA AGG AAA TG 3'; Reverse: 5' GA TCC AGA GTT CTG GCA CCA A 3'). Genomic DNA (gDNA) from day 30 hESC-RPE was isolated using the Promega Wizard genomic DNA isolation kit (Promega, Wisconsin, USA). The RPE65 promoter region was isolated from gDNA using PCR. Then the promoter was ligated into the pGreenFire Lenti-Reporter, oriented to drive the plasmid's endogenous copGFP. All completed reporters were confirmed by sequencing performed by Eton Bioscience Inc. (Eton Bioscience Inc., California, USA).

Cell Culture

Human embryonic kidney 293 cells (HEK293) used for viral production were obtained from ATCC and cultured in Dulbecco's Minimum Essential Media+Glutamate (DMEM, Life Technologies) on tissue culture plastic.

hESC H9 cells, donated from J. Thomson, were allowed to overgrow for 8-14 days in mTESR medium on Matrigel. The medium was then changed to XVIVO-10 medium containing no basic fibroblast growth factor (bfgf). Ninety days after the removal of bfgf, pigmented patches were enriched [4, 25]. Briefly, the non-pigmented cells were manually dissected and washed away with phosphate buffered saline (PBS). Pigmented patches were enzymatically digested with TrpLE express for 5mins at 37°C. Cells were then scraped, diluted in 1:10 volumes of XVIVO-10, spun at 1000rpm for 5mins and seeded at $1.0x10^5$cell/cm^2, yielding a homogenous hESC-RPE population. hESC-RPE were maintained in XVIVO-10 on Matrigel coated tissue culture plates, and enzymatically passaged every 30 days in the same method described above.

A negative control cell line, human umbilical vein endothelial cells (HUVECs), was cultured in Endothelial Growth Medium I (EGM) on 0.1% gelatin coated tissue culture plates. All cells were grown at 37°C 5% CO^2 in normoxic conditions.

Virus Production

Lenti-viral envelope (Plasmid # 12259) and packaging (Plasmid # 12260) plasmids were obtained from Addgene. These plasmids in combination with each reporter plasmid were tranfected into HEK293 cells using a calcium phosphate method. The transfection was stopped after 16h by aspirating the medium and adding fresh DMEM medium. This medium was subsequently collected at 48h and 72h after the initial transfection. Viral particles were concentrated using a PEG-it solution (SBI) and stored at -80°C until use.

Transduction of Viral Particles

hESC-RPE and HUVECs were transduced with viral particles immediately following cell passage, allowing particles to attack the cells on all sides, leading to a higher efficiency of infection. Antibiotic resistance was conferred within the viral genome of each reporter except the EF1α-eGFP vector. Both BEST1-copGFP and RPE65-copGFP reporters conferred resistance to neomycin, while MKi67-eGFP contained a blasticidin resistant gene. To select for cells expressing the reporters the BEST1-copGFP and RPE65-copGFP hESC-RPE cultures were treated with G418 at 400μg/ml and the MKi67-eGFP hESC-RPE culture with 4ng/ml of blasticidin for 3-10 days post-infection.

Cells were monitored over one month using an Olympus IX71 fluorescent microscope to ensure reporters maintained efficient tracking of desired behavior. After 30 days in culture the hESC-RPE containing the reporters were passaged and frozen down 2 days after plating. Cells were frozen in CryoSTOR10 and stored in the liquid nitrogen, forming four intermediate cell banks, one for each reporter.

Seeding of parylene substrates

Parylene substrates were obtained from California Institute for Technology through our collaboration for the California Project to Cure Blindness. Substrates were placed in a 24 well plate and washed twice with 70% ethanol for 15mins, then twice with PBS containing magnesium and calcium for 15mins. A 14.5mm cylinder ring was placed within the well to hold the substrates down. The substrates were coated with 10μg/ml human vitronectin (BD Biosciences, California, USA) for 2 hours at room temperature. Cells were then passaged and seeded onto coated substrates at $3.0x10^5$ cells per well in XVIVO-10 medium. 24-48 hours after initial seeding, substrates were

moved to a new 24 well plate and cultured for 30 days with a medium change every 2-3 days.

Results

EF1α-eGFP was constitutively expressed in hESC-RPE

The elongation factor 1 α promoter region is commonly used to drive expression of exogenous transgenes [26]. We utilized the ubiquitous and strong expression of the EF1α promoter to create a reporter that was constitutively active within our hESC-RPE. hESC-RPE were transduced with the EF1α-eGFP virus created as described in the *Methods* section. Thirty days after infection, hESC-RPE efficiently and continuously expressed eGFP (Fig. 16A). Although the cells expressing the exogenous reporter were not selected for, high efficiency of viral incorporation was achieved. In addition, hESC-RPE containing the EF1a-eGFP reporter were passaged onto a vitronectin coated parylene substrate and grown for thirty days, with maintained eGFP expression (Fig. 16B). In the future, these monolayers could be transplanted into a rat model of retinal dystrophy. This reporter will be useful for examining transplant location and cell migration.

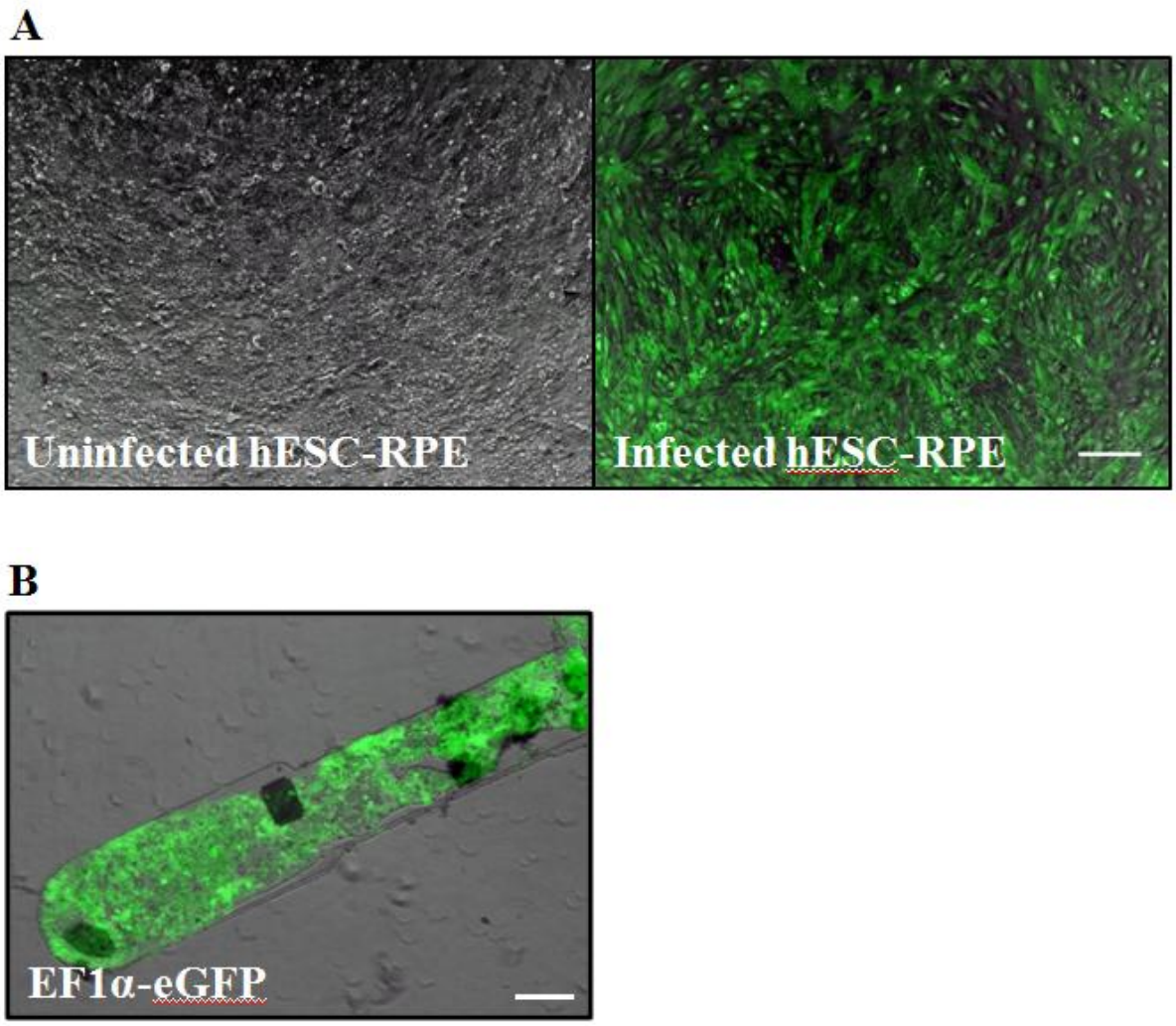

Figure 16. hESC-RPE transduced with EF1α-eGFP lentivirus, 30 days post-infection. (A) The uninfected cells show no eGFP expression, left panel; while the cells infected with the reporter show a high efficiency of eGFP expression, right panel. (B) hESC-RPE infected with the EF1α-eGFP reporter have been seeded onto a parylene substrate for transplantation. Scale bar (A)=100μm. Scale bar (B)=200μm.

BEST1-copGFP and RPE65-copGFP monitor hESC-RPE cell identity and maturity

BEST1 is found specifically in RPE and is believed to be a calcium activated chloride channel [27]. It is necessary for maintaining proper membrane conductance of the RPE, essential for functional vision [28]. hESC-RPE cells transduced with the BEST1-copGFP reporter expressed BEST1 indicated by the presence of copGFP (Fig. 17). In uninfected hESC-RPE and infected HUVECs (a negative control cell line), there was no transcription of BEST1 indicated by the lack of copGFP expression, supporting the specificity of the reporter to BEST1 expression within RPE.

RPE65 is a visual cycle protein found in mature RPE. It is required for all trans to 11-cis-retinoid isomerization, a critical step in recycling components involved in maintaining the photoreceptors' light sensing abilities [29]. RPE, not HUVECs, fluoresce copGFP following transduction of the RPE65-copGFP reporter indicating that this reporter was specific to RPE (Fig. 17).

These reporters will be useful to identify whether monolayer transplanted RPE maintain their mature markers of RPE identity, which could give insight into their functional abilities. In particular, it will help elucidate whether the bolus injection of hESC-RPE are able to mature after injection.

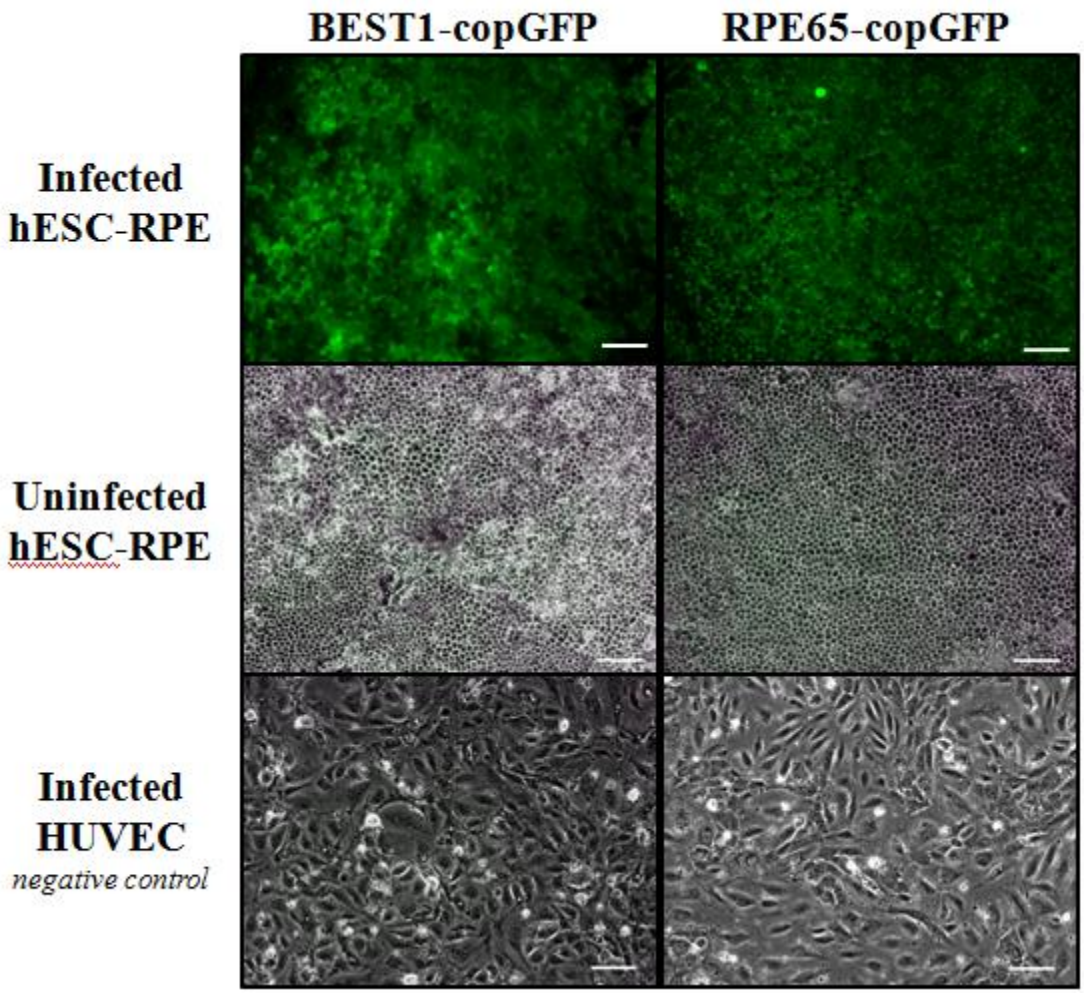

Figure 17. RPE specific reporter expression. BEST1, an RPE specific chloride channel, drives expression of copGFP. This expression was specific to RPE cells and not seen in uninfected hESC-RPE or infected HUVECs (negative control cell line) (left panel). RPE65, a mature protein in the visual cycle, was reported only in hESC-RPE (right panel). Scale bar=100μm.

MKi67-eGFP track cells undergoing mitosis

MKi67 is a critical component in cell cycle regulation [30]. hESC-RPE were transduced with a MKi67-eGFP reporter upon plating and monitored over 30 days (Fig. 18). hESC-RPE primarily proliferated during the first 8 days, as seen through expression of eGFP on day 3 and 8. The signal may appear less intense at day 3 than day 8 possibly because the cells were still building up eGFP to visible levels following the integration, transcription and translation of the exogenous transcript. The cells then began to shrink down and drop out of the cell cycle, depicted by the decrease in reporter expression from day 8 to 12. By day 30, minimal eGFP was detected. Although there was a small patch of fluorescent cells, this could be hESC-RPE re-entering the cell cycle to fill an area that underwent cell death. The MKi67-eGFP reporter will be useful for accurately monitoring cells within the cell cycle and give insight into whether there is aberrant proliferation upon transplantation.

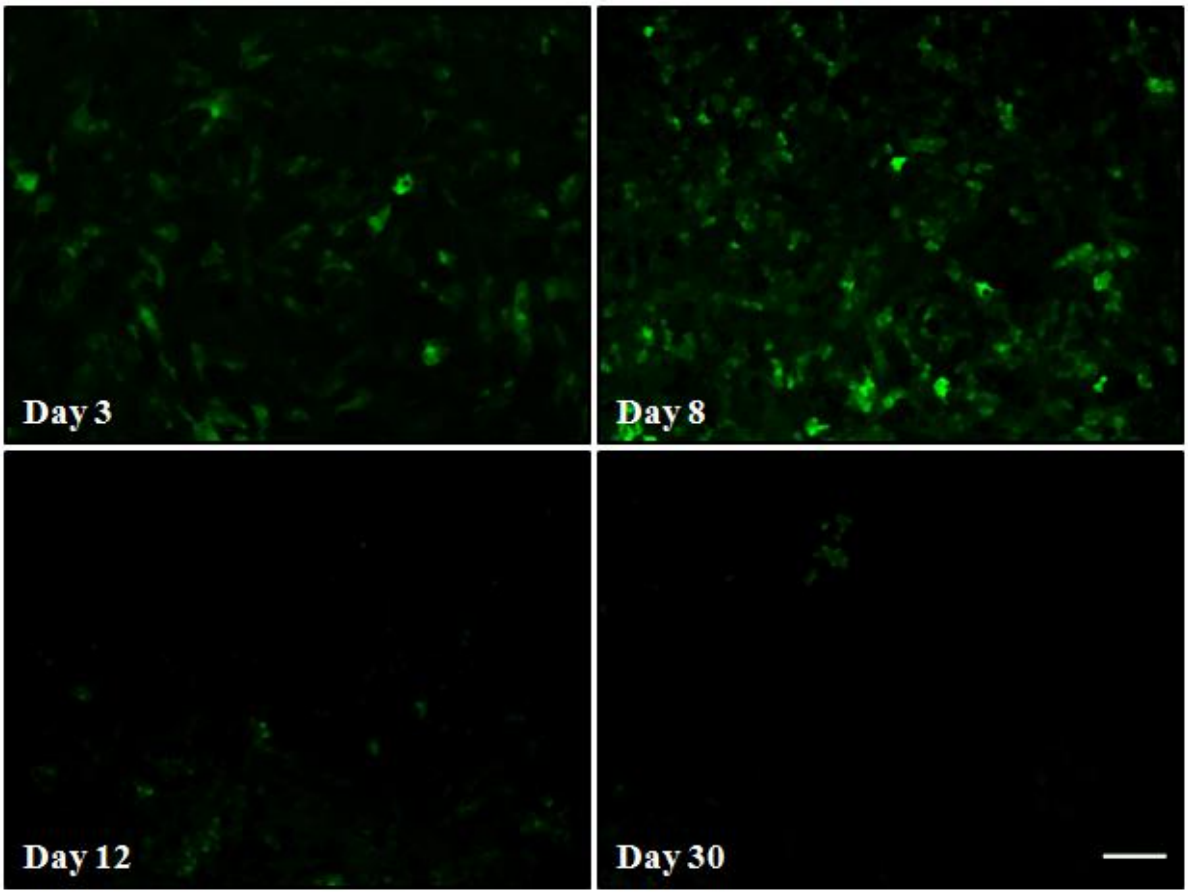

Figure 18. hESC-RPE were transduced with MKi67-eGFP upon plating and monitored over 30 days. MKi67 expression followed the known hESC-RPE proliferation timeline. hESC-RPE divide throughout the first 3-12 days and then shrink down and exit the cell cycle. Scale bar=100μm.

Discussion

Current work has created four reporters: the EF1α promoter driving eGFP expression, the BEST1 promoter driving eGFP, the RPE65 promoter driving eGFP, and the MKi67 promoter driving eGFP. EF1α, a constitutive marker, can track migration of transplanted cells; BEST1 and RPE65, more functional RPE genes, monitor mature RPE identity; while MKi67 will report any cells undergoing mitosis, a large concern of the FDA in stem cell therapies. All reporters have been transduced into hESC-RPE and ICBs have been created. Fluorescent color of the cells will correspond to the specific cell behavior, allowing transplanted hESC-RPE to be monitored in real time within the same animal.

Utilizing the power of these reporter cells in various animal models of ocular disease in which the RPE are affected, will be critical in progressing stem cell therapies towards successful outcomes in the clinic. They will give us valuable insight, through real time imaging, of how transplanted cells behave. Imaging specialists can carry out in vivo optical coherence tomography and fundus autofluorescence confocal scanning laser opthalmoscope techniques to analyze cell characteristics at various time-points after surgery. Optokinetics tests could monitor any changes in visual function to support reporter imaging data. In addition, further determination of the optimal surgical method could be uncovered through reporter expression patterns and optokinetic scores.

The overall goal of the creation of these molecular tools is to identify key behaviors of transplanted hESC-RPE to ensure the best surgical outcome for those suffering from the advanced form of Dry AMD and other ocular diseases. The ICBs of

hESC-RPE reporter lines await collaboration and transplantation to fully utilize their potential.

References

1. Schwartz, S.D., et al., *Embryonic stem cell trials for macular degeneration: a preliminary report.* Lancet, 2012. **379**(9817): p. 713-20.
2. Croze, R.H., *Differentiation of Pluripotent Stem Cells into Retinal Pigmented Epithelium*, in *Cell-Based Therapy for Retinal Degenerative Disease. Developmental Opthalmology*, Z.M. Casaroli-Marano RP, Editor. 2014, Karger: Basel. p. 81-96.
3. Vugler, A., et al., *Embryonic stem cells and retinal repair.* Mech Dev, 2007. **124**(11-12): p. 807-29.
4. Vugler, A., et al., *Elucidating the phenomenon of HESC-derived RPE: anatomy of cell genesis, expansion and retinal transplantation.* Exp Neurol, 2008. **214**(2): p. 347-61.
5. Schwartz, S.D., et al., *Human embryonic stem cell-derived retinal pigment epithelium in patients with age-related macular degeneration and Stargardt's macular dystrophy: follow-up of two open-label phase 1/2 studies.* Lancet, 2015. **385**(9967): p. 509-16.
6. Streilein, J.W., et al., *Immunobiology and privilege of neuronal retina and pigment epithelium transplants.* Vision Res, 2002. **42**(4): p. 487-95.
7. Sheridan, C., R. Williams, and I. Grierson, *Basement membranes and artificial substrates in cell transplantation.* Graefes Arch Clin Exp Ophthalmol, 2004. **242**(1): p. 68-75.
8. Ong, J.M. and L. da Cruz, *A review and update on the current status of stem cell therapy and the retina.* Br Med Bull, 2012.
9. Diniz, B., et al., *Subretinal implantation of retinal pigment epithelial cells derived from human embryonic stem cells: improved survival when implanted as a monolayer.* Invest Ophthalmol Vis Sci, 2013. **54**(7): p. 5087-96.
10. Kamao, H., et al., *Characterization of human induced pluripotent stem cell-derived retinal pigment epithelium cell sheets aiming for clinical application.* Stem Cell Reports, 2014. **2**(2): p. 205-18.
11. Hu, Z., M. Ulfendahl, and N.P. Olivius, *Central migration of neuronal tissue and embryonic stem cells following transplantation along the adult auditory nerve.* Brain Res, 2004. **1026**(1): p. 68-73.
12. Kokkinopoulos, I., et al., *Mature peripheral RPE cells have an intrinsic capacity to proliferate; a potential regulatory mechanism for age-related cell loss.* PLoS One, 2011. **6**(4): p. e18921.
13. Hentze, H., R. Graichen, and A. Colman, *Cell therapy and the safety of embryonic stem cell-derived grafts.* Trends Biotechnol, 2007. **25**(1): p. 24-32.
14. Tezel, T.H., L.V. Del Priore, and H.J. Kaplan, *Reengineering of aged Bruch's membrane to enhance retinal pigment epithelium repopulation.* Invest Ophthalmol Vis Sci, 2004. **45**(9): p. 3337-48.
15. Gullapalli, V.K., I.K. Sugino, and M.A. Zarbin, *Culture-induced increase in alpha integrin subunit expression in retinal pigment epithelium is important for improved resurfacing of aged human Bruch's membrane.* Exp Eye Res, 2008. **86**(2): p. 189-200.

16. Tang, C. and M. Drukker, *Potential barriers to therapeutics utilizing pluripotent cell derivatives: intrinsic immunogenicity of in vitro maintained and matured populations.* Semin Immunopathol, 2011. **33**(6): p. 563-72.
17. Zhao, T., et al., *Immunogenicity of induced pluripotent stem cells.* Nature, 2011. **474**(7350): p. 212-5.
18. Boyd, A.S., et al., *Concise review: Immune recognition of induced pluripotent stem cells.* Stem Cells, 2012. **30**(5): p. 797-803.
19. Glotzbach, J.P., et al., *An information theoretic, microfluidic-based single cell analysis permits identification of subpopulations among putatively homogeneous stem cells.* PLoS One, 2011. **6**(6): p. e21211.
20. Somoza, R.A. and F.J. Rubio, *Cell therapy using induced pluripotent stem cells or somatic stem cells: this is the question.* Curr Stem Cell Res Ther, 2012. **7**(3): p. 191-6.
21. Carr, A.J., et al., *Protective effects of human iPS-derived retinal pigment epithelium cell transplantation in the retinal dystrophic rat.* PLoS One, 2009. **4**(12): p. e8152.
22. Zambon, A.C., *Use of the Ki67 promoter to label cell cycle entry in living cells.* Cytometry A, 2010. **77**(6): p. 564-70.
23. Esumi, N., et al., *Analysis of the VMD2 promoter and implication of E-box binding factors in its regulation.* J Biol Chem, 2004. **279**(18): p. 19064-73.
24. Nicoletti, A., K. Kawase, and D.A. Thompson, *Promoter analysis of RPE65, the gene encoding a 61-kDa retinal pigment epithelium-specific protein.* Invest Ophthalmol Vis Sci, 1998. **39**(3): p. 637-44.
25. Croze, R.H., et al., *ROCK Inhibition Extends Passage of Pluripotent Stem Cell-Derived Retinal Pigmented Epithelium.* Stem Cells Transl Med, 2014. **3**(9): p. 1066-78.
26. Wang, R., et al., *Promoter-dependent EGFP expression during embryonic stem cell propagation and differentiation.* Stem Cells Dev, 2008. **17**(2): p. 279-89.
27. Marmorstein, A.D., et al., *Bestrophin, the product of the Best vitelliform macular dystrophy gene (VMD2), localizes to the basolateral plasma membrane of the retinal pigment epithelium.* Proc Natl Acad Sci U S A, 2000. **97**(23): p. 12758-63.
28. Rosenthal, R., et al., *Expression of bestrophin-1, the product of the VMD2 gene, modulates voltage-dependent Ca2+ channels in retinal pigment epithelial cells.* FASEB J, 2006. **20**(1): p. 178-80.
29. Boulanger, A., et al., *The upstream region of the Rpe65 gene confers retinal pigment epithelium-specific expression in vivo and in vitro and contains critical octamer and E-box binding sites.* J Biol Chem, 2000. **275**(40): p. 31274-82.
30. Schluter, C., et al., *The cell proliferation-associated antigen of antibody Ki-67: a very large, ubiquitous nuclear protein with numerous repeated elements, representing a new kind of cell cycle-maintaining proteins.* J Cell Biol, 1993. **123**(3): p. 513-22.

Appendix

Differentiation Method	iPSC line				
	DF19	DF4	DF6	MyCell	OAT
Spontaneous (SCAC)	+++	++	–	+++	–
Expedited (14-day)	+++	+	++	+++	+

(+++) Represents high RPE yield, (++) and (+) represent moderate to low RPE yield, and (-) indicates insufficient quantities of RPE were derived for characterization.

Supplemental Table 1. Line-to-line variation in iPSC-RPE derivation based on derivation protocol.

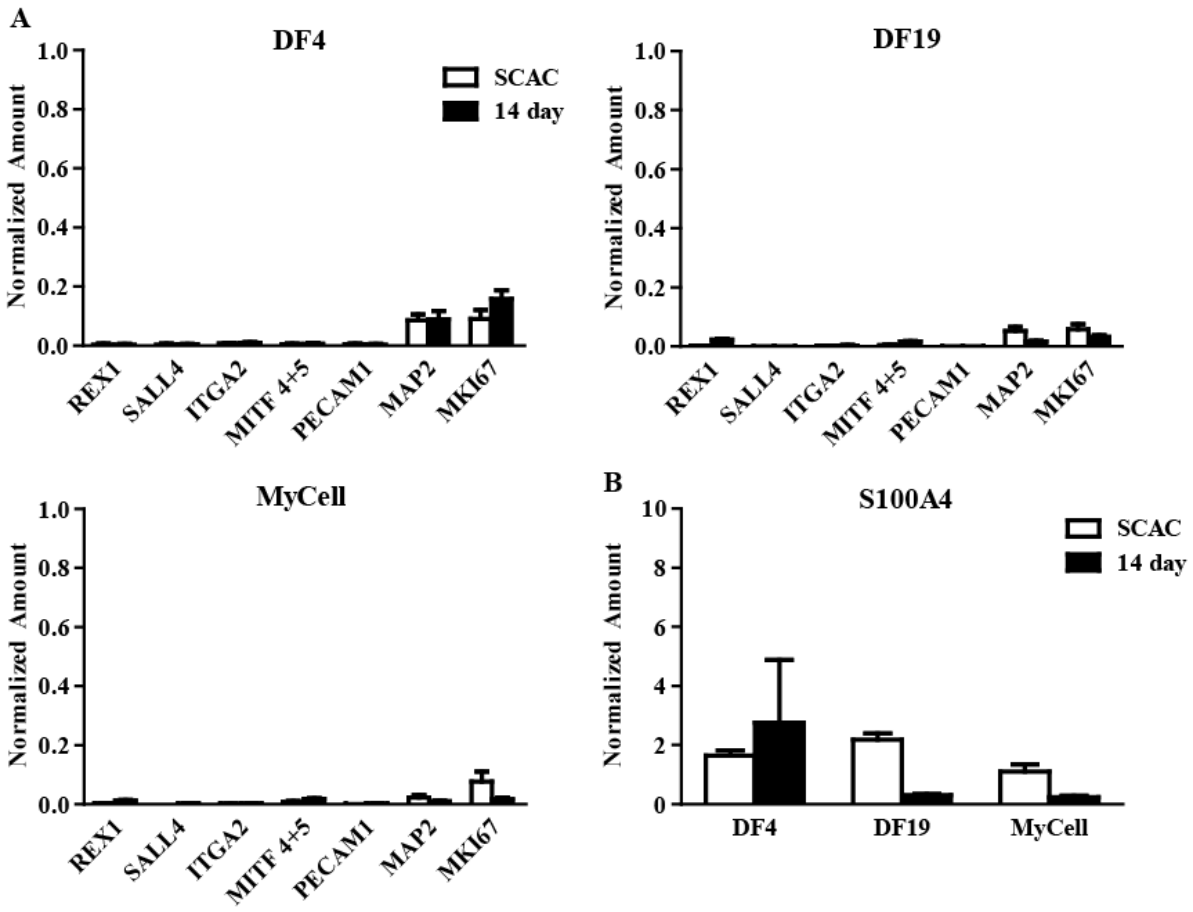

Supplemental Figure 1. Contaminate marker transcripts levels. (A) DF4, DF19 and Mycell iPSC-RPE contaminate markers are significantly lower than positive control values ($p \leq 0.05$). Positive control cell values for non-RPE genes: H9 hESC, Rex 1 (4.09±0.09), Sall4 (10.93±0.45); SMC, ITGA2 (2.02±0.24); HUVEC, PECAM (15.7±0.53); SH-SY5Y, MAP2 (0.78±0.29). (B) S100A4 contaminate expression for DF4, DF19 and Mycell iPSC-RPE are significantly lower than positive control, ($p \leq 0.05$) Hs27, S100A4 (20.13±1.09). Normalized to geometric mean of housekeepers, See *Methods* in Chapter 2. Error bars represent ± SEM. n=3.

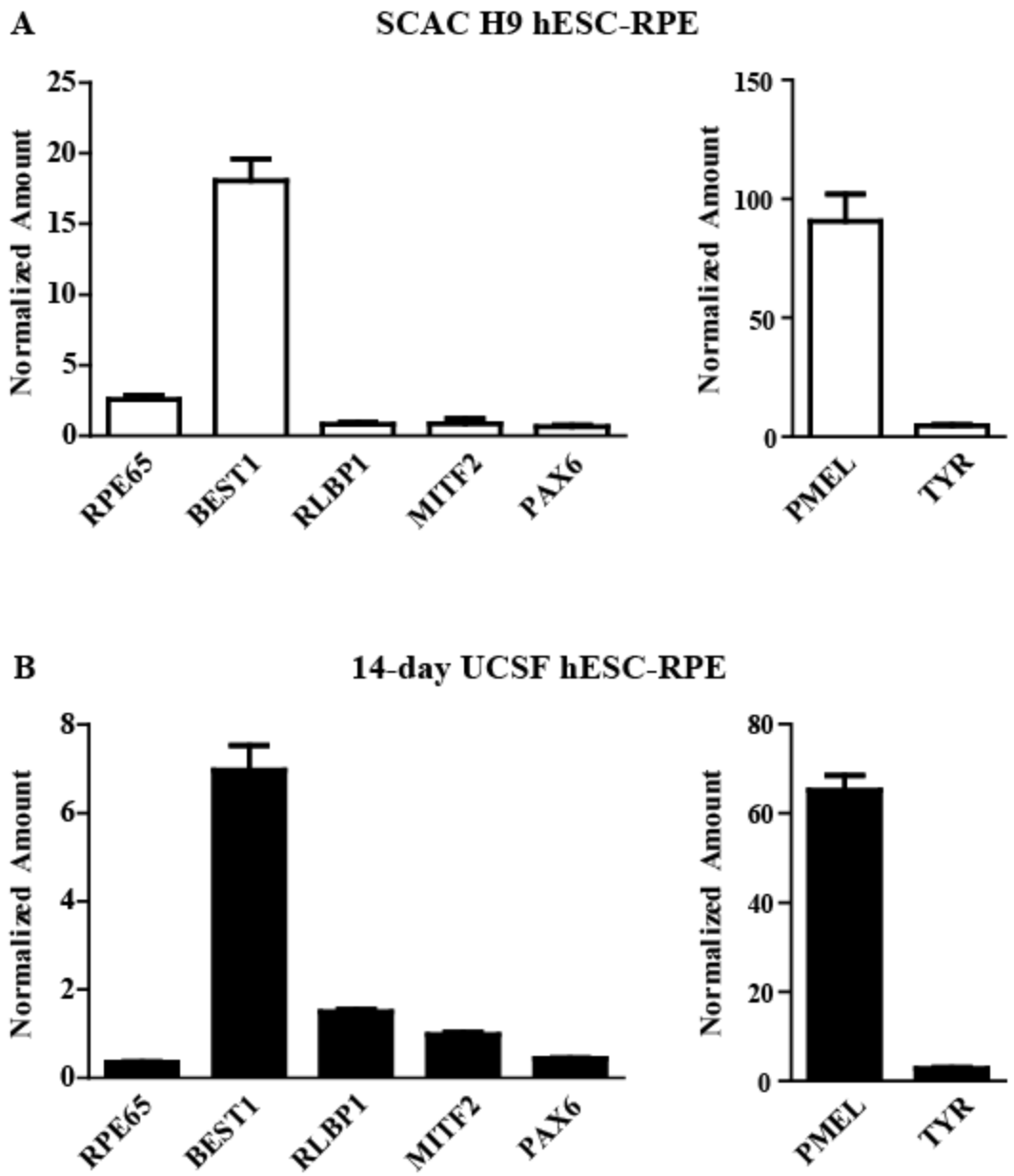

Supplemental Figure 2. Gene expression profiles for hESC-RPE passage 3 day 30 after thaw. RPE specific transcripts and PAX6, a neural retina marker, left panel. Pigmentation markers, right panel. (A) SCAC-derived H9 hESC-RPE gene profile. (B) 14-day-derived UCSF4 hESC-RPE gene profile. The two different hESC lines cannot be directly compared. Normalized to geometric mean of housekeepers, See *Methods* in Chapter 2. Error bars represent ± SEM. n=3.

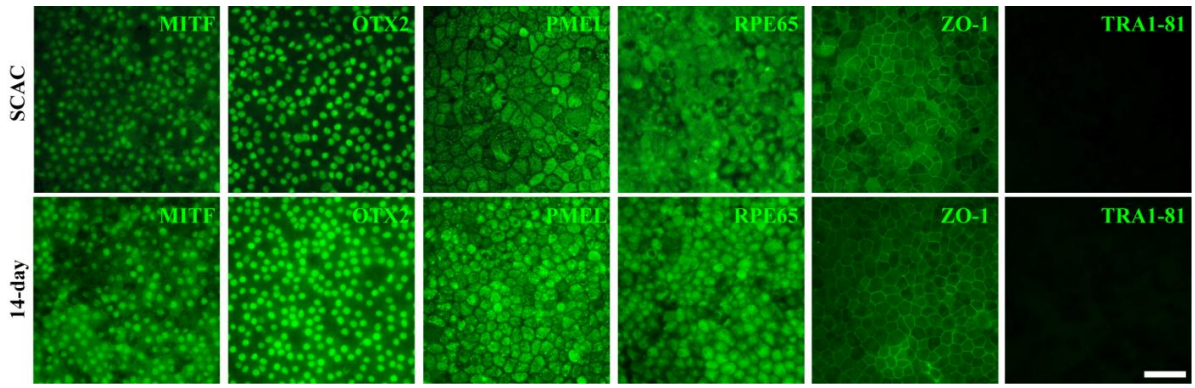

Supplemental Figure 3. Protein localization and expression in hESC-RPE. Immunofluorescence images of OTX2, MITF, PMEL, RPE65, ZO-1, and TRA1-81 are shown for passage 3, day 30 hESC-RPE derived by SCAC (H9-RPE) or 14-day directed differentiation (UCSF4-RPE). Scale bar represent 50μm.

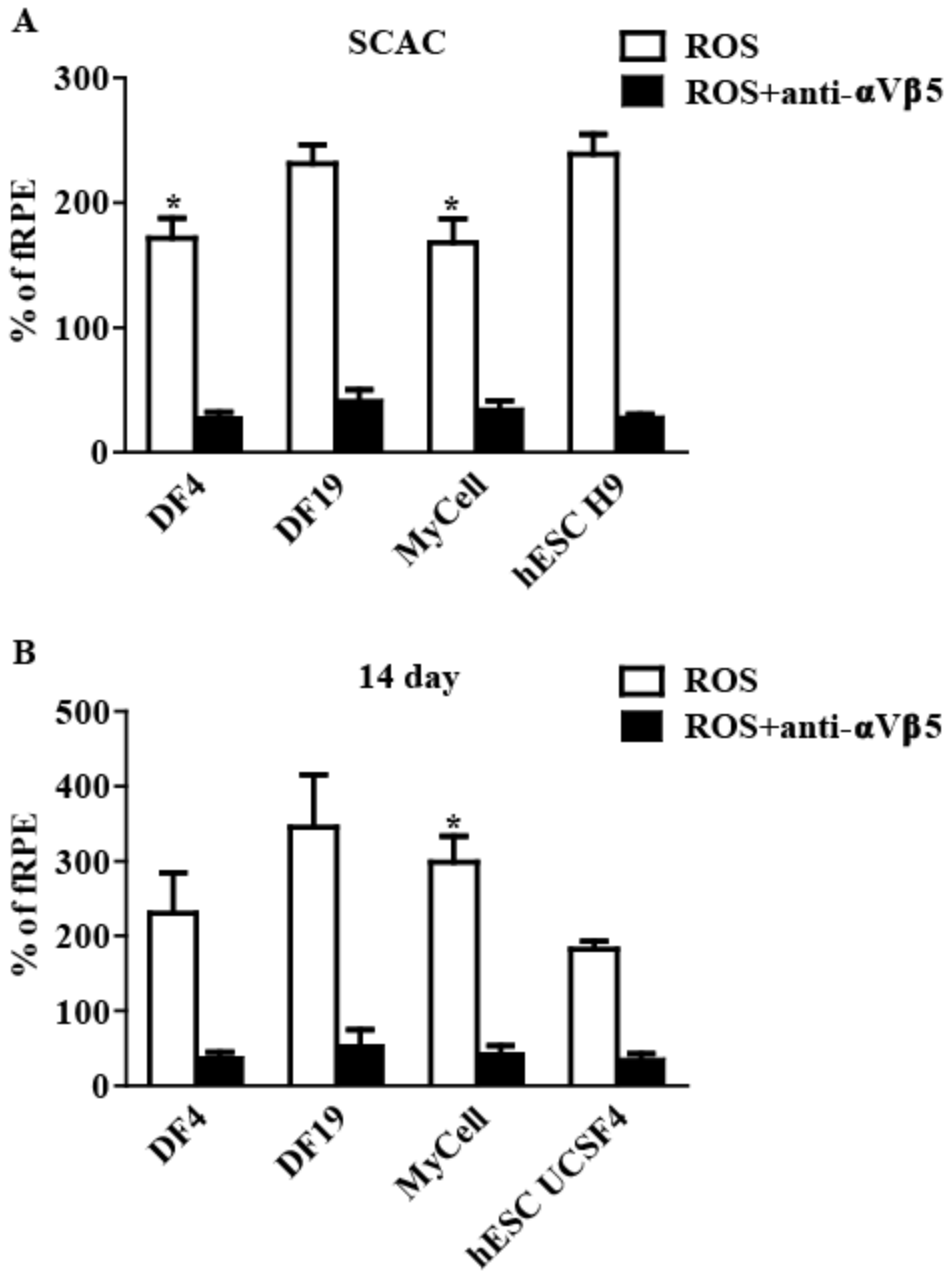

Supplemental Figure 4. iPSC-RPE phagocytosis compared to hESC-RPE phagocytosis. Rod outer segments (ROS) in the absence (white bars) or presence (black bars) of anti-αVβ5 represented as a percent of ROS fRPE integrated pixel density. (A) Phagocytosis of SCAC-derived DF4, DF9 and MyCell iPSC-RPE compared to SCAC-derived H9 hESC-RPE. DF4 and DF19 iPSC-RPE phagocytose less than H9 hESC-RPE. (B) 14-day-derived DF4, DF9 and MyCell iPSC-RPE compared to 14-day-derived UCSF4 hESC-RPE phagocytosis. MyCell iPSC-RPE phagocytose more than UCSF4 hESC-RPE. Reference Chapter 2 *Methods* for normalization method and statistics. Error bars represent ± SEM. *p≤0.05, compared to hESC within the same method. n=3.

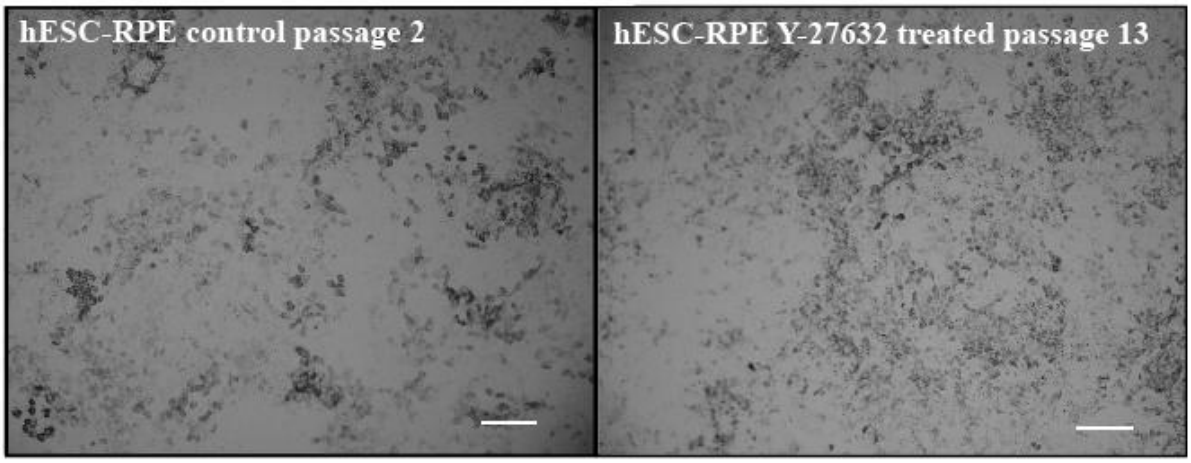

Supplemental Figure 5. Bright-field images of control passage 2 (left) and Y-27632 treated passage 13 (right) cells show similar patterns of pigmentation at day 30. Scale bar=100μm.

hESC-RPE control passage 3

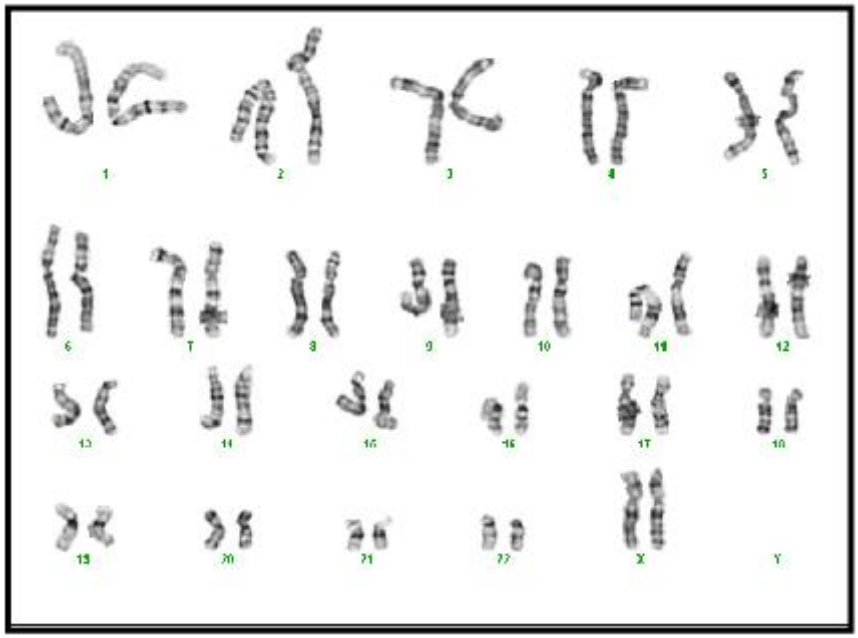

hESC-RPE Y-27632 treated passage 13

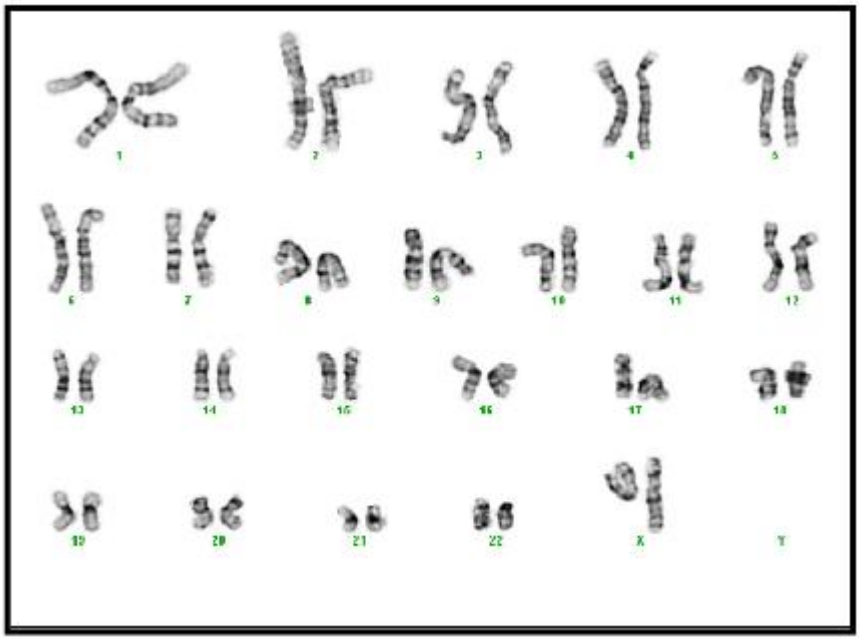

Supplemental Figure 6. Cytogenetic analysis reveals normal human female 46, XX karyotype for hESC-RPE passage 3 (top panel) and passage 13 (bottom panel) from the same enrichment. Y-27632 treatment does not create chromosome abnormalities.

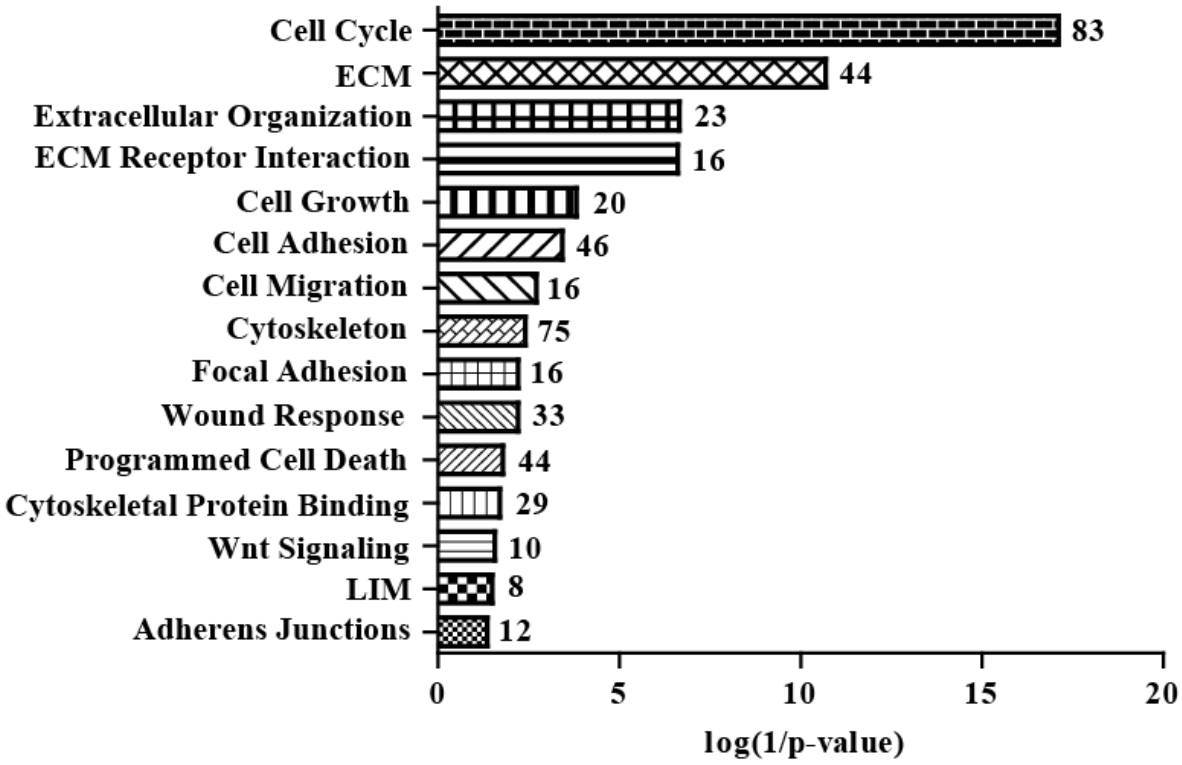

Supplemental Figure 7. The microarray data was transformed using the ratio: $\log_2$(Y-27632/Control) and put into the DAVID clustering software. Cell processes were graphed according to p-value. The number of genes within the cluster is indicated at the right of each bar.

A

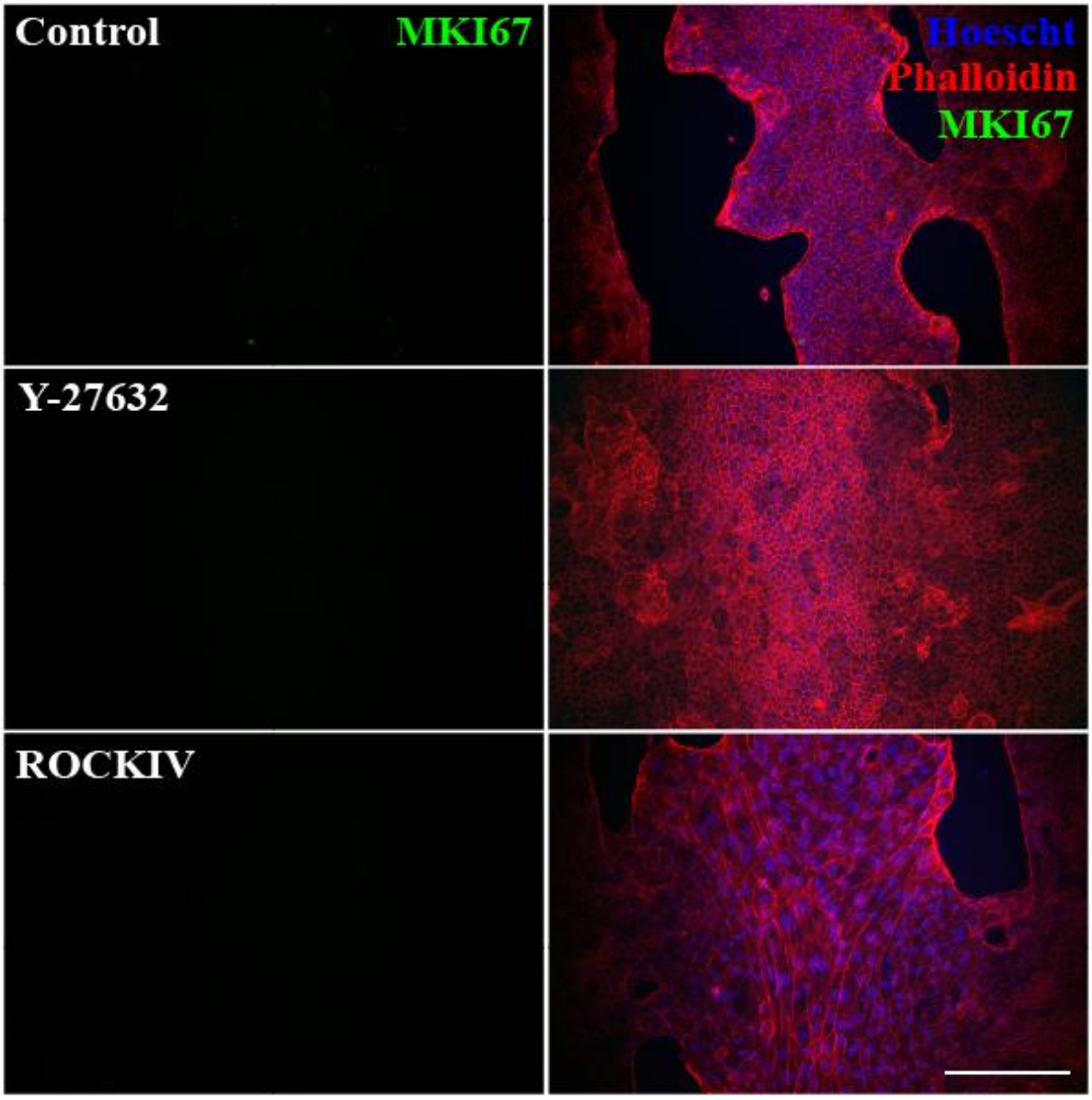

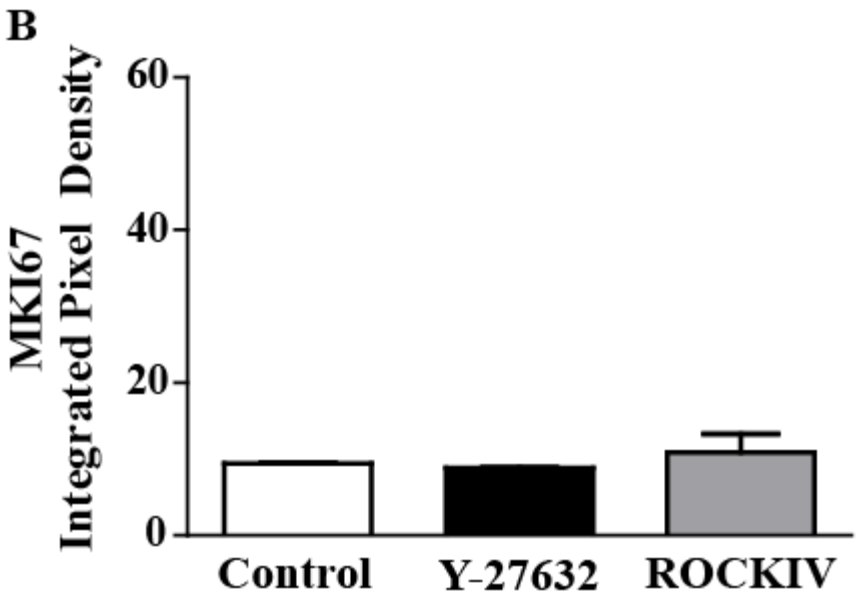

Supplemental Figure 8. Day 30 after scratch of hESC-RPE showed no residual MKI67 expression. hESC-RPE were scratched and treated with either 10μM Y-27632, 10μM ROCKIV or equal volume water as a control and immunocytochemistry was performed following 30 days in culture. Treatments were stopped after 14 days. (A) Left panel, MKI67 staining, right panel, overlay of Hoescht (blue, cellular DNA), Phalloidin (red, F-actin), and MKI67 (green, proliferation). (B) Quantification of intensity of MKI67 fluorescence following ICC within scratched region. Some residual integrated pixel density was detected by the software; however this was background. Scale bar (A)=200μm. Error bars represent ± SEM. n=2.